A NEW LOOK AT THE SUMMER ARCTIC FRONTAL ZONE

by

ALEXANDER MICHAEL DOMINIC CRAWFORD

B.A., Colgate University, 2012

A thesis submitted to the

Faculty of the Graduate School of the

University of Colorado in partial fulfillment

of the requirement for the degree of

Master of Arts

Department of Geography

2014

This thesis entitled:
A New Look at the Summer Arctic Frontal Zone
written by Alexander Michael Dominic Crawford
has been approved for the Department of Geography

_____
(Mark C. Serreze)

_____
(Peter Blanken)

_____
(John Cassano)

Date_____

The final copy of this thesis has been examined by the signatories, and we find that both the content and the form meet acceptable presentation standards of scholarly work in the above mentioned discipline.

Crawford, Alexander Michael Dominic (M.A., Geography)

A New Look at the Summer Arctic Frontal Zone

Thesis directed by Professor Mark C. Serreze

A notable characteristic of the summertime Arctic is the existence of a narrow band of strong horizontal temperature gradients spanning the coastlines of Siberia, Alaska, and western Canada that extends through a considerable depth of the troposphere. Past research has associated this summer Arctic Frontal Zone (AFZ) with contrasts in atmospheric heating between the Arctic Ocean and snow-free land, with its regional strength strongly influenced by topography. However, little is known about its variability, and questions persist regarding possible links with heating contrasts along the boreal forest-tundra ecotone. Output from the latest generation of global atmospheric reanalyses is used to better constrain and define the summer AFZ, including its spatial and seasonal characteristics. The relative importance of different factors linked to its variability are evaluated, and long-term trends in monthly AFZ strength are examined.

The summer AFZ is present in at least some areas from May through August and reaches its peak strength in July. It is manifested aloft as a separate Arctic jet feature at about 300 hPa. The summer AFZ is clearly associated with differential atmospheric heating, as evidenced by the sharp difference in surface energy balance terms between the Arctic Ocean and adjacent land. No evidence is found of links between the summer AFZ and the boreal forest-tundra ecotone. Interannual variations in monthly strength of the summer AFZ are spatially heterogeneous and primarily dependent on factors affecting temperature over land, especially variability in cloud cover, surface wind direction, and snow cover extent. Local variability in sea ice concentration is

also important through its control on temperatures over coastal seas. Snow cover is primarily important to monthly AFZ strength in May and June, while sea ice is more important in July and August. Throughout the period 1979 to 2012, monthly June AFZ strength increased throughout most of Eurasia. This strengthening is likely related to amplification of Arctic atmospheric warming over land from snow cover loss.

ACKNOWLEDGEMENTS

This material is based upon work supported by the National Science Foundation (NSF) Graduate Research Fellowship Program under Grant DGE 1144083 and by NSF Grant PLR 1417016. I would like to thank my adviser Mark Serreze for guiding me through this process and my committee members, Peter Blanken and John Cassano, for their insightful comments. I would also like to thank Allison Hurley for mentoring me in my first two years as a graduate student and to Karen Alley for her support both in the office and at home.

CONTENTS

TABLES

Table

FIGURES

Figure

1. INTRODUCTION

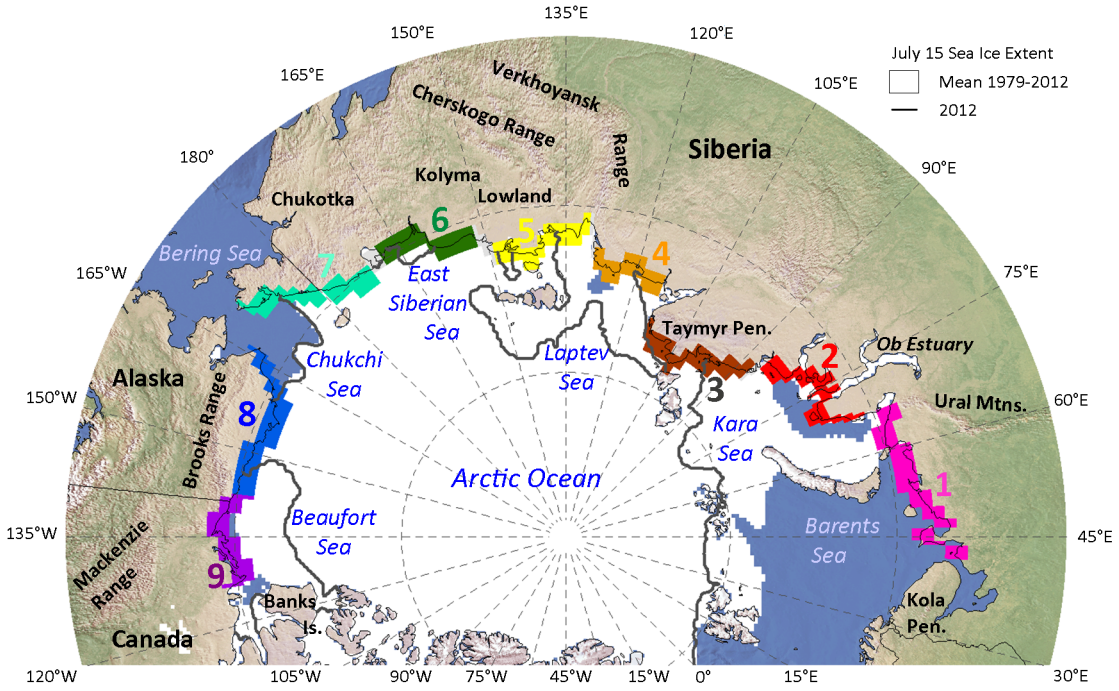

Figure 1. Location map of the summer Arctic frontal zone (AFZ) region showing geographic regions referred to in this study, sectors for which the summer AFZ is examined (colored shading; described in Section 4), the average mean July 15 sea ice extent for 1979-2012 (white shading), and the July 15 sea ice extent for 2012 (black line). The North Atlantic region, in which no summer AFZ is observed, has been omitted.

As the Arctic (**Figure 1**) loses its summer sea ice cover, the region becomes more accessible to marine transport, tourism, and extraction of energy resources. As the economic and strategic importance of the Arctic grows, so does the need to better understand its climate and weather. Extensive research has addressed large-scale aspects of the Arctic atmospheric circulation (Wu et al. 2006; Wang et al. 2009; Overland and Wang 2010; Stroeve et al. 2011), extratropical cyclone strength and frequency (Simmonds and Keay 2009; Simmonds and Rudeva 2012; Zhang et al. 2013), and their impacts on sea ice and the hydrologic cycle. However, less attention has been paid to regional scale features. The purpose of the present study is to better

define the mean characteristics and spatiotemporal variability of one such regional feature - the summer Arctic frontal zone.

Historically, studies of northern high-latitude fronts have had two distinct motivations, and thus the terms “Arctic front” and “Arctic frontal zone” have been applied to two distinct but related frameworks. The framework used here has its origin in attempts to explain why cyclone activity over the central Arctic Ocean reaches a maximum in summer. Dzerdzeevskii (1945) observed the prevalence of fronts along the northern coast of Siberia and identified this “Arctic frontal zone” (hereafter AFZ) as the origin of cyclones tracking into the Arctic Ocean. Building on this research, Reed and Kunkel (1960) calculated frontal frequencies from early surface analyses and confirmed the presence of a high-latitude frontal zone broadly focused along the Arctic Ocean coastlines of Siberia and Alaska. This frontal zone was distinct from the polar frontal zone to the south. They noted the persistence of strong horizontal temperature gradients from the surface up to about 500 hPa, a sharp tropopause fold, and a jet-like feature centered at about 250 hPa.

These seasonal features were attributed to differential heating of the atmosphere over land and ocean surfaces. The land surface, which loses its snow cover in spring, has a low albedo and warms strongly in response to downwelling radiation in summer. The land surface readily transfers this heat to the overlying atmosphere. By contrast, the Arctic Ocean absorbs much less incoming radiation because of its lingering sea ice cover and high albedo. Additionally, energy that is absorbed during summer is primarily used to melt sea ice and increase the sensible heat content of the ocean mixed layer (the top 10-30 m) and not merely the surface. Consequently, the surface stays relatively cool and heating of the atmosphere

above is limited. This heating contrast creates strong horizontal temperature gradients (the AFZ) along the coast. Reed and Kunkel (1960) also suggested that the AFZ might be enhanced by coastal mountain ranges, such as the Brooks Range in Alaska, which prevent cold air from pushing inland.

This interpretation found strong support in the much later study of Serreze et al. (2001) based on data from the National Centers for Environmental Prediction/National Center for Atmospheric Research (NCEP/NCAR) atmospheric reanalysis. They applied a thermal frontal parameter algorithm, which is the horizontal gradient of the horizontal temperature gradient (see also Hewson 1998) to 850 hPa temperature data, citing the strong influence of model parameterization on the boundary layer as the reason for choosing 850 hPa rather than a lower vertical level for analysis. Using this method, Serreze et al. (2001) resolved a summertime frontal zone along the coasts of Alaska and Siberia. Furthermore, they demonstrated that regions where the summer AFZ is strongest (eastern Siberia and Alaska) are preferred regions of summer cyclogenesis, and experience an especially high proportion of their annual total precipitation in summer. Cyclones that originate or intensify along this zone often track into the central Arctic Ocean, where they may impact the summer precipitation maximum over the Arctic Ocean (Serreze and Barrett 2008).

The other use of the terms “Arctic front” and “Arctic frontal zone” is to describe the southern boundary of Arctic air masses. (Arctic air masses originate over the Arctic Ocean and lie to the north of Polar air masses.) Bryson (1966) used air mass trajectory analysis to identify the southern boundary of the Arctic air mass in North America. He located an Arctic front whose mean July location extended from the Mackenzie River Delta southeastward across

Canada. This summer frontal zone was roughly co-located with the northern boundary of the boreal forest.

In contrast to the frontal zone described by Dzerdzeevskii (1945) and Serreze et al. (2001), this air mass boundary exists in all seasons, not just summer. In winter, Bryson (1966) observed that the mean location of the Arctic front pushed southward across most of Canada. The one exception was in the west along the Cordillera, where the frontal zone remained fixed near the Mackenzie River Delta. Whereas the summer position of Bryson's AFZ was co-located with the northern boundary of the boreal forest, the winter position was co-located with the southern boundary. Noting this, Bryson (1966) suggested that the boreal forest's extent might be controlled by the position of the AFZ.

The air mass framework has been revisited sporadically for North America (Barry 1967; Willis and Grice 1977; Scott 1992; Ladd and Gajewski 2010). Inverting Bryson's (1966) hypothesis, some have suggested that heating differences between the tundra and boreal forest may influence or determine the location of the Arctic front (Hare 1968; Krebs and Barry 1970; Hare and Ritchie 1972; Pielke and Vidale 1995). However, Beringer et al. (2001) found that the surface heat flux difference between tundra and boreal forest biomes is equal to the variation found *within* each biome. Comparisons between the mean July position of the Arctic front based on trajectory analysis and anomalies of the normalized difference vegetation index (NDVI) further question a vegetative control on the Arctic front; they instead suggest that variability in Arctic front position influences primary productivity (Ladd and Gajewski 2010).

One recent study has presented a perspective that combines these two frameworks. Liess et al. (2011) coupled climate and land surface models to project the impact of northward

advance of the boreal forest on the AFZ. While they found the strongest frontal expression along the coastline, they also found that the temperature gradient and jet stream intensified slightly with northward advance of the tree line. They concluded that although the land-ocean contrast may be primary to AFZ development, vegetation contrasts can also enhance AFZ strength.

To summarize, in the framework motivated by cyclone behavior, the AFZ is defined as an essentially fixed geographic area of seasonal baroclinicity. In the framework motivated by air mass description, the AFZ has a constant function but no fixed location. There is always an "Arctic front" because it is defined as the boundary between Arctic and polar air masses. This boundary will shift further south in winter and further north in summer. The regions of focus also differ for the two frameworks. The cyclone-motivated framework is usually applied to the Arctic Ocean basin whereas the air mass-motivated framework is more often associated with North America, and especially Canada. Hypotheses concerning the impact of Arctic fronts on biome boundaries and vice versa have been usually applied to the air mass framework; however, some studies (Lynch et al. 2001; Liess et al. 2011) have considered the role of vegetation in either.

The research presented here most closely follows the Arctic cyclone framework because it is intended as a foundation for future studies regarding Arctic cyclogenesis and precipitation patterns. The first goal is to take advantage of data from the latest generation of global atmospheric reanalyses to better constrain and define the AFZ, including its spatial and seasonal characteristics. Both the quality and the spatial resolution of these data are

improvements on the previous generation of global atmospheric reanalyses, so they provide a new look at old questions.

In addition to improved data, this research also addresses new questions about the summer AFZ. The second goal is to evaluate the relative importance of factors linked to AFZ variability, including surface winds, sea level pressure, topography, vegetation boundaries, snow cover, sea ice, and cloud fraction. Finally, the third goal is to examine long-term trends in summer AFZ strength. These last two goals are the groundwork for assessing more closely the role of the summer AFZ in the Arctic climate system, and in particular its influence on cyclogenesis and the hydrologic cycle. Understanding these processes becomes ever more relevant as the Arctic climate changes and the region becomes more accessible.

2. DATA SOURCES

2.1. Atmospheric Reanalyses

Atmospheric reanalyses provide gridded representations of atmospheric states spanning multiple decades. They are generated by blending observational data (such as from radiosondes, satellites, and buoy stations) and forecasts using a constant atmospheric model and assimilation system (Saha et al. 2010). The three reanalyses examined here are the National Aeronautics and Space Administration (NASA) Modern Era Retrospective-Analysis for Research and Applications (MERRA; Rienecker et al. 2011), the National Oceanic and Atmospheric Administration (NOAA) Climate Forecast System Reanalysis (CFSR; Saha et al. 2010); and the European Centre for Medium Range Weather Forecasting (ECMWF) interim European ReAnalysis (ERA-Interim; Dee et al. 2011). CFSR has the highest resolution at 0.50° of longitude by 0.50°of latitude and 64 vertical levels. MERRA has a resolution of 0.67^{o} longitude by 0.50^{o} latitude and 72 vertical levels. ERA-Interim has a resolution of 0.75° of longitude by 0.75° of latitude and 60 vertical levels. Data are available for the entire 1979-2012 period from ERA-Interim and MERRA. Data are only available for 1979-2009 from CFSR. Variables used for this study include monthly temperature and wind data from near the surface (2-m and 10-m) and at pressure levels from 1000 to 100 hPa, as well as sea level pressure and the various surface energy fluxes: net shortwave radiation, net longwave radiation, sensible heat, and latent heat. All reanalysis data was acquired as monthly means of daily means when available. Otherwise, daily and monthly means were calculated after acquisition.

An analysis for the central Arctic Ocean using tethersonde soundings from the Tara drifting ice station in 2007 (Jakobson et al. 2012) revealed that ERA-Interim produces more accurate temperature, humidity, and wind speed profiles in the lower atmosphere than does MERRA or CFSR. All three reanalyses exhibited warm biases at the surface and underestimated wind speeds throughout most of the lower atmosphere. Temperature measurements had lower accuracy during high wind conditions and temperature inversions. The warm bias in ERA-Interim (the worst performer, up to 2°C) may be related its treatment of sea ice. The most commonly observed surface temperatures in the Arctic Ocean are the freezing point of seawater, but surface temperatures in ERA-Interim have a tendency toward the melting point of sea ice (Lüpkes et al. 2010). CFSR performed the best with regard to surface parameters, likely because of its more complicated treatment of sea ice (Jakobson et al. 2012).

2.2. Sea Ice Concentration

Daily sea ice concentration and extent at a 25 km resolution for 1979 onwards were obtained from the combined satellite passive microwave record available from the National Snow and Ice Data Center (NSIDC; Cavalieri et al. 1996, updated 2008). Sea ice concentration is calculated using the NASA Team algorithm. Accuracy of the algorithm depends on ice conditions, methods, and locations used in individual validation studies. In general, ice concentration accuracy is within ±5% in winter, but falls to ±15% during summer, when melt ponds are present (Cavalieri et al. 1992). Because the NASA Team algorithm is based on tie-points for snow-covered sea ice, accuracy tends to be higher within the consolidated ice pack and decreases as the proportion of thin or new ice increases.

2.3. Snow Cover

Weekly snow cover at 25 km resolution for 1979 through 2011 was obtained from the Northern Hemisphere Equal Area Scalable Earth (EASE) Grid 2.0 Weekly Snow Cover and Sea Ice Extent product, also available from NSIDC (Brodzik and Armstrong 2013). Each grid cell indicates the presence or absence of snow cover. This product is based on the weekly NOAA/National Climatic Data Center snow cover extent Climate Data Record product, which is derived from manual analysis of a suite of visible and microwave satellite imagery, derived map products, and surface observations. It is least accurate in areas of varied topography and patchy snow cover, and accuracy varies throughout the record period because of changing data sources (Robinson 2013).

2.4. Cloud Fraction

Monthly means of cloud fraction were obtained from the Extended Advanced Very High Resolution Radiometer (AVHRR) Polar Pathfinder (APP-x) product, which has a 25 km resolution and extends from 1982 to 2012. Cloud detection is accomplished by applying a series of thresholding operations to modeled and sensor radiances. Monthly cloud fraction is calculated from the set of daily cloud masks (Key 2002). Different procedures are implemented for daytime versus nighttime, water clouds versus ice clouds, and high versus low zenith angles, but large zenith angles still yield high uncertainties (Key 2002). Issues with nighttime detection were addressed by comparing AVHRR to data from the year-long Surface Heat Budget of the Arctic Ocean (SHEBA) experiment from September 1997 to August 1998 (Key et al. 2001). Nighttime issues are of minor relevance to this study, which focuses primarily on the summer season.

2.5. Ancillary Data

Ancillary data include the International Bathymetric Chart of the Arctic Ocean (IBCAO) version 3 (Jakobsson et al. 2012), the Moderate Resolution Imaging Spectro-radiometer (MODIS) land cover dataset (MCD12Q1; Strahler et al. 1999), and the Combined Land-Surface Air and Sea-Surface Water Temperature Anomalies (Land-Ocean Temperature Index, LOTI) from the NASA Goddard Institute for Space Studies Surface Temperature Analysis (GISTEMP; Hansen et al. 2010). The IBCAO was used to identify the Arctic coastline (defined using the zero m contour/isobath). LOTI acted as an independent reference time series of surface temperatures, which is compared to the regional time series of summer AFZ strength.

The MODIS dataset was used to identify the major Arctic vegetation boundaries. Multiple classification systems are provided in these data, so the International Geosphere Biosphere Programme (IGBP) classification that matches the data used by Liess et al. (2011) was selected. Vegetation boundaries are diffuse, so rather than identify a distinct line to demarcate the forest-tundra boundary, past researchers have identified the forest-tundra ecotone as a zone of transition. This zone is also variably referred to as open woodland (e.g. Krebs and Barry 1970; Hare and Ritchie 1972) or open shrubland (e.g. Liess et al. 2011). The problem with using the open shurbland as the forest-tundra ecotone is that the open shrubland extends over a wide enough area to have its own diffuse boundaries with both the forest and tundra. For this study, the northern boundary of the forest and the southern boundary of the tundra were marked so that all groups of four contiguous grid cells identified as shrubland (digital numbers 6 and 7) lay in between. This resulted in a generously large ecotone, increasing the likelihood that the summer AFZ would be identified as co-located with the ecotone in this study. Where no

shrubland existed, the northern boundary of the forest was identified so that all groups of four contiguous gird cells identified as forest lay on the forest side of the boundary. This made the boundary more likely to be placed too far north as opposed to too far south.

3. AFZ STRUCTURE

3.1. Measuring the AFZ

The AFZ has previously been identified using a variety of metrics, including, 1000 to 500 hPa layer thickness (e.g. Kurashima 1968), trajectory analysis of streamlines (e.g. Bryson 1966), the vertical component of relative vorticity (e.g. Lynch et al. 2001), a thermal frontal parameter (e.g. Serreze et al. 2001), and the meridional temperature gradient (e.g. Liess et al. 2011). Often, such metrics have been used to identify individual fronts, with the location of the AFZ then determined by assessing frontal frequency during a particular period. Since prevailing theory concerning the summer AFZ in either framework highlights surface-atmosphere interactions, ideal measurements would be at or near the surface. However, atmospheric parameters from reanalyses are typically less accurate near the surface, which has led to use of 850 hPa as the most common level for examining AFZ location and strength (e.g. Barry 1967; Willis and Grice 1977; Serreze et al. 2001).

The present study uses the horizontal 2-m temperature gradient as the main measure of the summer AFZ (calculated from air temperatures 2 m above the surface). This simple metric is more straightforward than a thermal frontal parameter or other complex constructions, and using the 2-m level more closely relates to the differential surface heating argument than using the more common 850 hPa level. Despite improvements to atmospheric reanalyses, the influence of model parameterizations on the accuracy of near-surface variables is still a concern.

Temperature gradient magnitude fields were calculated using a modified Sobel operator. The Sobel operator calculates a zonal and meridional gradient using a 3 by 3 kernel. The four cells that share an edge with the center cell are weighted twice as heavily as the four cells sharing a corner. The reanalysis data are gridded on latitude and longitude, so the Haversine formula was included in the operator to convert to kilometers before calculating the gradient. Magnitude was then calculated as normally using the Pythagorean theorem.

Except where noted, summer AFZ strength is defined as the 2-m horizontal temperature gradient magnitude in units of K/100 km. The meridional temperature gradient is used to compare with the zonal winds or to contrast with temperature gradients in other seasons. The vertical structure of the summer AFZ is assessed using the meridional temperature gradient and zonal wind velocity up to 100 hPa.

3.2. Horizontal Structure of the AFZ

Figure 2 shows the spatial distribution of the average July horizontal 2-m temperature gradient magnitude north of 60°N for all three reanalyses. In general, horizontal temperature gradient magnitude is weakest in ERA-Interim (which has the lowest resolution) and strongest in CFSR (the highest resolution). All three reanalyses show exceptionally strong gradients along the Arctic coasts of Eurasia and western North America. This is the surface expression of the summer AFZ. No strong gradients are associated with the forest-tundra ecotone (between the dashed green and brown lines).

Coastal July temperature gradients are consistently strongest along the Laptev, East Siberian, and Beaufort Seas, exceeding 5.0 K/100 km in ERA-Interim and exceeding 7.0 K/100 km in CFSR. This is consistent with the proposition by Reed and Kunkel (1960) and Serreze et al.

(2001) that near-coastal mountain ranges like the Brooks Range in Alaska and the Cherskogo, Gydan, and Verkhoyansk Ranges in Siberia may enhance the AFZ by trapping cold Arctic air near the coast.

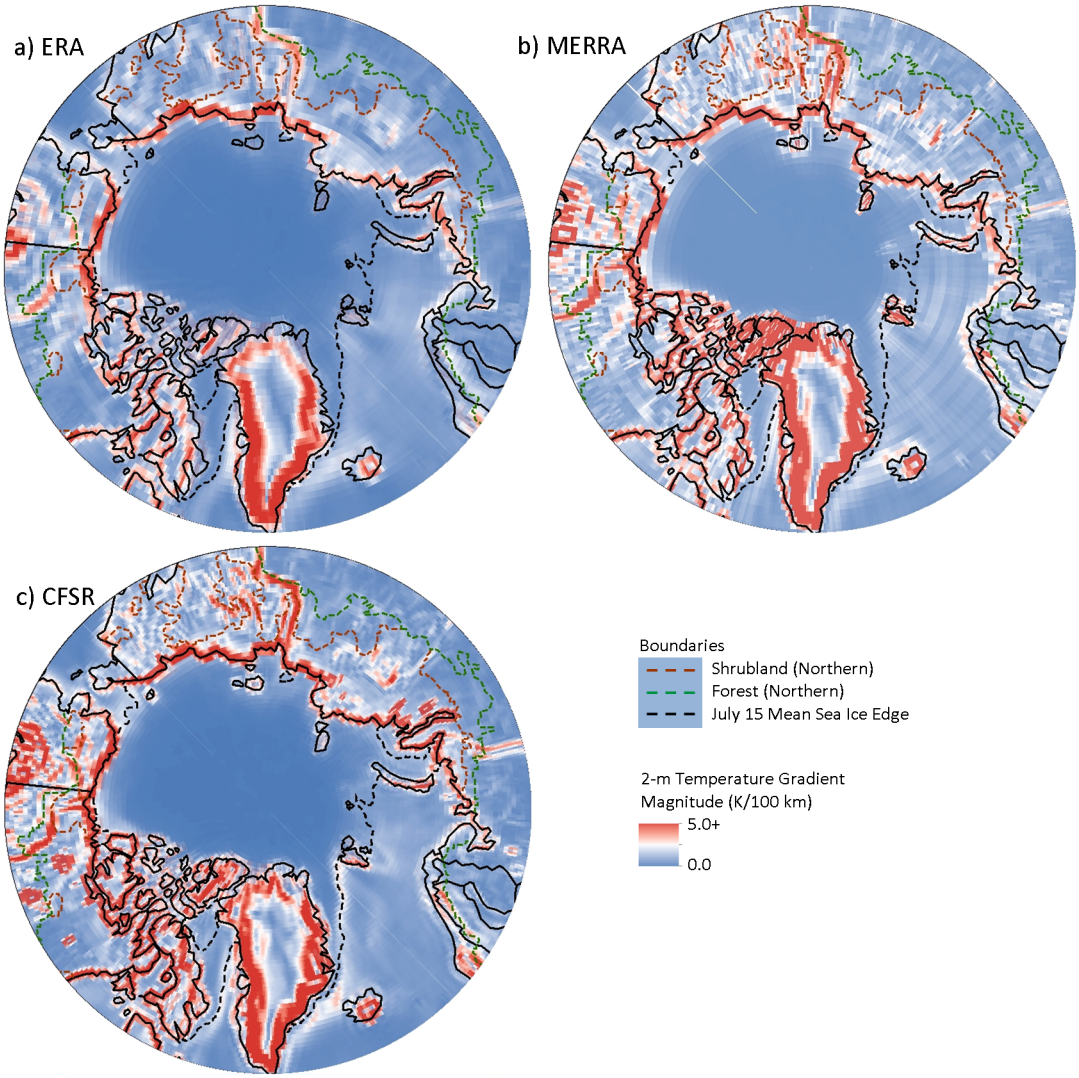

Figure 2: Mean July 2-m temperature gradient magnitude for 1979-2012 from a) ERA, b) MERRA, and c) CFSR. Dashed lines denote important boundaries, including the mean July 15 sea ice edge (black), the northern limit of the boreal forest (green), and the northern limit of the shrubland (brown). The boreal forest-tundra ecotone lies between these boundaries and contains open and closed shrubland.

Strong 2-m temperature gradients also exist in areas of pronounced topography, such as along the Greenland coast and along mountain ranges like the Mackenzie Range in Canada.

These occur in large part because the 2-m temperature field follows topography, so a grid cell with a higher elevation than its neighbor will tend to have a lower 2-m air temperature. CFSR and MERRA also resolve strong temperature gradients throughout the Canadian Arctic Archipelago, which has complex topography. Since MERRA represents the median option for both spatial resolution and AFZ strength, remaining results focus mostly on MERRA. Except where otherwise noted, CFSR and ERA-Interim show very similar results.

The presence of topographic temperature gradients may be viewed as a hindrance to studying the horizontal temperature gradients of the AFZ. Several more complicated methods of identifying fronts exist that might de-emphasize topographic gradients (see Section 3.1), but the resulting metrics are several steps removed from the physical mechanisms of energy (im)balance and differential heating that have been proposed as the causes of summer AFZ development. Another option is to use the potential temperature, which does further emphasize coastal gradient but does not completely eliminate topographic gradients. A third option would be to calculate the vertical component of the temperature gradient magnitude in each grid cell and then remove it or mask any grid cells for which the vertical component exceeds a certain threshold. These methods seem unlikely to result in perfect de-emphasis, so the surest method might be to simply mask out grid cells for which the topographic slope exceeds a certain threshold.

None of these methods have been employed here. In addition to the arguments for simplicity and for measuring as directly as possible the supposed mechanisms at work, there is the argument that the presence of topography likely plays a role in summer AFZ development. Although the grid cells adjacent to the coastline have little variation in elevation, mountain

ranges are located near and parallel the coastline in several places. These ranges, like the Brooks Range in Alaska (200 to 300 km from the coast), may facilitate summer AFZ development by obstructing the inland movement of cold Arctic air (Reed and Kunkel 1960; Serreze et al. 2001). In other words, removing the topographic signal might obscure the reality of topographic influence on horizontal temperature gradients.

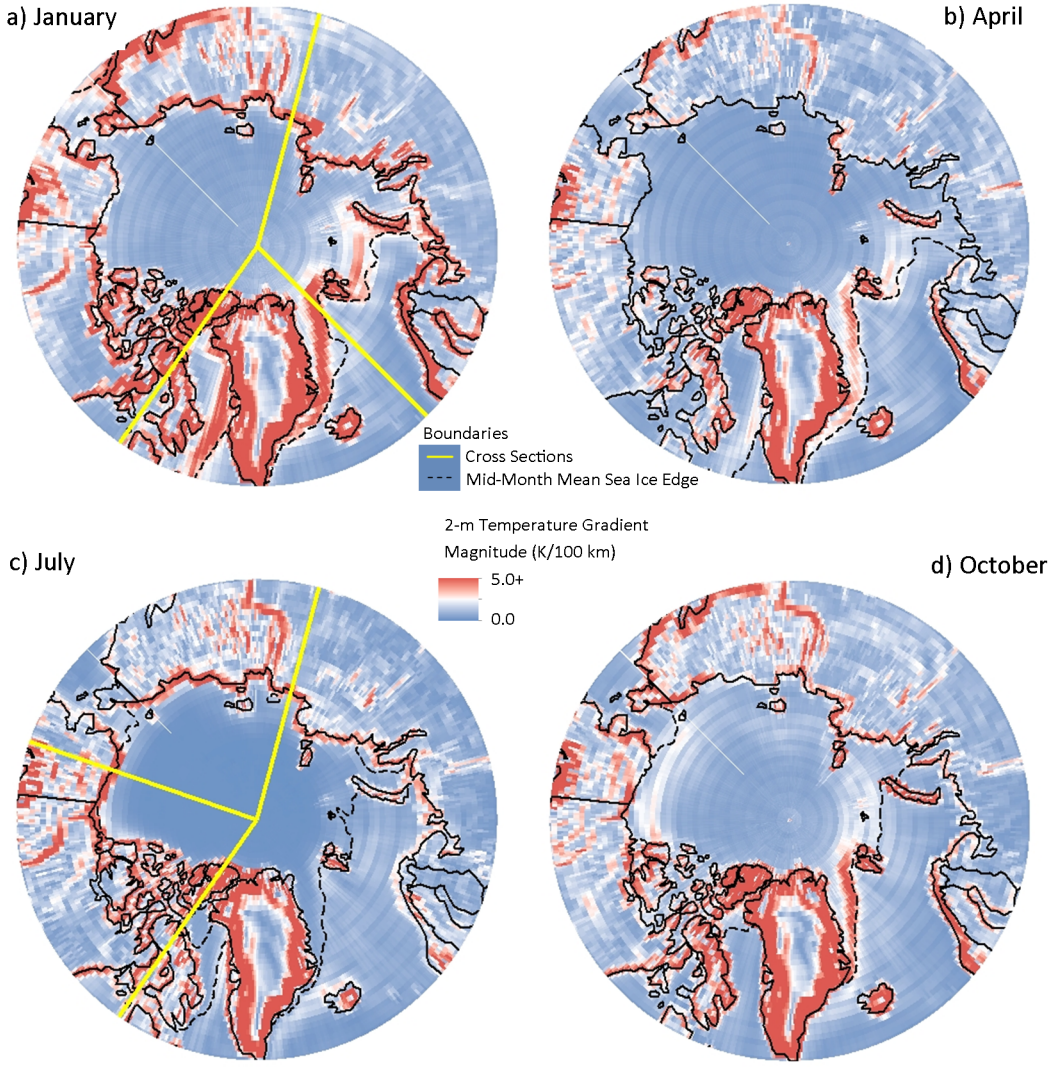

Figure 3: Mean 2-m temperature gradient magnitude for the four mid-season months for the period 1979-2012. Sold yellow lines indicate the locations of latitudinal cross sections presented in Figures 5 (July) and 6 (January). Dashed black lines indicate the mid-month mean sea ice edge (1979-2012). Data from MERRA.

Strong 2-m temperature gradients are also not unique to summer. Coastal gradients are weak in April and October but are quite strong in January (**Figure 3**). As discussed below, these winter coastal gradients differ greatly from those in summer by being confined to a shallow layer. Winter also sees strong temperature gradients along the sea ice edge in the North Atlantic Ocean that extend through a deep layer of the atmosphere; winter cyclone formation and deepening along the ice edge is known to be quite common.

Summer atmospheric heating differences on either side of the coastal boundary are clearly expressed in terms of the surface energy balance. **Figure 4** shows net longwave (red), net shortwave (green), and net allwave (black) radiation at the surface as well as the sensible (gold) and latent (blue) heat fluxes along a latitudinal transect at 120°E longitude averaged for a) July and b) January 1979-2012 (from MERRA). Longitude 120^{o}E lies in an area of the AFZ with average strength (see Section 4.3). Furthermore, in not being influenced by islands or estuaries, it provides a clean depiction of surface flux contrasts. This and subsequent cross sections extend all the way to the Equator in order to help place the summer AFZ in a wider context.

Traveling northward in July (Figure 4a), all four energy balance terms see a pronounced decrease in magnitude crossing the coast. The drop in the net shortwave flux is due to the high albedo of sea ice and demonstrates that the land surface absorbs more incoming radiation than the ocean surface. The decrease in magnitude of the negative net longwave flux manifests a decrease in upward longwave radiation because the land surface is substantially warmer than the ocean surface.

The surplus of net allwave radiation at the land surface is mostly balanced by the upward sensible and latent heat fluxes, which transfer energy into the lower atmosphere. The

ocean surface also has a net radiation surplus, but this is mostly balanced by ice melt or increasing sensible heat storage in the ocean. In fact, because the ocean surface remains at the melting point of sea ice until melting concludes, the temperature of the ocean surface is colder than the overlying atmosphere and the sensible heat flux is downward for coastal waters. This makes the contrast for the sensible heat flux over land and ocean particularly stark. Since the upward longwave radiation and sensible heat fluxes to the lower atmosphere are greater over land, the air overlying land is heated more than the air overlying ocean, which explains the development of strong horizontal temperature gradients near the surface.

This portrayal of how the summer AFZ develops is reminiscent of localized sea breezes that often develop on summer afternoons at beaches along Cape Cod or on the Jersey Shore. The land surface heats up more readily than the ocean surface and transfers energy to the overlying air column. In addition to a horizontal temperature gradient, this sets up a horizontal pressure gradient across the shoreline that leads to local circulation and the familiar cooling sea breeze. Similarly, the summer AFZ develops because the land surface heats more readily than the ocean surface and transfers energy to the lower atmosphere, creating a horizontal temperature gradient across the coastline.

However, the summer AFZ differs from the sea breeze scenario in several aspects. First, the AFZ exists on a much wider spatial scale. The summer AFZ is observed across the Arctic Ocean coastline for thousands of kilometers from the Kola Peninsula eastward to the Canadian Arctic Archipelago (Figure 2). Second, whereas the sea breeze is fleeting, existing only during the afternoon, the summer AFZ persists twenty-four hours a day throughout the entire summer. In the mid-latitudes, the land surface cools off in the evening and becomes cooler

than the ocean surface at night. In the Arctic, nighttime is short or non-existent in summer. Additionally, lingering sea ice cover suppresses ocean temperatures, preventing them from rising above the melting point of sea ice and accentuating the albedo difference between ocean and land. Several other differences become apparent when observing the vertical structure of the summer AFZ (Section 3.3).

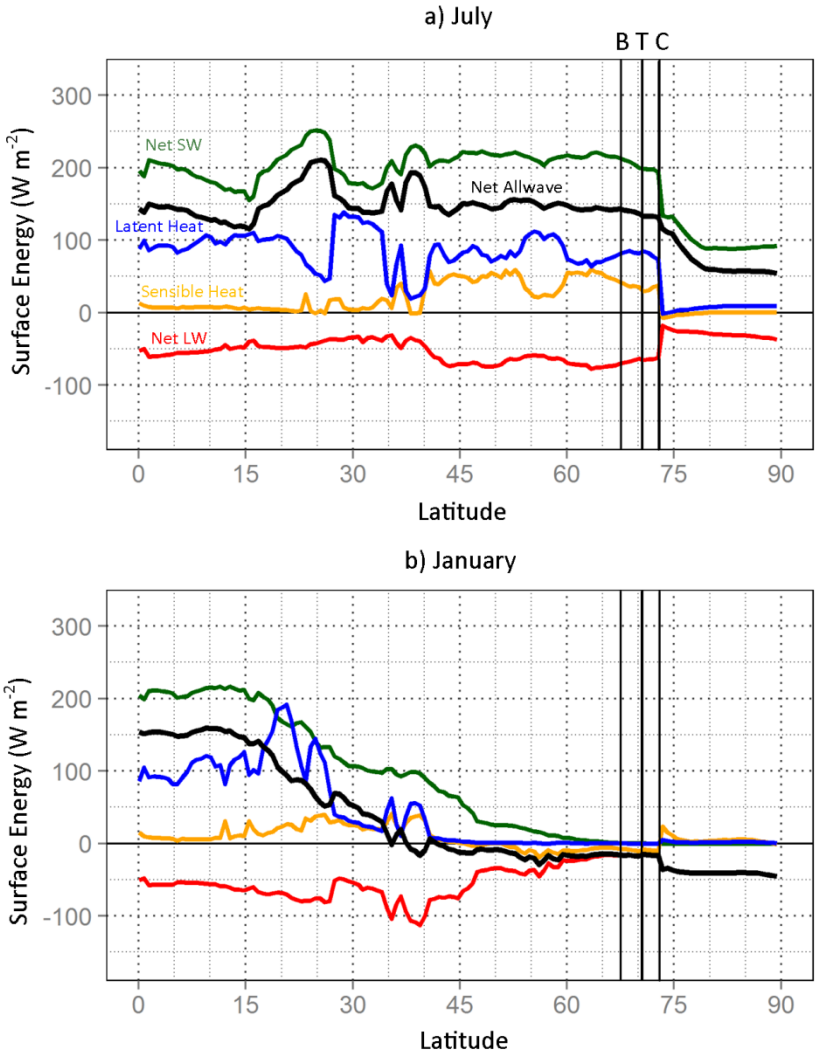

Figure 4: Latitudinal cross sections of mean surface energy balance components along 120°E in a) July and b) January for the period 1979-2012. Radiation fluxes are positive downwards and turbulent fluxes are positive upwards. The Siberian coastline (C), southern boundary of the tundra (T), and northern boundary of the boreal forest (B) are also marked. Data from MERRA.

Unlike across the coastline, no pronounced changes in the surface energy balance are seen across the forest-tundra ecotone. Some decline in the magnitude of net shortwave radiation, net longwave radiation, and the sensible heat flux is observable when travelling from the boreal forest to the tundra, but the differences in these fluxes between the two vegetation cover types are less than the differences they exhibit between land and ocean. Furthermore, because the boundary between forest and tundra is so diffuse, any energy differences associated with the two sides of that boundary are seen as gradual transitions. The coastline, on the other hand, is a sharp and clearly defined boundary, so the energy differences associated with the coastline are similarly stark. Therefore, the resulting temperature gradients are substantially stronger across the coastline than across the ecotone.

Although net shortwave radiation is at or near zero during January and net radiation is negative, sharp shifts still exist in both the net longwave and sensible heat fluxes along the coastal boundary (Figure 4b). Upward heat fluxes are greater from the ocean because the ocean stored substantially more heat during summer and now releases it, especially by areas of open water and thin sea ice. The difference in energy fluxes is manifested as temperature gradients with reversed direction (higher temperatures to the north) compared to the summer AFZ (Figure 4a). By contrast, temperatures across the winter sea ice edge in the Atlantic sector of the Arctic are lower to the north, in the same manner as for the summer AFZ.

3.3. Vertical Structure of the AFZ

Figure 5 shows latitudinal cross sections of the average July meridional temperature gradients from MERRA at a) 120°E, b) 80°W, and c) 154°W. These longitudes were chosen to illustrate regional differences in the expression of the AFZ. Vertical cross sections at the same

longitudes from CFSR and ERA-Interim (not shown) are very similar to those from MERRA, although CFSR shows a greater range of temperature gradient strengths and wind velocities. ERA-Interim results are virtually indistinguishable from MERRA except that the archived fields from MERRA have topography masked out. At both 154°W and 120°E, the zone of strongest temperature gradients (> 5.0 K/100 km) occurs near the surface at the Arctic Ocean coastline. At 154°W, the boreal forest-tundra ecotone lies a few degrees south of this narrow zone. The distinction is subtler at 120°E, where both the coastline and ecotone lie within the zone. However, whereas temperature gradients associated with the coast (73.0°N) exceed -0.4 K/100 km up to almost 400 hPa, temperature gradients associated with the ecotone (70.6°N) fall below that magnitude above the 800 hPa level.

A remarkable characteristic of the summer AFZ is its large horizontal scale. It extends laterally, with varying strength, for thousands of kilometers from the Kola Peninsula (41°E), along the Siberian Coast, across to Alaska, and over to the Canadian Arctic Archipelago (126°W; Figure 2). Furthermore, the roughly zonal orientation of this entire stretch of coastline results in temperature gradients that have predominantly the same orientation as the basic latitudinal (equator to pole) temperature gradient. The presence of strong meridional temperature gradients through such a deep layer of the atmosphere along such a vast zonal expanse is sufficient to produce a zonal jet-like feature at the tropopause, north of and distinct from the polar front jet (Figures 5d and f). This jet-like feature was also noted by Reed and Kunkel (1960) and Serreze et al. (2001).

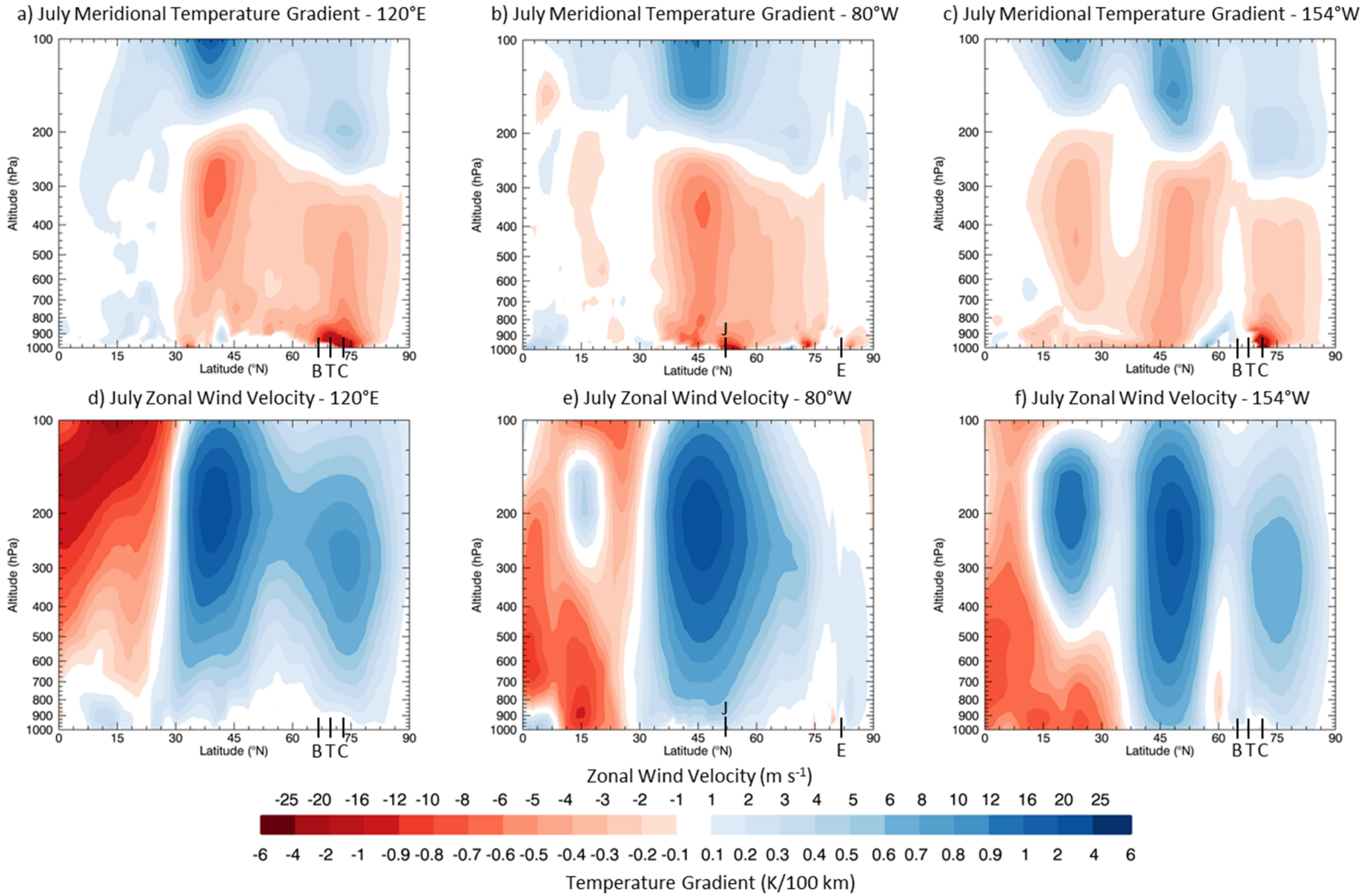

Figure 5: Latitudinal cross sections of mean July meridional temperature gradient (a-c) and zonal wind velocity (d-f), averaged for the period 1979-2012 from MERRA. Cross sections are along longitudes 120°E (a and d), 80°W (b and e) and 154°W (c and f). Also marked are the Arctic Ocean coastline (C), the southern boundary of tundra (T), the northern boundary of boreal forest (B), the northern shore of Ellesmere Island (E), and the southern coast of James Bay (J).

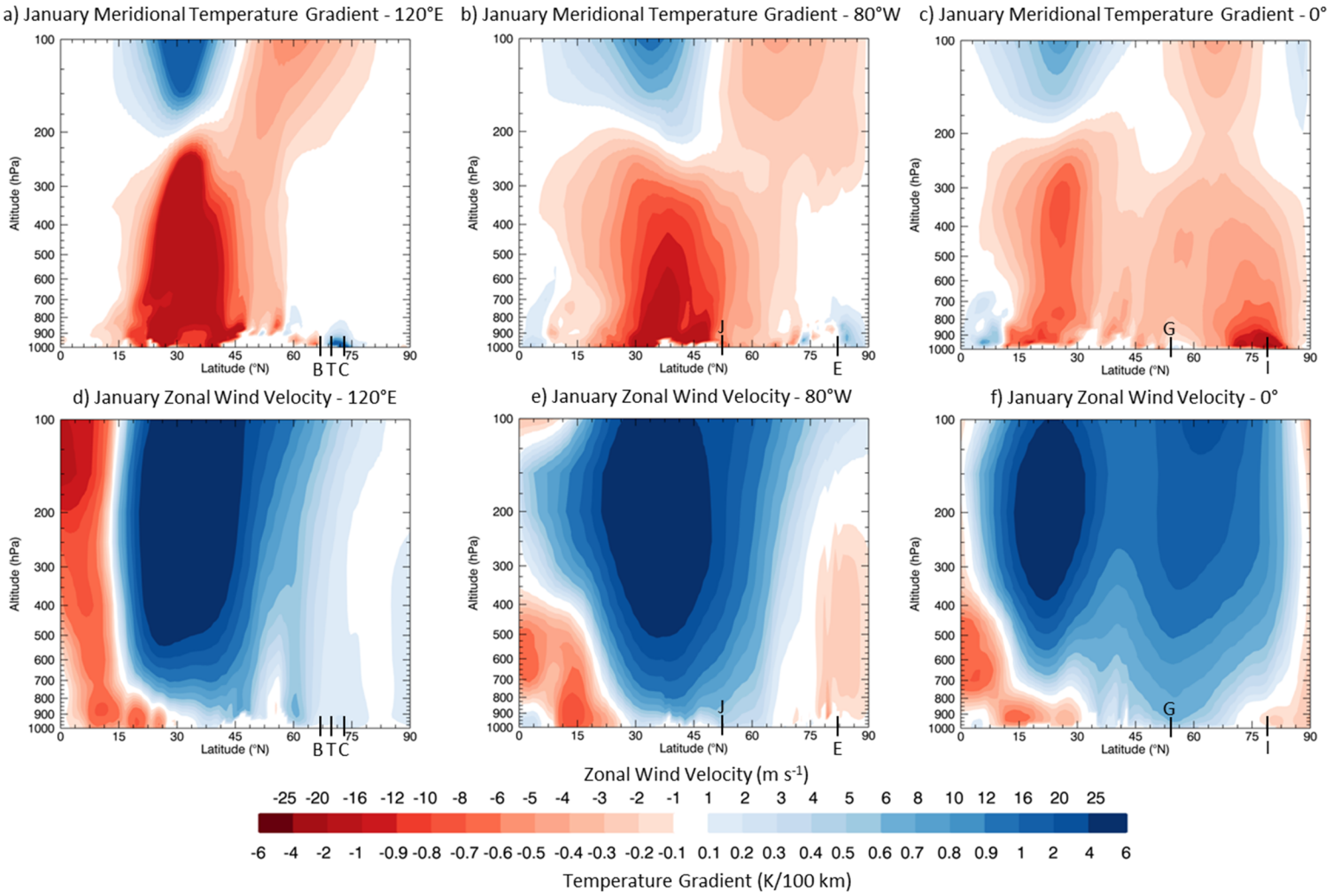

Figure 6: Latitudinal cross sections of mean January meridional temperature gradient (a-c) and zonal wind velocity (d-f), averaged for the period 1979-2012 from MERRA. Cross sections are along longitudes 120°E (a and d), 0° (b and e) and 154°W (c and f). Also marked are the Siberian coastline (C), the southern tundra boundary (T), the northern boreal forest boundary (B), the mean January sea ice edge in the Norwegian Sea (I), and the island of Great Britain (G).

Strong temperature gradients in July are also associated with the shores of the Great Lakes, James Bay, and the Canadian Arctic Archipelago along 80°W (Figure 5b), but like gradients along the boreal forest-tundra ecotone, these do not impact the atmosphere substantially above 800 hPa. Comparisons between the cross sections of zonal wind velocity at 120°E and 154°W (Figures 5d and f) and at 80°W (Figure 5e) demonstrate the close association of the Arctic jet with the AFZ. Along 120°E, the coast, the zone of strong temperature gradients, and the Arctic jet are each located at 73°N. Along 154°W, these features exist at 71°N. Since their positions are apparently less variable throughout July at 154°W, the polar jet (47°N) and sub-tropical jet (22°N) are also distinguishable at this longitude, revealing a three-jet structure in July. The strong Arctic temperature gradients exhibited at 80°W (Figure 5b) have neither the zonal breadth nor the vertical depth to produce a jet-like feature aloft and only one jet is evident at 45°N (Figure 5e).

Arctic jet-like features are also restricted to strong horizontal temperature gradients whose orientation enhances the basic latitudinal temperature gradient. For instance, the Hudson Bay Lowlands in Manitoba are similar to the AFZ since both regions experience a contrast of snow-free land with lingering sea ice in summer (Rouse 1991). In both cases, substantial surface temperature gradients develop, but along the Manitoba coast these gradients are predominantly zonal in nature. These Hudson Bay gradients do not reinforce the basic latitudinal temperature gradient, so they are weaker than gradients found, for example, along the Beaufort Sea coast (Rouse 1991). Additionally, no jet-like feature is produced along the coast of Hudson Bay. Cross sections of meridional temperature gradients and zonal winds at 95°W look very similar to those at 80°W (Figures 5b and 5e).

In contrast to July, strong near-surface temperature gradients in January (**Figure 6**) along the coast at 120°E are positive (temperatures increasing to the north). A positive meridional temperature gradient works against the basic latitudinal temperature gradient, resulting in a neutral wind regime aloft (Figures 6a and 6d). Meridional temperature gradients are also positive throughout much of the Canadian Arctic Archipelago (e.g. at 80°W; Figures 6b and 6e), and like at 120°E, 80°W shows no jet-like feature at Arctic latitudes in winter. In other words, the AFZ is only distinct from other high latitude land-sea contrasts during summer.

At 0° longitude, the strong, deep gradients in winter lie along the sea ice edge in the North Atlantic Ocean (Figure 6c). This strong and deep baroclinicity is associated with winter cyclone formation and deepening (Tsukernik et al. 2007; Bader et al. 2011). In this manner, the winter sea ice edge and the summer coastline are roughly analogous. Both are zones of high baroclinicity produced by surface contrasts that enhance the basic latitudinal temperature gradient and both are associated with cyclogenesis. However, no separate high latitude winter jet exists at this longitude (Figure 6f), which presumably reflects the effects of the ice edge being masked by large variability in the position of the polar front jet in this region.

4. SPATIAL VARIABILITY OF THE SUMMER AFZ

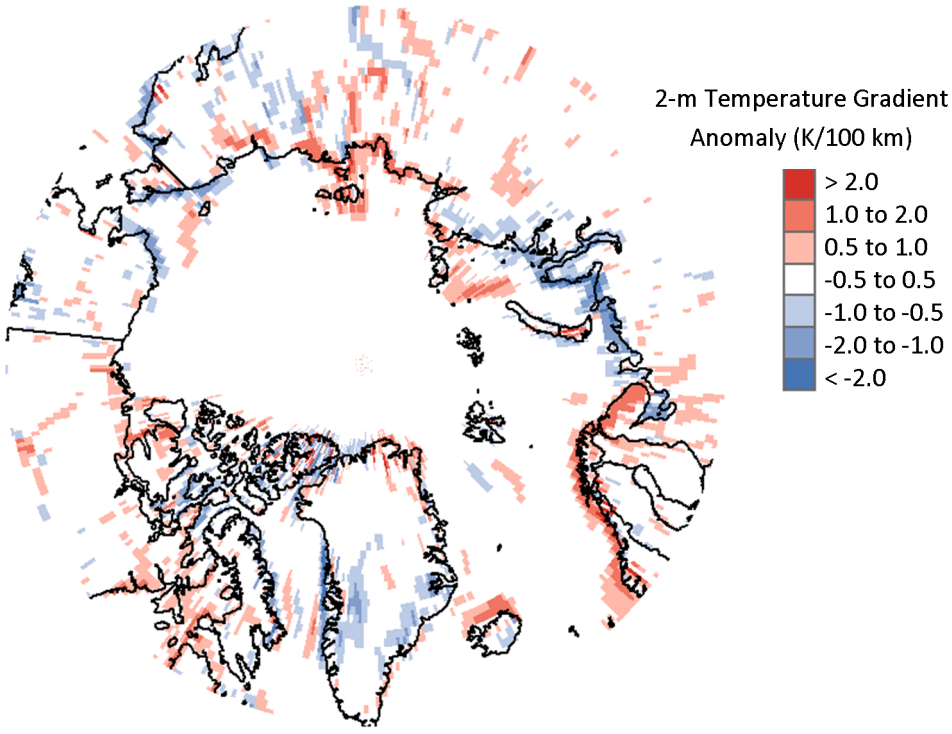

Figure 7: Anomaly of July 2-m temperature gradient magnitude in 1997 calculated with respect to 1979-2012 averages (from MERRA).

To help illustrate both the spatial and temporal variability of AFZ strength, **Figure 7** shows the 1997 anomaly of the July horizontal 2-m temperature gradient magnitude with respect to the 1979-2012 average. Like most years, 1997 exhibits substantial spatial heterogeneity in the anomaly of AFZ strength. Gradients are weaker than average bordering much of the Barents, Kara, and Chukchi Seas but are stronger than average bordering the Laptev Sea. This heterogeneous behavior argues against treating the summer AFZ as a single unit when measuring variation in strength. For this reason, a cluster analysis was conducted to identify the natural summer AFZ regions, or “sectors”, based on year-to-year variations in

strength. No standard method of clustering appears to exist in climatology research, so the methods used to define these clusters will be described in detail.

4.1. Cluster Analysis Methods

Since the summer AFZ is associated with the coast (see Section 3), AFZ "points" were defined as the average longitude and latitude of the Arctic Ocean coastline (from IBCAO) within each longitudinal band of the reanalysis data from 41°E eastward to 126°W, excluding the Bering Strait. (These are the longitudes at which the summer AFZ is present.) AFZ strength was measured using the mean of the 2-m temperature gradient magnitude from the two reanalysis grid cells with the closest latitude and longitude to each AFZ point.

Clustering was conducted separately for each reanalysis. For ERA-Interim and MERRA, the monthly July anomaly of AFZ strength for each year from the 1979-2012 average was used as one of the 34 dimensions of the cluster analysis. CFSR was treated the same way except that only 31 dimensions were used (one for each year in the range 1979-2009).

Three different clustering methods were used: a centroid method (k-means), and two hierarchical methods (average linkages and Ward's minimum variance method). Although using different processes, all three methods attempt to assign clusters so that each observation is more similar to members of its own cluster than it is to members of other clusters. In this case, the AFZ strength at locations that are part of the same sector will be stronger than normal in the same year and weaker than normal in the same year, but no (or only weak) correlation exists for locations that are part of different sectors.

Centroid clustering uses an iterative process to minimize the Euclidean distance between the centroid of a cluster and each of its members in n-dimensional space (34 or 31

dimensions, depending on the reanalysis). More specifically, the k-means process used for this study involves five steps:

1) A set of k unique cluster centroids is randomly distributed throughout n-dimensional space.
2) Each point in n-dimensional space (each point along the AFZ) is assigned to the closest centroid based on Euclidean distance, which results in k clusters.
3) For each cluster, the mean position of the members is calculated.
4) The cluster centroids are moved to match the calculated mean.
5) Steps 2) through 4) are repeated until the centroids no longer move or for 100 iterations, whichever occurs first.

This iterative process minimizes the sum of the squared distance between the mean of each cluster and each member. The ideal number of clusters (k) was determined by running a k-means for all values of k from 2 to 20 and then calculating the average silhouette width for each result. The silhouette width for a cluster is the difference between "within similarity" (the average similarity between each pair of elements in that cluster) and "cross similarity" (the average similarity between each pair of elements in that cluster and its most similar cluster). Average silhouette width is the average for all clusters in a result. Thus, higher average silhouette width results from high similarity within a cluster and low similarity across clusters. For each reanalysis, the k-means solution with the highest average silhouette width was selected for further consideration.

Linkages clustering methods entail sequentially combining clusters based on similarity. More specifically, the steps are:

1) Initially, each point is assigned to its own single-member cluster.
2) An n by n similarity matrix is calculated for all clusters.
3) The two clusters that are most similar are combined to make a larger cluster.
4) Steps 2) and 3) are repeated, sequentially reducing the number of clusters until only one cluster containing all points remains.

Several flavors of linkages clustering methods exist because there are several ways to determine which two clusters are "most similar". The similarity of clusters can be compared using their most similar members (single-link), their least similar members (complete-link), or the average of all links between members in each cluster (average-link). Single-linkage tends to result in clusters with low in-cluster similarity, which may not be physically meaningful. Complete-linkage results in tighter clusters, reducing the chance of finding statistical illusions that are not physically meaningful, but it is also very sensitive to outliers. Average-linkages represents a compromise that alleviates but does not eliminate those two concerns.

Ward's method follows the same logic as the linkage methods, except it combines clusters based on which combination will result in the largest R^2 value for the entire dataset. This R^2 value is calculated as the difference between the total sum squares (TSS) for the dataset and the residual sum of squares (RSS) not explained by the clustering assignments. This difference is then divided by TSS to yield R^2. TSS is a constant value for each dataset, being the sum of the squared distances between each point and the overall mean of the dataset. RSS changes depending on the cluster assignments. It is the sum of the squared distances between each point and its cluster mean. RSS increases as the number of clusters decreases because each cluster is forced to encompass greater variation, but at each step in the process, the

combination that minimizes the increase in RSS will also maximize the R^2 value for that particular step.

All three of these methods are commonly used in climatology research (Kalkstein et al. 1987). However, a researcher's preference for one method over the others varies depending on the data and the application (e.g. Gong and Richman 1995; Bunkers et al. 1996; Shahgedanova et al. 1998; Unal et al. 2003). A potential benefit of hierarchical methods is that they are deterministic and reproducible; repeated iterations of the same process will always yield the same result. Centroid methods may yield different results depending on the initial conditions. This issue was addressed by performing 100 iterations of each k-means clustering process and selecting the best result from those iterations. A potential benefit of centroid methods is that they are less computationally heavy, but the reanalysis datasets only contains hundreds of points in the AFZ, so this is not a concern.

With no clear and objective reasoning to choose one method over the others, all three methods were employed and compared. Since the number of clusters for hierarchical cases is always somewhat subjective (or else pre-determined), the number of clusters for the hierarchical cases was chosen to match the k-means case. This allowed for more direct comparison of how the different methods sectorialized the summer AFZ.

4.2. Sectors of the Summer AFZ

The clustering process resulted in nine different solutions (three reanalyses, each secotrialized using three methods). A final decision on the best solution was made using additional criteria. First, points belonging to the same sector had to be contiguous. Spatial information was purposefully omitted from the clustering analyses so that only naturally

occurring sectors would be identified. Second, physical justification had to be present for sector boundaries (e.g. abrupt changes in topography or coastline orientation). Third, results had to be reproducible using each reanalysis.

The sectors shown in Figure 1 are derived from a compromise amongst ideal solutions from the three clustering methods and three reanalyses. Of the three methods, average-linkages was clearly the worst, grouping the vast majority of points into a single cluster. K-means and Ward's method produced reasonable numbers of similarly populated clusters. The tendency of Ward's method to produce clusters of roughly equal size was previously observed by Kalkstein et al. (1987) and Shahgedanova et al. (1998). However, the centroid methods in these same studies created many single-member clusters and one large cluster comprising most of the observations. For the AFZ data, this type of result was restricted to average linkages. These disparate results emphasize how no single clustering method is appropriate for all applications.

Greater confidence was given to the Ward's method and k-means solutions because each produced contiguous clusters with logical boundaries that match abrupt changes in topography or coastline orientation for all three reanalyses. Based on average-silhouette width, the ideal k-means solution includes six clusters in MERRA, seven in CFSR, and nine in ERA-Interim. The three Ward's method solutions of the same size for each reanalysis show close agreement, making six total reasonable solutions. Although neither the CFSR nor the MERRA solutions show as many clusters as for ERA-Interim, all of the geographical cluster boundaries in the CFSR and MERRA solutions are within one grid cell of the boundaries from the ERA-Interim Ward's method solution. Differences in spatial resolution also cause a few grid cells to straddle

cluster boundaries. Therefore, the compromise solution presented in Figure 1 identifies sectors using the boundaries of the ERA-Interim Ward's method with one caveat: The few grid cells that could not be definitely assigned to one sector were omitted from subsequent analysis. This solution represents a balance of statistical metrics of similarity, variation amongst the reanalyses, and physical justifications for making divisions.

Table 1: Description of AFZ Sectors Based on Cluster Analysis

Sector	Range (Longitude)	Length (km)	Land Side	Ocean Side	Eastern Boundary
1	41°E - 67°E	1545	European Russia	Barents Sea	Baydaratskaya Bay & Ural Mountains
2	67°E - 85.5°E	1006	Ob & Yenisei Estuaries	Kara Sea	Pyasina Bay
3	87°E - 114°E	1072	Taymyr Peninsula	Kara/Laptev Seas	Khatanga Bay
4	114°E - 129°E	612	Lena Delta	Olenekskiy Bay (Laptev Sea)	Verkhoyansk Range
5	130.5°E - 149°E	776	Kolyma Lowland	Laptev/East Siberian Seas	Ularyoskaya Bay
6	151°E - 168.5°E	692	Kolyma Lowland	East Siberian Sea	Chaunskaya Gulf
7	171°E - 171°W	1015	Chukotka	East Siberian/ Chukchi Seas	Bering Strait
8	166°W - 143°W	1057	Alaska	Chukchi/Beaufort Seas	Griffin Point
9	143°W - 126°W	761	Western Canada	Beaufort Sea	Banks Island

Geographical descriptions of each sector are provided in **Table 1**. Several of the geographic features mentioned are labeled in Figure 1. Using the compromise solution, Sector 1 encompasses the European Russia portion of the AFZ, extending from the Kola Peninsula (41°E) to Baydaratskaya Bay (67°E), where the Ural Mountains reach the coast of the Kara Sea. Most of its ocean portion lies within the Barents Sea. Sector 2 (67°E to 85.5°E) comprises the Kara Sea coastline between the Urals and the Taymyr Peninsula. The Ob River and Yensei River estuaries dominate this sector, and obscure the boundary between land and ocean. The Taymyr Peninsula is Sector 3 (87°E to 114°E). It extends across more degrees of latitude than any other

sector and reaches the furthest poleward. Sector 4 extends from Khatanga Bay (114°E) to the Verkhoyansk Range (129°E), which reaches the coast just east of the Lena River Delta. This area is bordered by Olenekskiy Bay, a part of the western Laptev Sea. The Kolyma Lowland is divided into Sectors 5 (130.5°E to 149°E) and 6 (151°E to 168.5°E). The division between these sectors is a kink in the coastline by Ularvoskaya Bay. Sector 7 comprises Chukotka, extending from Chaunskaya Gulf (171°E) to the Bering Strait (171°W). This is the only sector for which the landmass to the south extends for less than 1000 km. (It becomes as narrow as 200 km.) Sector 8 (166°W to 143°W) contains most of Alaska and is divided from Sector 9 at Griffin Point, which is not especially distinct except for being the same area where the highest points in the Brooks Range stand less than 100 km from the Beaufort Sea coast. In contrast, most of the Brooks Range is 200 to 300 km from the coast. Sector 9 extends from Point Griffin to Banks Island (126°W) and the Canadian Arctic Archipelago. The boundaries between Sectors 1-2, 3-4, 7-8, and 8-9 are universal to the clustering solutions from all three reanalyses.

4.3. Variability in Peak AFZ Strength by Sector

Division of the summer AFZ into sectors was conducted using the annual anomaly of July temperature gradients; however, these sectors also differ from each other in average temperature gradient strength. The box and whisker plots in **Figure 8** show the interannual variability of July 2-m temperature gradient magnitude by AFZ sector. In general, the summer AFZ is stronger in Siberia (Sectors 4-6) and North America (Sectors 8-9) and weaker along the Barents and Kara Seas (Sectors 1-3) and in Chukotka (Sector 7). Notably, the absolute strongest expression of the summer AFZ is in Sector 8, where the Brooks Range parallels the coast about 200 to 300 km inland. In addition to spatial variability by sector, July AFZ strength also

demonstrates substantial interannual variability. The range for each sector is at least 2 K/100 km. Excluding strong outliers, Sector 6 has the largest range at about 4 K/100 km, and in several sectors, the strongest observed July AFZ is twice the magnitude of the weakest. So although the AFZ is a consistent feature of the summer Arctic climate system, its peak monthly strength can vary substantially.

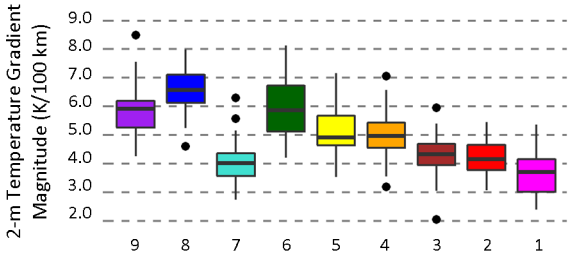

Figure 8: Interannual variability of July 2-m temperature gradient magnitude by AFZ sector for the period 1979-2012. The box contains the median and first and third quartiles, the whiskers extend to the most extreme values lying within 1.5 times the interquartile range, and the dots represent outliers. Data from MERRA.

4.4. Seasonal Development of the Summer AFZ

In addition to variability in its peak strength, the timing of AFZ development also varies across sectors. **Figure 9** shows the average meridional 2-m temperature gradient for each sector for all months. All sectors show the pattern of negative gradients in the summer (when air over land is warmer than air over ocean) and positive gradients in the winter (when air over land is colder). However, the summer regime is substantially shorter. Winter lasts from October through March or April (six or seven months), while summer lasts from May or June through August (three or four months). Summer temperature gradients are strongest in July for all sectors.

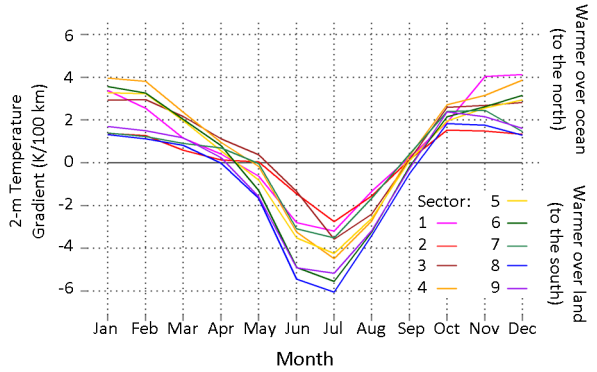

Figure 9: Seasonality of mean monthly meridional 2-m temperature gradient for the period 1979-2012 from MERRA. The color of each line corresponds to the sector colors in Figures 1 and 8.

Observing the nine lines on Figure 9 more closely, it becomes apparent that the timing of the transition from winter to summer regimes is highly variable by sector. April, May, and June may all be a month of transition, depending on the sector. In stark contrast, the transition from summer to winter is uniform across the entire AFZ. All sectors are clearly in a summer mode in August, neutral in September, and in a winter mode by October. This suggests that the processes giving rise to the summer AFZ are more spatially heterogeneous than the processes leading to its autumn decay.

Figure 9 provides a good snapshot of the overall seasonal cycle of 2-m temperature gradients, but the box plots in **Figure 10** and **Figure 11** better demonstrate the spatial variation in each month. The winter regime (Figure 10) begins in October, during which the median temperature gradient for each sector is between +1.0 and +3.0 K/100 km. Rarely in any sector is the gradient stronger than +4.0 K/100 km. Temperature gradient strength varies more by sector in subsequent months, depending on how much colder 2-m temperatures become over land in comparison to over the Arctic Ocean.

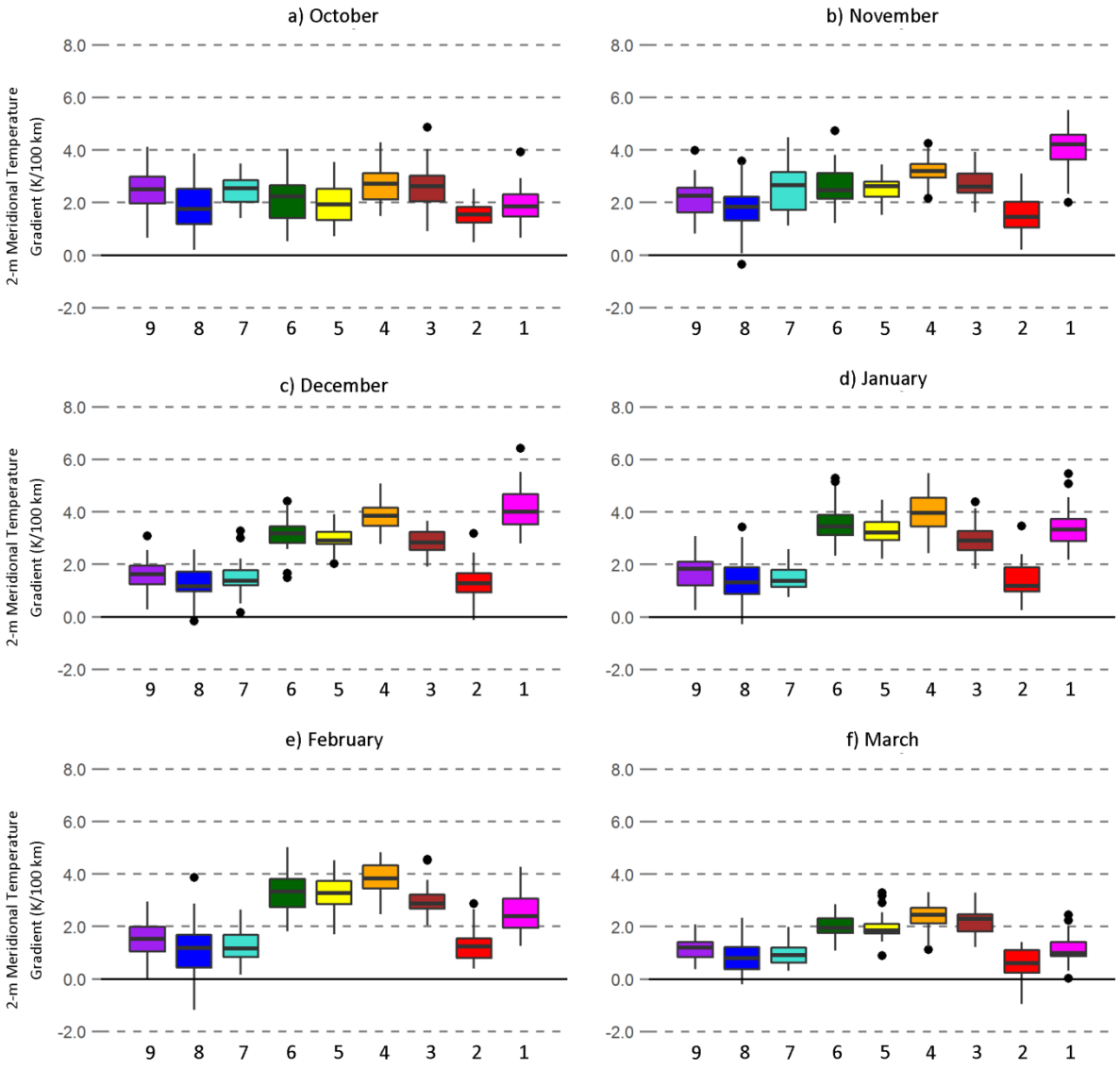

Figure 10: Interannual variability of monthly 2-m meridional temperature gradient by sector during winter for the period 1979-2012. Data from MERRA.

For instance, temperature gradients along the Beaufort Sea (Sectors 8 and 9) are typically strongest in October, and slowly decline throughout the winter. They can even turn slightly negative in Sector 8 in any month. On the other hand, the Barents Sea coast (Sector 1) experiences peak winter temperature gradients in November and December. The later peak for Sector 1 seems to occur because coastal Barents Sea waters retain their warmth for longer than the Beaufort Sea and prolong their ice-free period well into December. Meanwhile, snow cover

accumulates almost uniformly across all coastal land areas. The lingering of warmth in the coastal Barents Sea while land temperatures plummet enhances winter temperature gradients. This is evidence of the Gulf Stream's influence on the Barents Sea. The transport of warm water from the south prevents the Barents Sea from cooling as quickly as the other coastal seas.

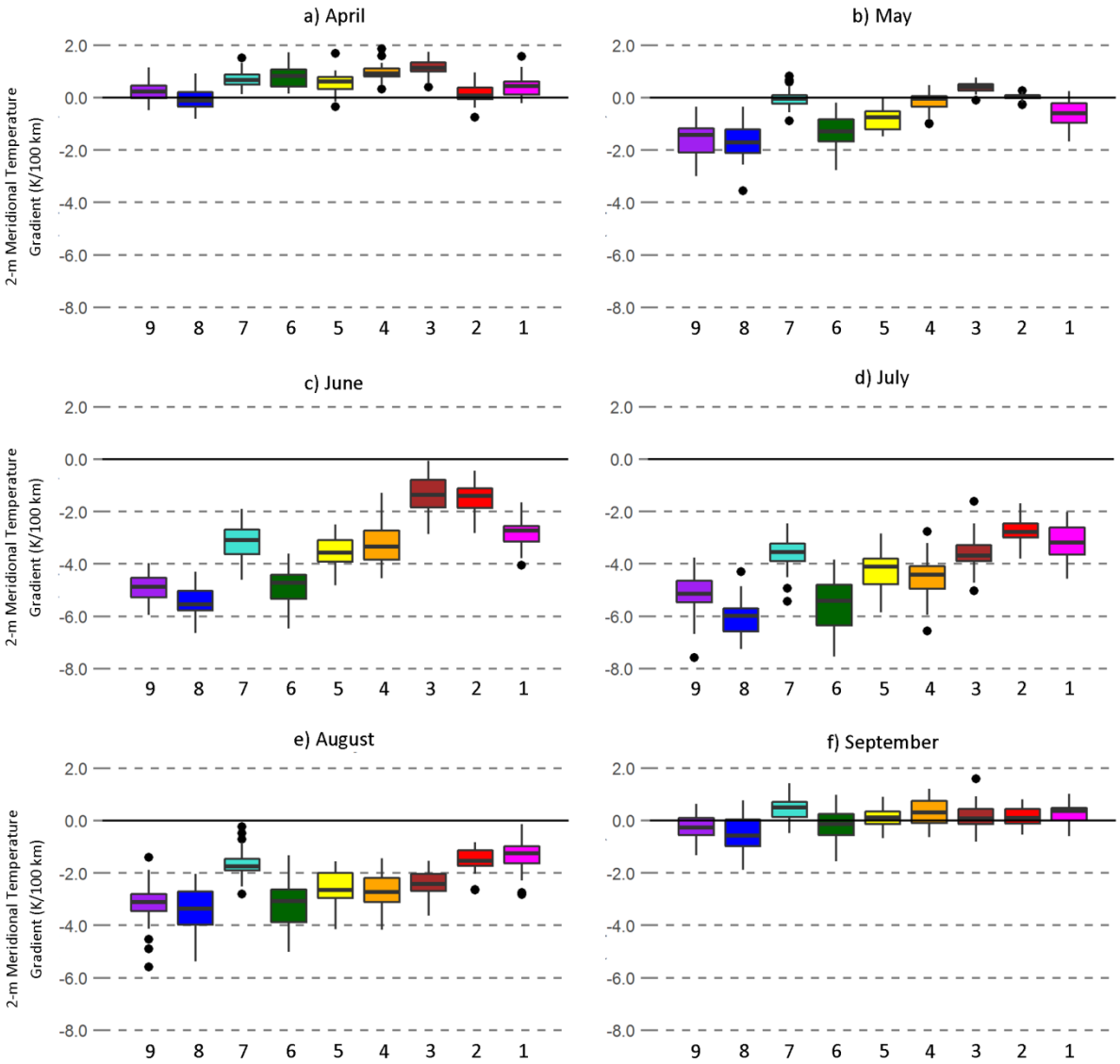

Figure 11: Interannual variability of monthly 2-m meridional temperature gradient by sector during summer for the period 1979-2012. Data from MERRA.

Siberia (Sectors 4-6), meanwhile, typically sees its strongest winter temperature gradients in December and January. Rather than being a signal of especially warm water, this instead most likely represents exceptionally cold land related to the seasonal Siberian High.

These sectorial differences can also be observed in cross sections of the energy balance at various longitudes. At 48°E (Sector 1; **Figure 12**), for instance, large upward latent and sensible heat fluxes over the Barents Sea contrast strongly with a neutral latent heat flux and downward sensible heat flux over European Russia in both October and January. The magnitude of these fluxes seems to relate to how much open water is present. A measurable upward latent flux from the Arctic Ocean exists in October at 90°E (Sector 3; **Figure 13**), 120°E (Sector 4; **Figure 14**) and 154°W (Sector 8; **Figure 15**), but this flux is notably absent in January. October follows the September sea ice minimum, so ample open water exists in coastal seas, but by January, sea ice cover has returned to most sectors. The relatively warm Barents Sea (Sector 1) is a key exception.

As the Arctic begins to warm in spring, 2-m meridional temperature gradients begin to shift from positive to negative (Figure 11). However, as observed in Figure 9, this transition occurs at different times for different sectors. At one extreme, Sectors 6, 8, and 9 all develop negative meridional temperature gradients in May and are usually stronger than -4.0 K/100 km in both June and July. At the other extreme, Sectors 2 and 3 do not become negative until June, when they average weaker than -2.0 K/100 km. They rarely exceed -4.0 K/100 km, and only ever in July.

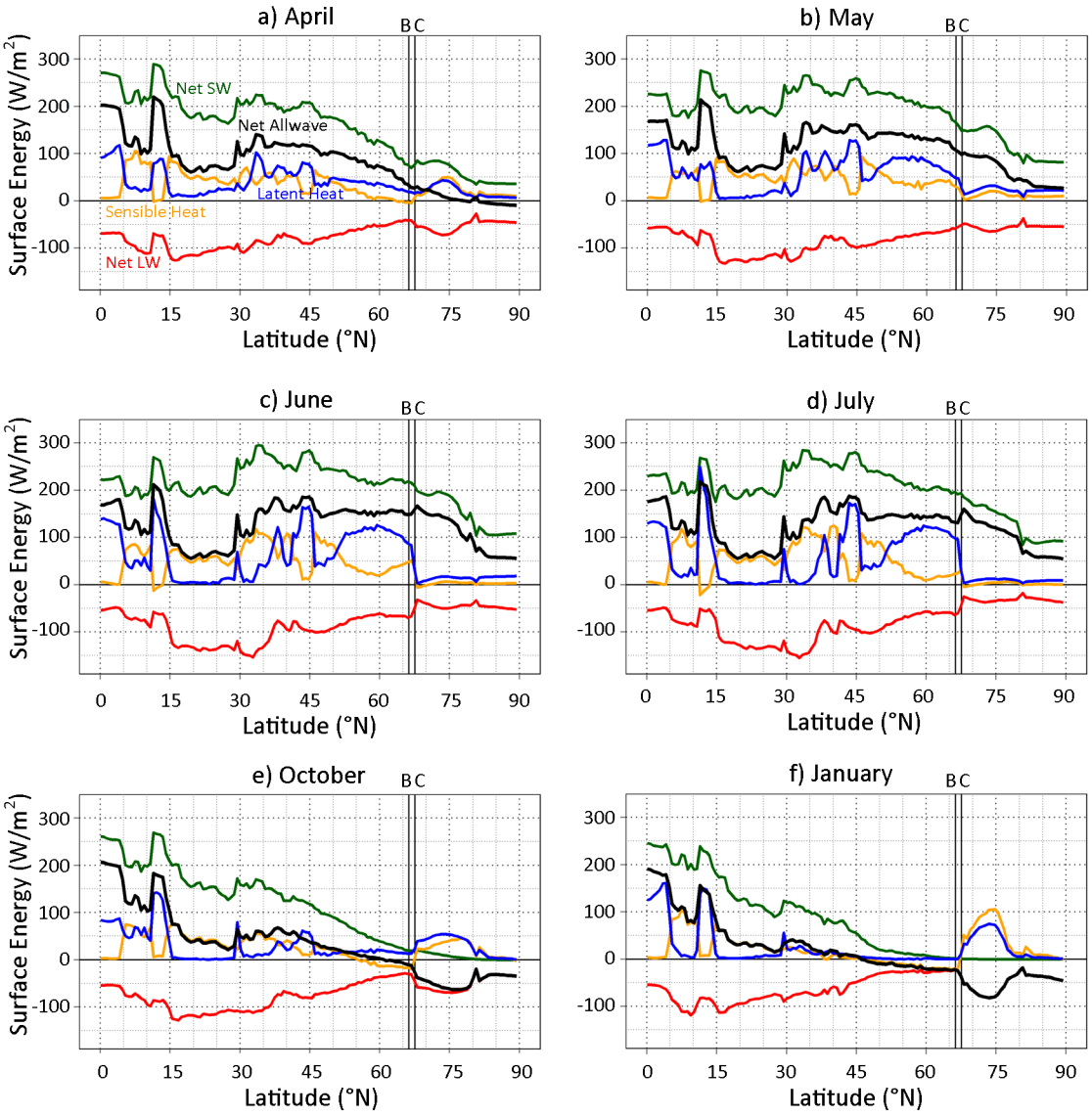

Figure 12: Latitudinal cross sections of mean surface energy balance components along 48°E in a) April, b) May, c) June, d) July, e) October, and f) January for the period 1979-2012. Radiation fluxes are positive downwards and turbulent fluxes are positive upwards. The Russian coastline (C) and northern boundary of the boreal forest (B) are also marked. Data from MERRA.

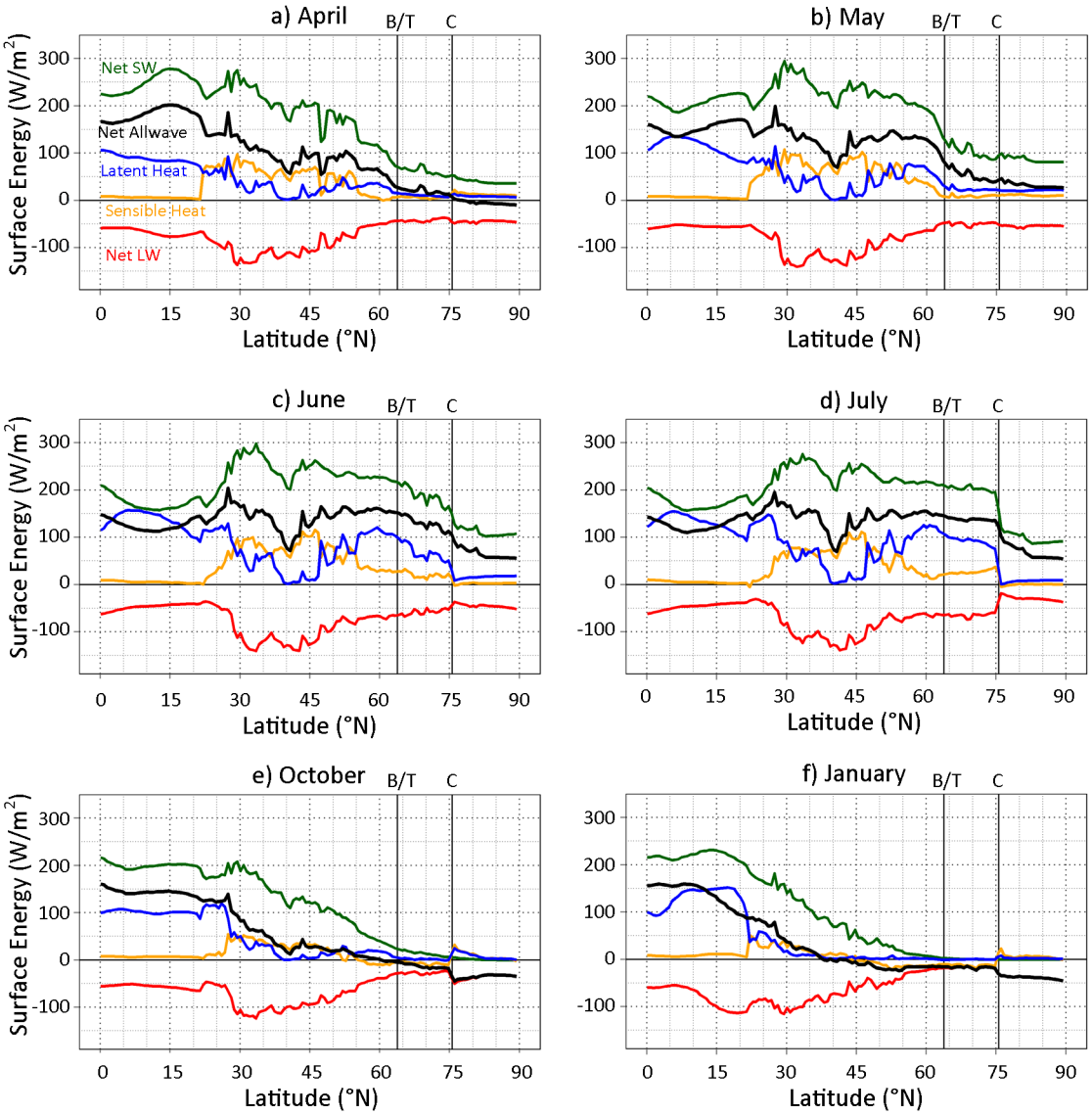

Figure 13: Latitudinal cross sections of mean surface energy balance components along 90°E in a) April, b) May, c) June, d) July, e) October, and f) January for the period 1979-2012. Radiation fluxes are positive downwards and turbulent fluxes are positive upwards. The Siberian coastline (C), southern boundary of the tundra (T), and northern boundary of the boreal forest (B) are also marked. Data from MERRA.

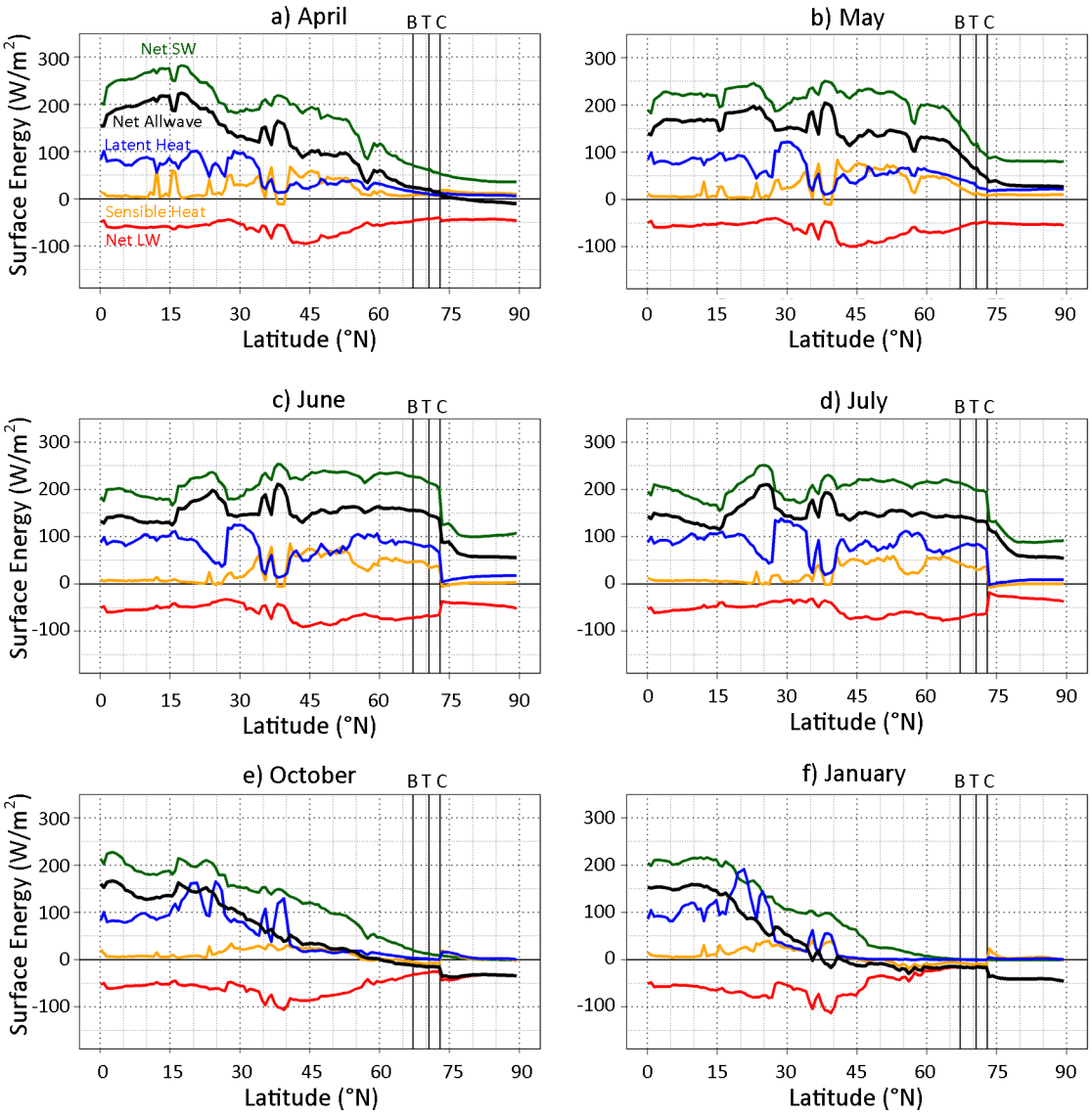

Figure 14: Latitudinal cross sections of mean surface energy balance components along 120°E in a) April, b) May, c) June, d) July, e) October, and f) January for the period 1979-2012. Radiation fluxes are positive downwards and turbulent fluxes are positive upwards. The Siberian coastline (C), southern boundary of the tundra (T), and northern boundary of the boreal forest (B) are also marked. Data from MERRA.

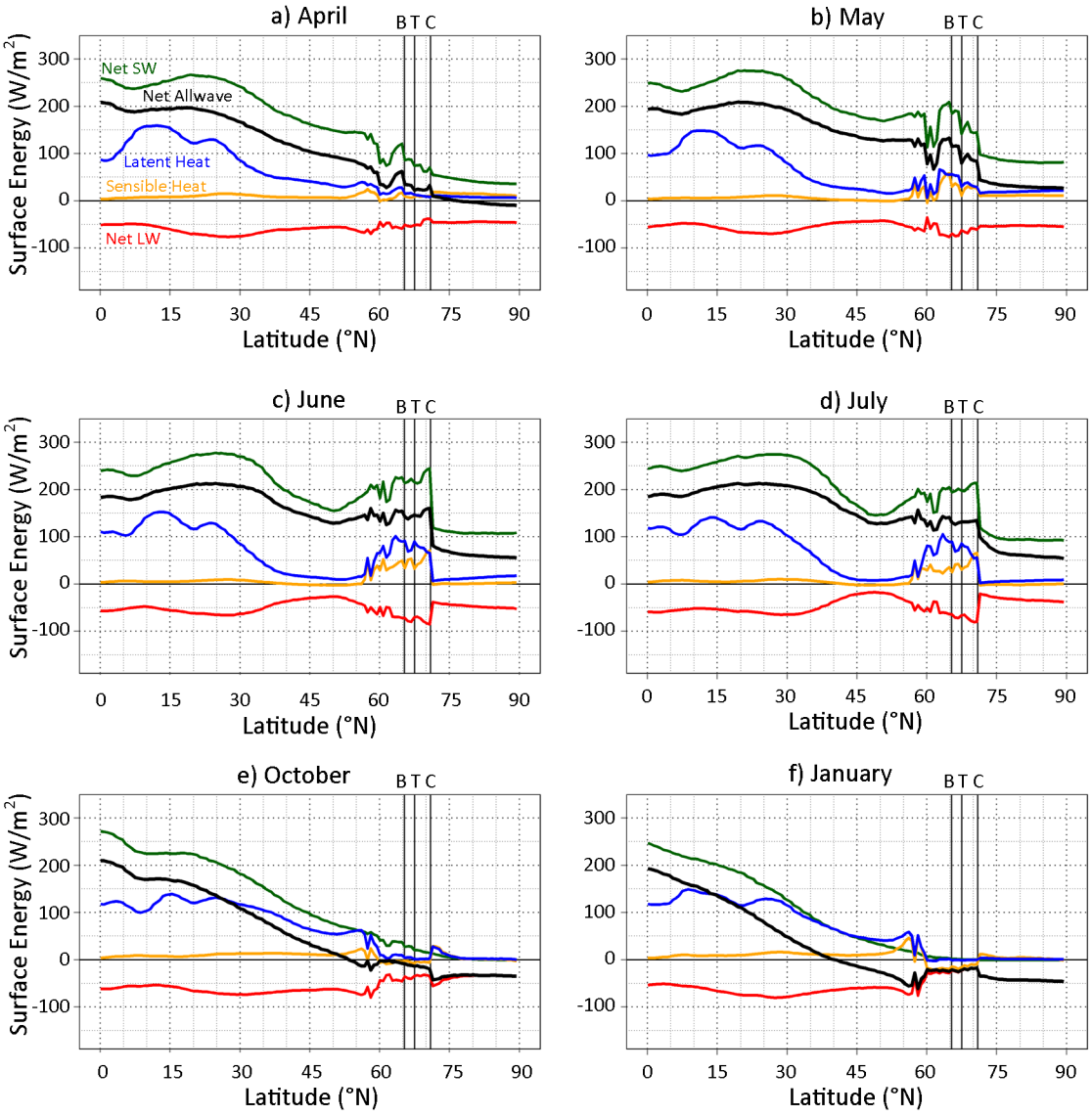

Figure 15: Latitudinal cross sections of mean surface energy balance components along 154°W in a) April, b) May, c) June, d) July, e) October, and f) January for the period 1979-2012. Radiation fluxes are positive downwards and turbulent fluxes are positive upwards. The Alaskan coastline (C), southern boundary of the tundra (T), and northern boundary of the boreal forest (B) are also marked. Data from MERRA.

As in winter, snow cover and sea ice concentration appear to be very important to these spatial differences. **Figure 16** compares box plots for each sector depicting a) July AFZ strength and b) the difference in timing of seasonal sea ice retreat and snow cover retreat. Retreat is measured as "retreat day", or the day on which the percent coverage of sea ice or snow cover

falls below 60% in the area within 250 km of the coast. (See Section 5.1 for a more detailed explanation of methods.)

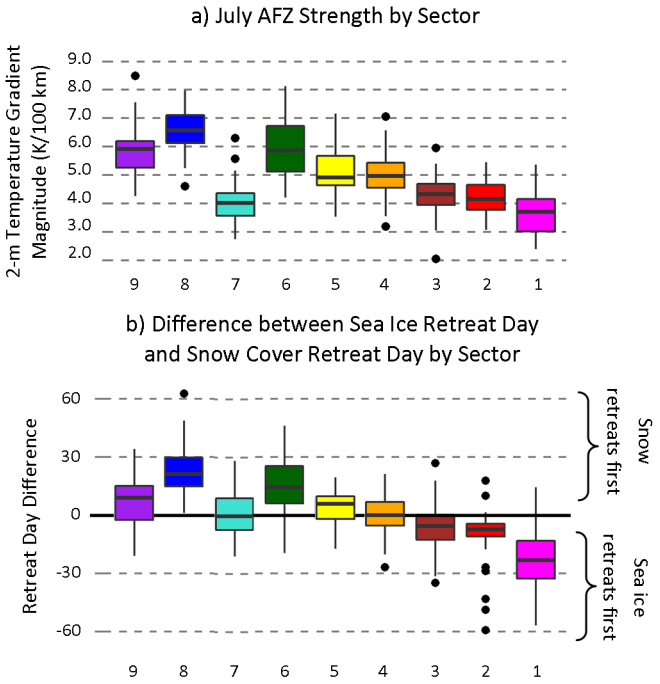

Figure 16: Interannual variability of a) July 2-m temperature gradient magnitude and b) the difference between sea ice and snow cover retreat days by AFZ sector for the period 1979-2011. Positive differences indicate that snow cover fell below 60% within 250 km of the coastline before sea ice concentration. The box contains the median and first and third quartiles, the whiskers extend to the most extreme values lying within 1.5 times the interquartile range, and the dots represent outliers.

In Figure 16b, positive values indicate that snow cover retreat occurs before sea ice retreat, and negative values indicate that sea ice retreats first. This metric exhibits substantial year-to-year variations, but a signal is observable through the noise. The three sectors that develop a summer AFZ in May and become strong in June are the same three sectors with the most positive mean values for retreat day difference (Figure 16b). Of these three, the strongest peak strength is found in Sector 8 (Alaska), where the snow cover retreat day occurs on average three weeks before the sea ice retreat day. Both snow and sea ice are highly reflective,

increasing surface albedo and decreasing the net shortwave radiation flux in sunlit months. The more quickly snow or sea ice retreats, the more quickly the underlying surface can transfer energy into the lower atmosphere. Since the summer AFZ involves higher air temperatures over land and lower air temperatures over the ocean, it will be enhanced if snow cover retreats more quickly than sea ice. In Alaska, it is as if the air overlying land has a three-week head start against the air overlying water. And since air overlying land already heats up more quickly than air overlying water, this head start encourages especially rapid development of the summer AFZ, which in turn allows the summer AFZ to become especially strong by the time it reaches its peak strength in July.

Sectors 4, 5, and 7 show slower summer AFZ development (Figure 11). In these sectors, snow cover and sea ice retreat at about the same time (Figure 16). Air overlying land receives no head start, so the summer AFZ does not develop quite as rapidly and its peak strength is not quite as strong as in Sectors 6, 8, and 9.

Sectors 1 and 2 are the southernmost sectors (Figure 1), and their coastal waters are influenced by the Gulf Stream. In fact, although its coastal waters experience sea ice in winter, the majority of the Barents Sea typically remains below 60% sea ice concentration all year. Sea ice retreat tends to occur before snow cover retreat in these sectors, especially in Sector 1 (Figure 16). Whereas especially warm waters mean strong temperature gradients in winter for Sector 1, they mean just the opposite in summer. Accordingly, these two sectors demonstrate the weakest peak summer temperature gradients in the AFZ (Figure 11).

Sector 2 is also affected by two large estuaries of the Ob and Yenisei Rivers (Figure 1). These estuaries disrupt the land-sea boundary, making the distinction between continent and

ocean less clear. As a result, the physical processes that differentiate land and ocean surfaces are not as neatly segregated as in other sectors and the temperature gradients are muted in both seasons. The Ob River estuary is the longest in the world, making this issue especially problematic. The temperature gradients in Sector 2 are the closest to neutral or second closest to neutral in every month (Figure 10 and Figure 11).

As with winter, the spatial differences in summer AFZ strength can also be observed in the energy balance cross sections of Figure 4. Sector 4 (Figure 14) is the median case. In April, no distinct shift in any parameter can be observed along the coastline or the two vegetation boundaries. All fluxes become gradually weaker and approach zero between 65°N and 75°N. In May, this transition becomes steeper because all fluxes increase more rapidly in magnitude at lower latitudes than at higher latitudes. The difference in net shortwave radiation between 65°N and 75°N becomes especially acute, shifting from less than 50 W/m^2 to over 100 W/m^2. However, a truly narrow summer AFZ is not apparent until June. In this month, the transition zone is focused precisely at the coastline. The difference in net shortwave radiation between 27°N and 72°N (45° of latitude) is about 60 W/m^2; this is the same as the difference in net shortwave radiation between two grid cells (0.5° of latitude) at the coastline. Similarly sharp transitions at the coastline also occur for the net longwave, sensible heat, and latent heat fluxes. And as discussed in Section 3.2, these sharp transitions persist through July.

Longitude 154°W (Figure 15) is representative of the extremely strong summer AFZ in Sector 8. Unlike at 120°E, the coastline and the two vegetation boundaries are correlated with minor transitions in the various energy terms even in April. However, the more notable difference between these two longitudes occurs in May, when the summer AFZ is already

noticeable, especially in terms of energy gains at the surface from shortwave radiation. In June, the transfer of energy from the land surface to the lower atmosphere by radiative and turbulent fluxes is greatly increased, while the upward transfer of energy from the ocean surface remains about the same as in May. This represents the rapid strengthening of the AFZ in late spring as the snow cover retreats.

Notably, the boreal forest-tundra ecotone is also a significant boundary for energy balance terms in May at 154°W, but not in June. A difference in albedo is suggested by the net shortwave flux. According to Pielke and Vidale (1995), the latent heat flux has often been proposed as the balancing mechanism for the greater surplus of energy over the boreal forest. However, they instead propose the sensible heat flux as the chief mechanism in their study. The data presented here show notable differences in both turbulent heat fluxes between boreal forest and tundra, suggesting that both mechanisms are relevant. However, the differences in energy fluxes associated with the ecotone are small in comparison to the differences observed between land and ocean surfaces. Furthermore, the ecotone shows no definite change in energy terms in June and July, while the coastline witnesses further disparities between land and ocean and an especially strong AFZ.

The influence of a warmer ocean in Sector 1 is observable along 48°E (Figure 12). In May, although the latent and sensible heat fluxes are stronger over land than over the water immediately adjacent to the coast, a large area of open water in the Barents Sea has a moderating affect on the contrast. As land continues to warm and the summer regime becomes more dominant, this effect fades, and the latent heat flux in particular shows a strong land/sea

contrast, but the sensible heat flux contrast is small in comparison to the one observed at 154°W or even 120°E.

Omitted from the previous discussion was Sector 3, which comprises most of the Taymyr Peninsula. Sector 3 is the only sector still clearly in a winter mode in May (Figure 11). Looking at the energy terms (Figure 13), the turbulent fluxes are essentially unchanged across the coastline boundary, but the ocean surface still has a slightly more negative net longwave flux than the land surface. Sector 3 is the farthest north of any sector in the AFZ, and it has the islands of Severnaya Zemlya to help pin sea ice near the coast. Both snow cover and sea ice retreat typically occur later in Sector 3 than in other sectors, and the sea ice lingers especially long in comparison to Sectors 1 and 2. This helps keep the ocean surface (and by extension the near-surface air over the ocean) colder through summer in Sector 3 than in Sectors 1 and 2, which can be observed by comparing the net longwave radiation for July just north of the coastline in Figure 13 with that in Figure 12. For these reasons, Sector 3 is the last to transition to a summer regime, but when it does, it develops a summer AFZ more rapidly than Sectors 1 and 2 and experiences stronger temperatures gradients than both of them by July.

4.5. Seasonal Development of the Summer Arctic Jet

As discussed in section 3.3, the summer AFZ is accompanied by a seasonal Arctic jet. The seasonal development of this Arctic jet aloft follows a similar pattern to the development of meridional temperature gradients near the surface. Figures 17-20 show latitudinal cross sections of monthly zonal wind velocity along the same four longitudes used for the energy balance terms in Figures 12-15. **Figure 17** (48°E) represents areas where the summer AFZ is relatively weak (Sectors 1-2). **Figure 18** (90°E) represents Sector 3, which develops a summer

mode later than other sectors. The median case is represented by **Figure 19** (120°E), which lies in Sector 4. **Figure 20** (154°W) shows a cross section through Sector 8 and represents the strongest areas of the summer AFZ (especially Sectors 6, 8, and 9).

Only April through September are depicted in these figures. Monthly cross sections of October through March are well represented by the zonal winds in January at 120°E (Figure 6b). In these winter months, the strongest westerly winds are centered over about 30°N. The polar-night jet is evidenced at Arctic latitudes by a tendency for westerly winds to strengthen with height; especially evident in Sectors 6-9 (not shown). However, zonal winds in the lower atmosphere are weak and form no distinct jet-like feature at the tropopause. Recall from Section 3.3 that the positive meridional temperature gradients that exist near the surface at the Arctic coastline in winter work against the basic latitudinal temperature gradient and are not conducive to the development of a westerly jet-like feature aloft.

Comparing Figures 17-20 with Figure 11 shows the connection between the development of the summer AFZ and the development of an Arctic jet. In April, the area of winds between 8 and 15 m/s start extending slightly farther north, just as the meridional temperature gradients become neutral in most sectors. This behavior is most apparent at 154°W (Figure 20), which lies in the only sector for which mean April 2-m meridional temperature gradients are negative. The lingering effect of the polar-night jet is also evidenced in April, as the 8 m/s isopleth extends up beyond 100 hPa.

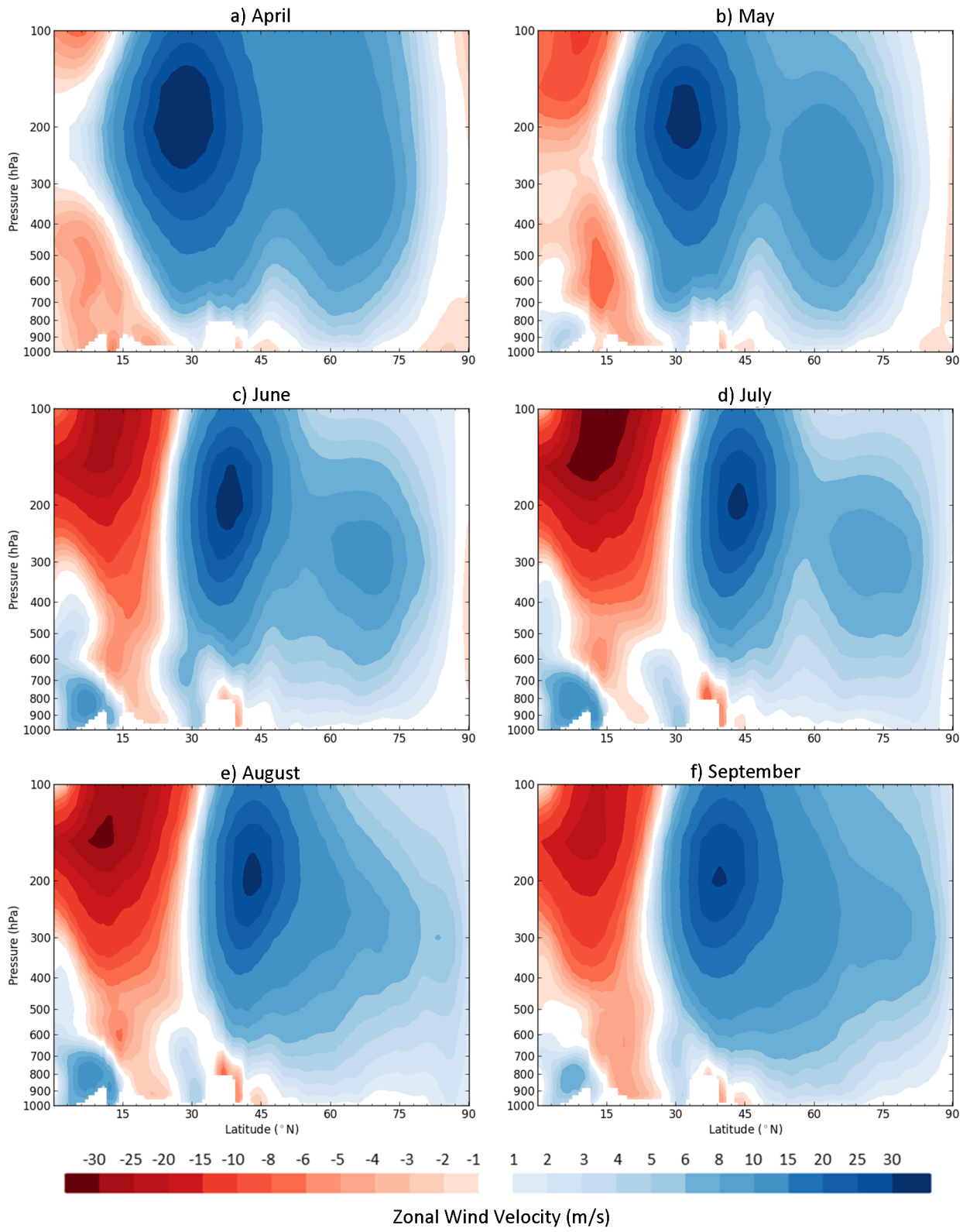

Figure 17: **Latitudinal cross sections of mean monthly zonal wind velocity for summer months along longitude 48°E**, averaged for the period 1979-2012 from MERRA.

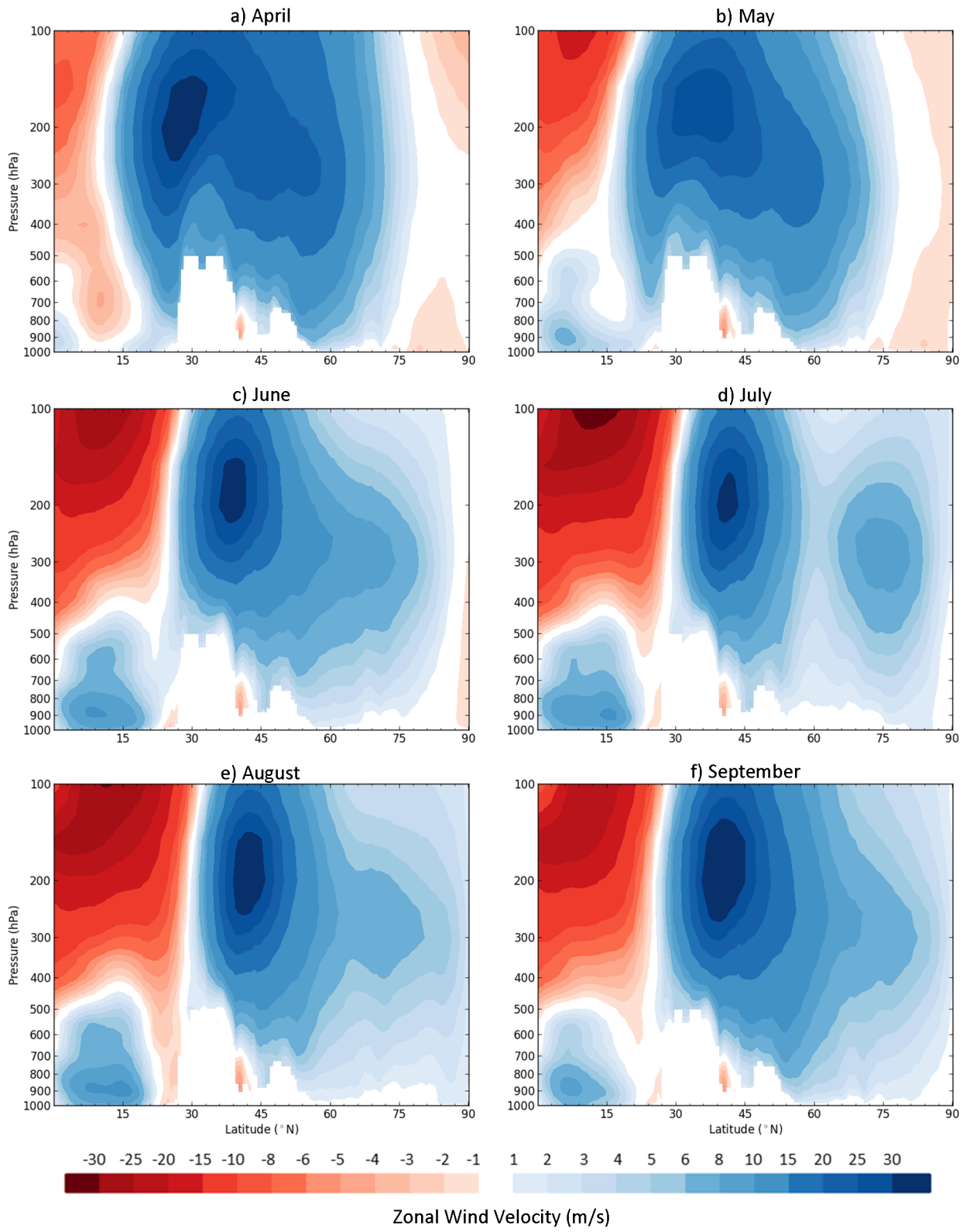

Figure 18: **Latitudinal cross sections of mean monthly zonal wind velocity for summer months along longitude 90°E**, averaged for the period 1979-2012 from MERRA.

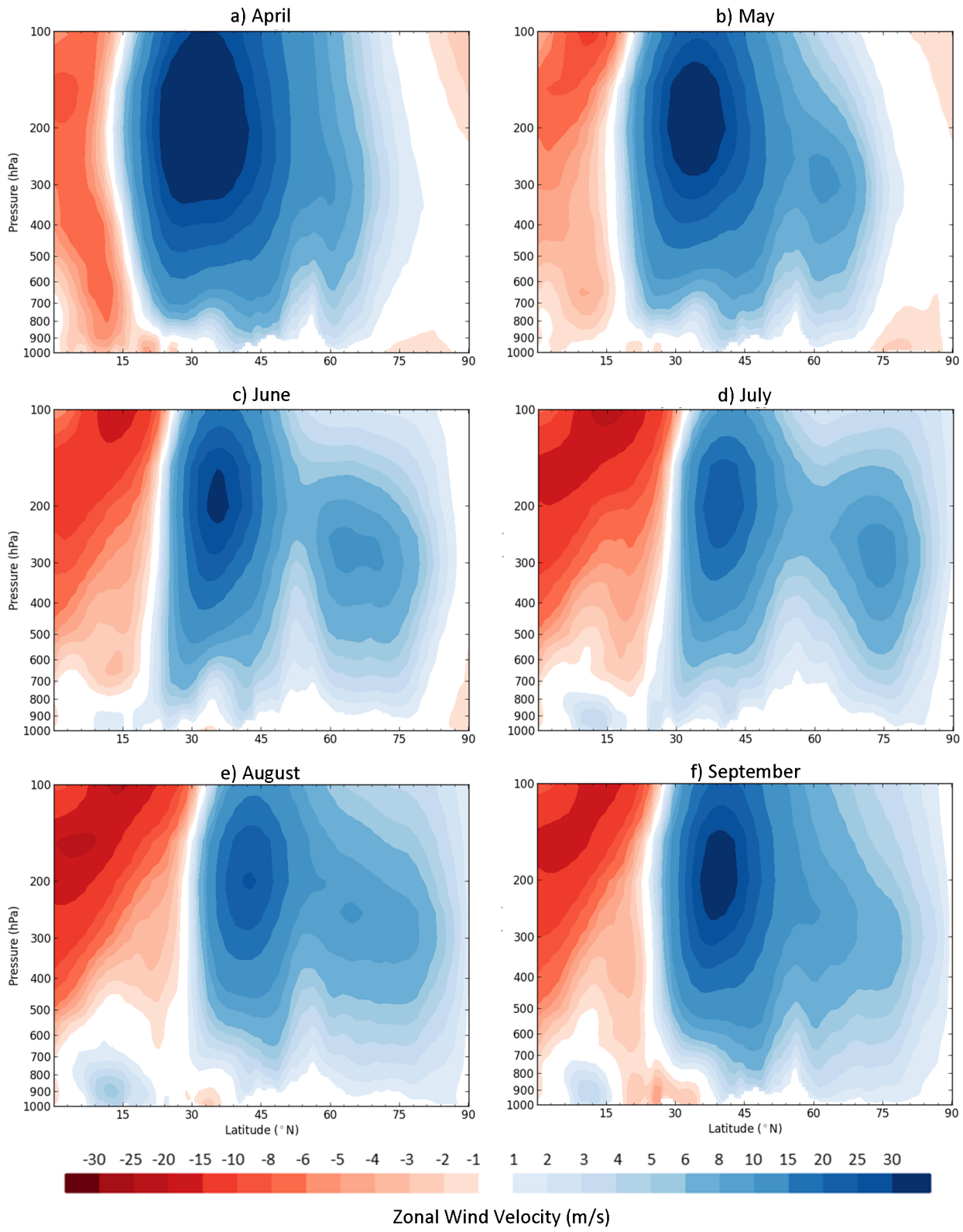

Figure 19: **Latitudinal cross sections of mean monthly zonal wind velocity for summer months along longitude 120°E**, averaged for the period 1979-2012 from MERRA.

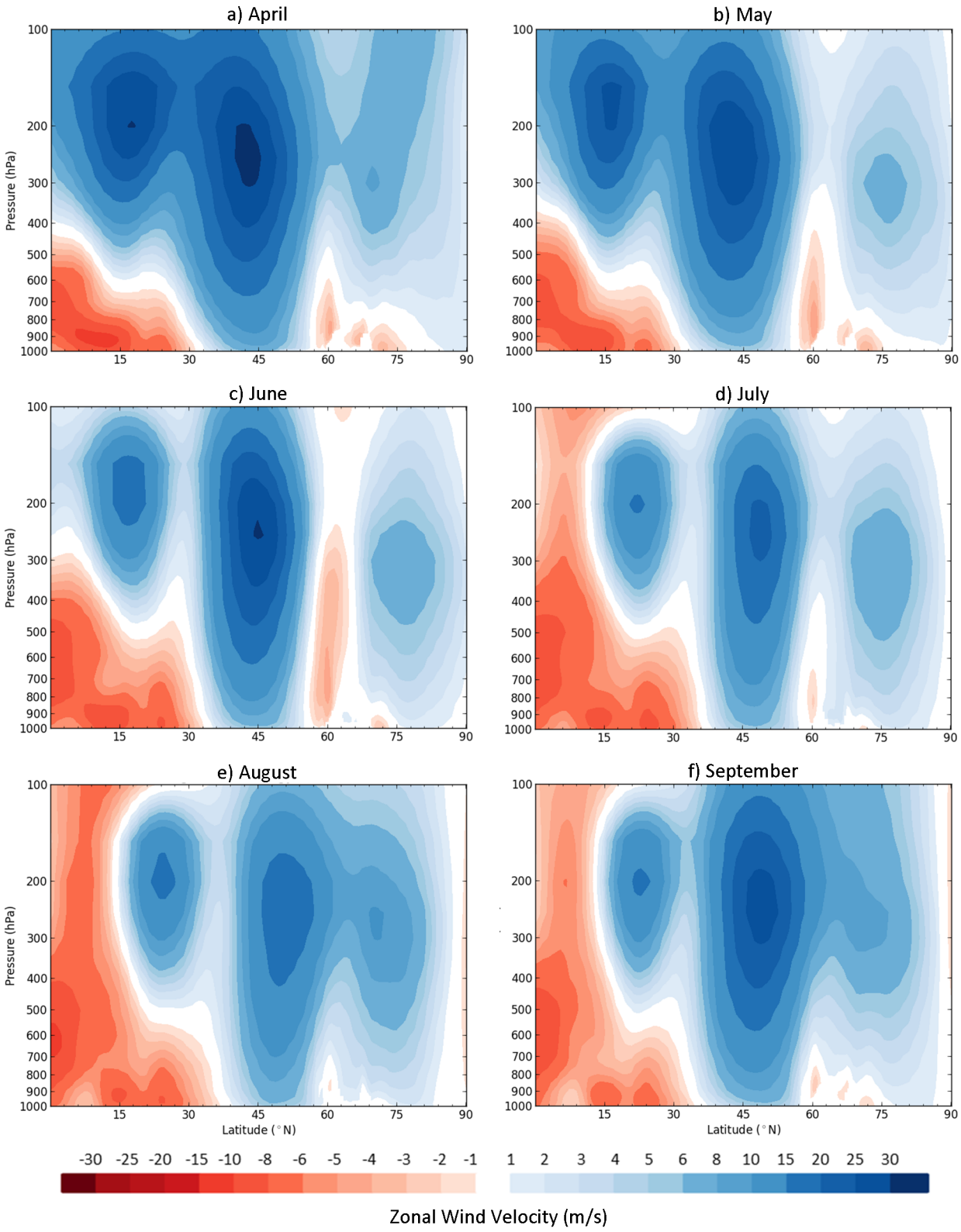

Figure 20: **Latitudinal cross sections of mean monthly zonal wind velocity for summer months along longitude 154°W**, averaged for the period 1979-2012 from MERRA.

No signs of a polar-night jet remain in May, but at all longitudes except 90°E (Figure 18), a closed isopleth centered north of 60°N indicates the formation of an Arctic jet. The feature is most distinct at 154°W (Figure 20), well defined at 48°E (Figure 17), and weakly defined at 120°E (Figure 19). This matches the relative strength of the AFZ in each sector in May. Sector 8 is the strongest, followed by Sector 1 and Sector 4, which is still essentially neutral in May.

By June, the Arctic jet becomes as well defined at 120°E as at 48°E, and it is slightly more distinct by July. At both longitudes, the mean location of the jet shifts northward from about 65°N in June to 75°N in July. No such northward shift is observed at 154°W; the feature is already located over 75°N in May. Meanwhile, an Arctic jet does not become completely distinct from the polar front jet at 90°E until July.

The polar front jet also shifts northward throughout the summer, so although westerly Arctic winds in August are as strong as or stronger than in July, the jet-like feature is less separated from the polar front jet and so less distinct. By September, the jet has diminished to a state similar to April at most longitudes (June for 90°E), reflecting the transition back to neutral AFZ temperature gradients.

Several aspects of this development and diminishing match the pattern of the summer AFZ. The strengths of both features wax and wane in tandem, and the same spatial variability observed in the summer AFZ temperature gradients is reflected by the strength and distinctiveness of the summer Arctic jet. Sectors in which the summer AFZ develops later also witness later development of an Arctic jet, and the Arctic jet is most distinct where the summer AFZ is strongest. The developing phase lasts longer than the diminishing phase, and the diminishing phase demonstrates less spatial heterogeneity.

However, several differences between the summer AFZ and the summer Arctic jet merit mentioning. First, an Arctic jet seems to form more quickly than the summer AFZ. Although positive, the 2-m meridional temperature gradients in Sector 8 are not particularly strong in May, averaging weaker than -2.0 K/100 km. In Sector 4, the temperature gradients are essentially neutral in May, but a separate jet center is clearly beginning to form in Figure 19b. Second, although an Arctic jet may be more distinct from the polar front jet at 154°W than at other longitudes, it is not stronger than in other sectors. In fact, the fastest Arctic jet wind speeds are observed at 120°E. Third, although spatial variation is apparent in the development of an Arctic jet in April through June, the cross sections for July show a fairly homogeneous feature across the four longitudes (including 90°E). Lastly, the center of the Arctic jet shifts northward throughout the season in some sectors, so its mean monthly position is not always located directly over the coastline. These differences warrant a closer and more quantitative examination of spatial variability in the Arctic jet and its relationship with the summer AFZ.

4.6. Variability in the Summer Arctic Jet by Sector

Although several studies have noted the association of the AFZ and the Arctic jet in both space and time (Reed and Kunkel 1960; Shapiro et al. 1987; Serreze et al. 2001; Liess et al. 2011), none has yet devised a systematic way of measuring the strength and location of this jet on an annual basis. The location of the jet was found at each longitude in the reanalyses by identifying the grid cell in latitude-pressure space with the maximum wind speed that lay north of 66.5°N and south of 85°N. The minimum latitude is necessary to avoid the polar jet stream. The maximum latitude omits several years in which grid cells directly over the North Pole observe especially strong westerly winds even though there is not sufficient longitudinal

breadth at such extreme latitudes to reasonably identify a jet. No pressure limits were set, but even without them, the jet is always found between 400 and 200 hPa and the interquartile range lies entirely between 300 and 250 hPa for all sectors. The identified grid cell was treated as the center of the jet. To calculate the strength of the jet, the zonal velocity was averaged for all grid cells within 50 hPa and 1.5° of latitude of center. Thus the metric for jet strength is measuring the core area of the jet and not just a single grid cell.

In addition to AFZ strength, **Figure 21** also shows the spatiotemporal variability of Arctic jet core velocity and latitude over the period 1979-2012. Both metrics for the Arctic jet core demonstrate less spatial variability than the 2-m temperature gradients used to measure AFZ strength. The median July Arctic jet core velocity for each sector lies between 10 and 14 m/s, and the median latitude lies consistently between 72°N and 75°N. No significant difference exists between any two sectors for either metric. Using these metrics provides quantitative evidence of greater homogeneity in the Arctic jet than in the summer AFZ.

These findings highlight an important limitation of dividing the AFZ into sectors: the boundaries between sectors are not as distinct as the color fills in Figure 1. The strong meridional temperature gradients in Sector 7, for example, do not produce zonal winds aloft in isolation from the temperature gradients in Sector 6. Furthermore, the Arctic jet develops in part because the summer AFZ has a broad longitudinal extent. Strong meridional temperature gradients in Sector 6 alone would probably not be sufficient to create an Arctic jet; otherwise, we would see jets along the coasts of Canadian islands or Hudson Bay. Instead of being developed sector by sector, the Arctic jet develops from the overall presence of the summer AFZ. Therefore, the lack of spatial variability in the Arctic jet is understandable. Additionally,

note that the range of the mean location for the Arctic jet core (72°N to 75°N) only directly matches the coast in Sectors 4 and 5, which are the most centrally located sectors (by longitude) of the AFZ. The Arctic jet actually lies slightly north of the coastline in the easternmost and westernmost sectors.

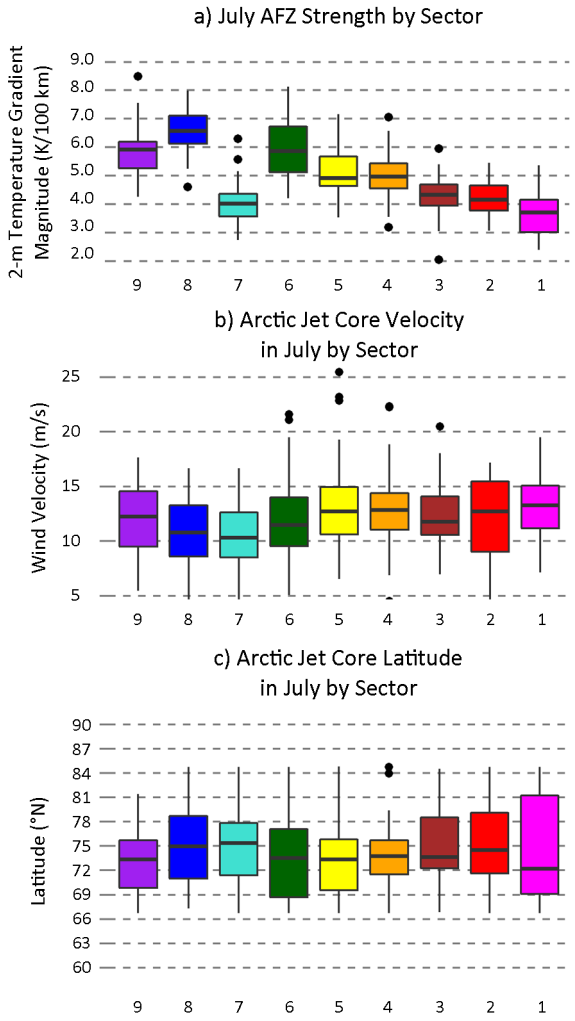

Figure 21: Interannual variability of a) July 2-m temperature gradient magnitude, b) July Arctic jet core velocity, and c) July Arctic jet core latitude by AFZ sector for the period 1979-2012. The box contains the median and first and third quartiles, the whiskers extend to the most extreme values lying within 1.5 times the interquartile range, and the dots represent outliers. Data from MERRA.

Whereas spatial variability is minimal for the Arctic jet core velocity and latitude, temporal variability is substantial. In fact, depending on the year, the Arctic jet may be found at practically any latitude between 66.5°N and 85°N. But how closely does this variation in location and strength match variation in strength of the summer AFZ? **Table 2** shows the coefficients and R^2 values for simple linear regression models between July AFZ strength and July Arctic jet core velocity and latitude. In six out of nine sectors, a stronger AFZ leads to a small but significant increase in Arctic jet core velocity. In Sector 2 (Kara Sea), variation in AFZ strength accounts for 40% of the variation in Arctic jet core velocity, but Sector 9 (eastern Beaufort Sea) is the only other area where the explanatory power of AFZ strength exceeds 15%. Along the Beaufort (Sectors 8-9) and Kara Seas (Sectors 2-3), a stronger AFZ is also associated with a more northerly Arctic jet. This relationship is once again strongest in Sector 2, but once again, AFZ strength can only explain a small amount of Arctic jet variation.

Table 2: Relationship Between Arctic Jet Core and Meridional Temperature Gradients – July 1979-2012 (MERRA)

Sector	Velocity		Latitude	
	Coefficient	R^2	Coefficient	R^2
1	**+1.71**	0.13	+1.31	0.02
2	**+5.05**	0.40	**+6.64**	0.34
3	-0.70	0.02	**+2.98**	0.15
4	+1.60	0.10	+0.90	0.02
5	**+2.09**	0.12	+0.13	0.00
6	**+1.43**	0.13	+0.52	0.01
7	**+1.84**	0.13	+1.46	0.04
8	+0.20	0.00	**+2.30**	0.13
9	**+2.40**	0.29	**+2.23**	0.17

Results for simple linear regression models regressing the a) velocity (m/s) and b) latitude (°N) of the Arctic jet's core area (100 hPa by 3° of Latitude) on the surface meridional temperature gradient (K/ 100 km) for July 1979-2012. **Bold** values are significant at the $p < 0.05$ level. Data from MERRA.

Focusing on significance alone would be misleading in this case. Significance of a coefficient at $p < 0.05$ means that, if there was really no relationship between AFZ strength and the Arctic jet core, a coefficient of that magnitude would be observed in collected data only five out a hundred times by random chance. But the magnitude of a coefficient does not indicate how much variation in the Arctic jet core can be explained by variation in AFZ strength. And a significant coefficient does not necessarily explain a large amount of variation.

The R^2 value thus becomes especially important. The R^2 value measures how much of the total variation in the Arctic jet core parameter is being explained by variation in AFZ strength for each sector. Low R^2 values indicate that although the presence of the summer AFZ is related to the Arctic jet's development, AFZ strength in a particular sector is far from the only factor influencing interannual variation in the strength of the zonal wind. Several reasons may exist, but in general the weak relationship probably results from a combination of how the two features are measured and the complexity of their relationship within a broader climate system.

For instance, as discussed above, the Arctic jet seems to act more like a single coherent unit than the AFZ in terms of interannual variability. Since interannual variation in Arctic jet velocity is coherent at a broader horizontal scale, it may be expected that the AFZ strength – Arctic jet core velocity relationship is stronger for larger sectors. By comparing the sector lengths in Table 1 to the regression results in Table 2, however, this is apparently not the case. Five sectors exceed 1,000 km in length: 1-3, 7, and 8. Three of these five sectors display a significant relationship between meridional temperature gradients and Arctic jet core velocity and two do not. Of the four sectors with lengths below 1,000 km, three display a significant

relationship and one does not. So although the length of sectors may have a meaningful influence on results, such an influence is not apparent in these data.

Alternatively, it may be suspected that the Arctic jet core velocity would be better predicted by including the meridional temperature gradients from upstream sectors as additional independent variables in the regression models. Doing this increases the R^2 value (and adjusted R^2) substantially for Sectors 3 and 4, but it weakens the relationship for Sectors 2, 5, and 6 (not shown). Therefore, it is unclear whether the mismatch of longitudinal scales of variation for the two features is adequately addressed using this method.

To complicate the relationship further, the Arctic jet may respond to not only a broader longitudinal scale, but also a broader latitudinal scale. As shown in Figure 5, the narrow zone of strong meridional temperature gradients encompassed by the summer AFZ are enhancing the overall latitudinal temperature gradient. Without the AFZ, no Arctic jet develops in the climatology (Figure 5e; Figure 6), but notably, while the measurement of AFZ strength used here encompasses only 2 to 3° of latitude (depending on the reanalysis), the zone of negative meridional temperature gradients associated with the formation of an Arctic jet is at least 10° of latitude (Figure 5). The coastline certainly seems to be the center of activity, but Arctic jet development is affected by a broader set of horizontal temperature gradients than simply the particularly strong ones at the coast.

Lastly, factors leading to the formation of an Arctic jet are also broad in vertical extent. The metric used for summer AFZ strength is the 2-m temperature gradient, but the formation of a jet-like feature at 300 hPa requires consistently strong and negative meridional temperature gradients throughout the troposphere. As noted in Section 3.3, the vertical depth

of strong meridional temperature gradients is one aspect that sets the coastal AFZ apart from other areas with strong near-surface temperature gradients.

A more specific example of the broader context for the Arctic jet is better understood by considering Figure 11a and Figure 20a. Both figures show the month of April. In this month, the 2-m meridional temperature gradients in Sector 8 (Figure 11a) make the switch from positive to negative. They reach a point of complete neutrality, when temperatures over land and ocean are equal. The summer AFZ develops from this clean slate, this neutral state. Looking aloft, no such clean slate is afforded the zonal winds at Arctic latitudes (Figure 20a). The westerly wind regime between 300 and 250 hPa fluidly morphs from being the lower reaches of the polar-night jet's influence to being the center of a new summer Arctic jet. The transition is swift, and the winds never stop blowing or reverse direction. In other words, one reason why the timing of development of the summer AFZ and the summer Arctic jet are not particularly well correlated is because they develop from different contexts.

This collection of disparities is not meant to suggest that the two features are unconnected. The seasonal and spatial correlations observed between Figure 11 and Figures 17-20 are strong qualitative evidence for an association. However, isolating the effect of the summer AFZ on the summer Arctic jet on an interannual basis is difficult without controlling for that broader context, and at least with the current methods, the relationship is not robust enough on an interannual basis to merit using the Arctic jet core velocity or location as additional measures of AFZ strength and vice-versa. Accordingly, the statistical analyses in the remainder of this study will focus exclusively on the temperature gradients that define the

summer AFZ. The impacts of the summer AFZ on the Arctic climate system will be considered in greater depth in future research.

5. FACTORS INFLUENCING INTERANNUAL VARIABILITY

5.1. Methods

To assess factors that influence interannual variability of summer AFZ strength, a series of regression models was constructed to relate mean monthly AFZ strength, 2-m temperatures over both land and ocean, and a series of influencing variables. A separate model was constructed for each sector and for each month in the summer AFZ regime (May-August). Since not all variables share the same temporal range, only the years for which all variables are available were used in the regression models (1982-2011 for MERRA and ERA-Interim and 1982-2009 for CFSR).

The 2-m temperatures and the influencing variables were masked to a distance of 250 km from the coastline. Next, three mean values were calculated for each masked variable: one for water grid cells on the ocean side of the coastline (i.e. a water mask with lakes and estuaries excluded), one for land grid cells on the continent side of the coastline (i.e. a land mask with islands excluded), and one for all grid cells on either side of the coastline.

Four multiple linear regression models were constructed for each combination of sector, month, and reanalysis: a) regressing AFZ strength on 2-m temperatures over land and ocean (AFZ-T), b) regressing 2-m temperatures over land on all land-influencing variables (LandT-var), c) regressing 2-m temperatures over ocean on all ocean-influencing variables (OceanT-var), and d) regressing AFZ strength on all influencing variables (AFZ-var).

The LandT-var and OceanT-var model types each include six influencing variables: cloud fraction, sea level pressure, wind speed, two wind components, and a metric for either snow cover or sea ice. The AFZ-var type includes both snow cover and sea ice, bringing the total to seven independent variables. All variables were converted to anomalies before use in regression models. The benefit of doing this is that any unbiased model should have an intercept of zero. Models with significant intercepts indicate the presence of some overall bias in the models towards stronger or weaker AFZ strength. Anomalies were used instead of z-scores so that the per unit change impact for each variable on AFZ strength can be easily interpreted from the results. The relative importance of each influencing variable to interannual variability in AFZ strength is measured using the partial coefficient of determination (the partial R^2). Several criticisms can be made about the multiple linear regression methods used here. These are better explained when examining the results, so they are reserved until the discussion in Section 5.6.

Three variables required further processing: the wind component measures, the sea ice metrics, and the snow cover metrics. First, the seasonal retreat of snow cover and sea ice concentration each spring and summer makes them distinct from other potential influencing variables. It was supposed that using a single metric to capture that seasonal retreat might be more meaningful for the AFZ (which also develops seasonally) than simply using the average monthly cover or concentration. To capture variability in the timing of sea ice retreat, daily sea ice concentration was averaged for the area within 250 km of the coastline for each point along the AFZ. The day on which that average sea ice concentration fell below 60% was recorded for each year and called the “retreat day”. These retreat days were then averaged for each sector.

The 250 km distance balances the desire for measuring only the fairly narrow AFZ with the coarse spatial resolution of the input data. The 60% average concentration threshold balances the desire to capture the timing of substantial sea ice retreat with the desire for a threshold that is reached in all sectors each year. Thresholds below 60% proved problematic because the average sea ice concentration often does not fall below the threshold.

Snow cover loss was measured in the same manner as sea ice retreat (spatial average with 60% threshold), only using the "retreat week" since the data were provided at weekly resolution. Lower thresholds could have been used for snow cover since it is nearly absent by July in all sectors, but using different thresholds did not significantly change relationships between snow cover and AFZ strength. For that reason, 60% was chosen to provide more comparison opportunities with sea ice retreat. (See Section 6 for an example of such comparisons.)

Each model was constructed multiple times, alternatively using either the monthly average or the annual retreat value for snow cover and/or sea ice, but only the model with the highest explanatory power (highest R^2) is presented below.

Second, wind fields based on local coordinate systems were created to test the relationship between AFZ strength and the strength of across-shore and along-shore winds. A local coordinate system was constructed for each AFZ point using the orientation of the local coastline as the x-axis. First, for each AFZ point, the angle was found between local coastline orientation at that point and a parallel that intersected that point. Next, the 10-m u and v wind components were converted into local along-shore (x) and across-shore (y) wind components by rotating axes the appropriate amount for each point. For local across-shore winds, positive y

is blowing offshore (from the land). Negative y is blowing onshore (from the ocean). Henceforth, positive y will be called an offshore wind and negative y will be called an onshore wind. For along-shore winds, positive x is blowing so that the coastline is to the right of the wind vector. Negative x is blowing so that the coastline is to the left of the wind vector. Each model was constructed twice, once using u and v wind components and once using local x and y wind components. Only the models using local x and y wind components are presented below, but the models using u and v components show almost identical results. This exemplifies the approximately zonal orientation of the Arctic coastline and the summer AFZ: meridional winds and zonal winds are broadly equivalent to across-shore winds and along-shore winds, respectively.

Since nine sectors, four months, and three reanalyses result in 108 iterations of each model type, only results from MERRA are presented below. In general, ERA-Interim provides a good match with MERRA, showing the same overall trends and only minor differences to which variables are significant in each model. CFSR usually yields fewer significant variables, which can be partly attributed to its small n value (28 years instead of 30). Additionally, as discussed in Section 2, the coarser resolutions of MERRA and ERA-Interim yield smoother fields of data with fewer extremes. Aggregation of data into sectors is more influenced by outliers in CFSR, which may also obscure trends and relationships.

5.2. Near-Surface Air Temperatures and AFZ Strength

Regressing AFZ strength on land and ocean 2-m temperatures within 250 km of the coastline (AFZ-T models) yields different R^2 values for each sector and each month (**Tables 3a - 3d**). For June, July, and August, these models explain between 79% and 97% of the variance in

AFZ strength. The explained variance is not 100% for any case because the temperature gradient magnitude of any grid cell is not restricted to land-ocean contrasts, and the spatial scales do not perfectly align. As expected, warmer air over land strengthens the summer AFZ, while warmer air over ocean weakens the summer AFZ for all sectors in each summer month. The low values of the intercepts indicate that bias from the model is small, on the order of 1% of AFZ strength variability.

Table 3a: AFZ-T Models for May

Sector	R^2	Land	Ocean	Intercept
1: Barents Sea	**0.74**	**+0.29**	**-0.27**	+0.01
2: Kara Sea	**0.38**	**-0.19**	+0.12	**+0.01**
3: Taymyr Peninsula	**0.76**	**-0.25**	**+0.20**	**+0.01**
4. West Laptev Sea	**0.35**	**+0.14**	-0.07	-0.02
5: Kolyma Lowland W	**0.82**	**+0.25**	**-0.19**	0.00
6: Kolyma Lowland E	**0.92**	**+0.37**	**-0.25**	-0.01
7: Chukotka	0.07	+0.05	-0.02	+0.01
8: Alaska	**0.81**	**+0.32**	-0.08	0.00
9: East Beaufort Sea	**0.93**	**+0.44**	**-0.44**	+0.01

Results for multiple linear regression models regressing May AFZ strength (K/100 km) on land and ocean 2-m temperatures (K) for 1982-2011. **Bold** values are significant at $p < 0.05$. Reanalysis data from MERRA.

Table 3b: AFZ-T Models for June

Sector	R^2	Land	Ocean	Intercept
1: Barents Sea	**0.90**	**+0.51**	**-0.36**	0.00
2: Kara Sea	**0.92**	**+0.46**	-0.14	0.00
3: Taymyr Peninsula	**0.93**	**+0.50**	**-0.47**	0.00
4. West Laptev Sea	**0.92**	**+0.52**	-0.23	+0.01
5: Kolyma Lowland W	**0.88**	**+0.48**	**-0.26**	0.00
6: Kolyma Lowland E	**0.93**	**+0.59**	**-0.48**	0.00
7: Chukotka	**0.90**	**+0.56**	-0.22	0.00
8: Alaska	**0.84**	**+0.46**	+0.05	-0.02
9: East Beaufort Sea	**0.79**	**+0.66**	**-0.58**	-0.04

Results for multiple linear regression models regressing June AFZ strength (K/100 km) on land and ocean 2-m temperatures (K) for 1982-2011. **Bold** values are significant at $p < 0.05$. Reanalysis data from MERRA.

May is more complicated because, as shown in Figure 11, only five out of nine sectors develop a summer AFZ in May. For Sectors 2, 4, and 7, depending on the year, meridional temperature gradients in May are either slightly negative (summer mode), slightly positive (winter mode) or neutral. Since AFZ strength is measured as the temperature gradient magnitude, a stronger AFZ may occur in these sectors in May if temperatures over land are either especially high or especially low. Linear models are insufficient for capturing this type of variation, and the R^2 values are consequentially low.

Table 3c: AFZ-T Models for July

Sector	R^2	Land	Ocean	Intercept
1: Barents Sea	**0.91**	**+0.73**	**-0.64**	-0.01
2: Kara Sea	**0.87**	**+0.60**	**-0.50**	-0.02
3: Taymyr Peninsula	**0.97**	**+0.62**	**-0.46**	+0.01
4. West Laptev Sea	**0.88**	**+0.61**	**-0.31**	+0.03
5: Kolyma Lowland W	**0.95**	**+0.48**	**-0.28**	+0.02
6: Kolyma Lowland E	**0.98**	**+0.55**	**-0.46**	+0.01
7: Chukotka	**0.92**	**+0.73**	**-0.65**	-0.01
8: Alaska	**0.86**	**+0.70**	**-0.59**	-0.05
9: East Beaufort Sea	**0.86**	**+0.65**	**-0.57**	-0.02

Results for multiple linear regression models regressing July AFZ strength (K/100 km) on land and ocean 2-m temperatures (K) for 1982-2011. **Bold** values are significant at $p < 0.05$. Reanalysis data from MERRA.

Since Sector 2 is in the winter mode slightly more often in May, the coefficient for land 2-m temperatures is negative. This indicates that the dominant temperature gradient mode in May is enhanced when air over land is cooler. Sector 4 is just the opposite. May is in the summer mode slightly more often, so more often than not stronger gradients are associated with warmer air over land. Sector 7 is so equally balanced between summer and winter cases that a linear model is useless. For these sectors, using the meridional temperature gradient as a measure of AFZ strength would be more appropriate in May, but using temperature gradient

magnitude better matches the coastal alignment of the summer AFZ temperature gradients and the use of local wind components, which are not perfectly meridional.

Table 3d: AFZ-T Models for August

Sector	R^2	Land	Ocean	Intercept
1: Barents Sea	**0.88**	**+0.62**	**-0.57**	+0.01
2: Kara Sea	**0.92**	**+0.72**	**-0.62**	+0.01
3: Taymyr Peninsula	**0.97**	**+0.58**	**-0.48**	**+0.00**
4. West Laptev Sea	**0.85**	**+0.67**	**-0.58**	-0.01
5: Kolyma Lowland W	**0.96**	**+0.55**	**-0.39**	+0.03
6: Kolyma Lowland E	**0.97**	**+0.52**	**-0.38**	+0.02
7: Chukotka	**0.89**	**+0.52**	**-0.41**	+0.02
8: Alaska	**0.85**	**+0.62**	**-0.48**	-0.02
9: East Beaufort Sea	**0.90**	**+0.63**	**-0.58**	+0.01

Results for multiple linear regression models regressing August AFZ strength (K/100 km) on land and ocean 2-m temperatures (K) for 1982-2011. **Bold** values are significant at $p < 0.05$. Reanalysis data from MERRA.

Finally, Sector 3 is notable in May for being the only case with a sector still clearly in the winter mode. Temperature gradients are positive in Sector 3 in May, so cooler air over land and warmer air over ocean promote stronger gradients. Since the summer AFZ is of chief concern, May results for Sectors 2-4 and 7 could be omitted from this analysis, but including some token neutral or winter cases provides a minor check on other interpretations. Models explaining variation in temperatures should be consistent in all cases. Models explaining temperature gradient magnitude should differ between winter and summer cases and should have less explanatory power (lower R^2) in neutral cases. This expectation is observed in the AFZ-T models.

Separating 2-m temperatures over land and ocean is useful because it helps to clarify the physical processes underlying the statistics. Although the coast represents a sharp surface boundary, cloud cover, sea level pressure, and surface wind anomalies may be similar on either

side of the boundary. For example, in any AFZ sector, a northerly wind anomaly over land is likely associated with a northerly wind anomaly over the ocean. This is potentially problematic because if the same process affects land and ocean temperatures in the same manner (e.g. reduces both), this will have opposing impacts (e.g. cooler land weakens the summer AFZ while a cooler ocean strengthens it). To determine whether a variable influencing AFZ strength is insignificant because it has little thermal impact or insignificant because land and ocean tendencies are competing, the following sets of regression models are conducted on land and ocean temperatures separately. These are the LandT-var and OceanT-var models. The final set of models (AFZ-var) considers monthly AFZ strength directly.

All model types are introduced first for July because that is the month with peak AFZ strength. The physical relationships described for July are also applicable to other months, but the relative importance of some independent variables changes throughout the development of the summer AFZ. Accordingly, the same models will also be examined for May, June, and August in order to compare them to July.

5.3. July Models for Near-Surface Air Temperature of Land and Ocean

Across the entire AFZ, July sea ice concentration and the across-shore component of wind velocity are the most important factors influencing ocean 2-m temperatures (**Table 4a**). Above-average sea ice concentration means the surface has an above-average albedo and absorbs less incoming shortwave radiation than normal. It also means that a greater percentage of the surface area is using absorbed energy to melt ice rather than increase the upper ocean heat content and hence sea surface temperature. This process results in a negative regression

coefficient for sea ice concentration. In most sectors, a sea ice concentration reduction of 20-30% is associated with a 1 K decrease in 2-m temperature.

In summer, an offshore wind is associated with warm air advection because it blows from warm continents. On the other hand, an onshore wind blows from over the cold Arctic Ocean. Thus, offshore winds are associated with higher 2-m temperatures over the ocean, and the y wind component has a positive coefficient. This relationship is strongest in Sector 5 and 6 (Kolyma Lowland), where a 1 m/s increase in offshore winds (or a 1 m/s decrease in onshore winds) is associated with a 1 K increase in 2-m temperatures.

Partial coefficients of determination show that sea ice concentration is the most important factor in the Barents, Chukchi, and Beaufort Seas (Sectors 1 and 7-9), while the offshore winds are the primary factor in the Laptev and East Siberian Seas (Sectors 4-6). These factors combined explain 70-86% of all variation in the ocean 2-m temperatures of each sector.

Whereas the models for ocean 2-m temperatures show uniformity, the models for land 2-m temperatures (**Table 4b**) show substantial heterogeneity. For instance, increased July snow cover or later annual snow cover retreat makes land 2-m temperatures lower. However, this is only a significant factor for four out of nine sectors, and only in Alaska (Sector 8) is snow cover the dominant factor.

Table 4a: OceanT-var Models for July

Sector	R^2	Cloud Fraction	SLP	Sea Ice	X Wind	Y Wind	Wind Speed	Intercept
1	**0.78**	-0.02	+0.02	**-0.13^**	-0.18	**+0.91***	+0.06	0.00
2	**0.71**	0.00	+0.02	**-0.03***	**-0.28'**	**+0.54***	-0.01	0.00
3	**0.71**	-0.01	+0.02	**-0.02***	-0.10	**+0.31^**	-0.05	-0.02
4	**0.81**	+0.01	+0.01	**-0.03^**	-0.11	**+0.69^**	-0.22	+0.01
5	**0.70**	+0.02	+0.06	**-0.03***	-0.13	**+0.96^**	-0.28	+0.02
6	**0.86**	**+0.03**	+0.10	**-0.03***	+0.05	**+0.98^**	+0.11	0.00
7	**0.73**	-0.04	+0.06	**-0.05^**	+0.01	**+0.49'**	+0.20	+0.08
8	**0.82**	-0.03	-0.01	**-0.04^**	-0.12	**+0.69'**	+0.09	+0.07
9	**0.84**	**-0.07**	+0.01	**-0.06***	-0.24	**+0.76**	+0.21	+0.04

Multiple linear regression model results for July 2-m temperatures (K) over ocean within 250 km of Arctic Ocean coastline by sector. **Bold** values are significant at $p < 0.05$. The symbols ', *, and ^ indicate a partial coefficient of determination over 5, 10, and 20%, respectively. Variables include cloud fraction (%), sea level pressure (hPa), 10 m x wind (m/s), 10 m y wind (m/s), and 10 m wind speed (m/s). Sea ice is measured as percent concentration in all sectors. Reanalysis data from MERRA.

Table 4b: LandT-var Models for July

Sector	R^2	Cloud Fraction	SLP	Snow Cover	X Wind	Y Wind	Wind Speed	Intercept
1	**0.77**	-0.10	+0.06	**-0.24'**	-0.34	**+1.46***	-0.61	-0.03
2	**0.83**	**-0.11'**	-0.02	**-0.41'**	**-0.63***	**+1.19^**	0.04	**+5.52'**
3	**0.78**	**-0.10'**	+0.02	-0.11	-0.14	**+0.62'**	**-0.83'**	+1.40
4	**0.79**	**-0.10'**	-0.03	**-0.10'**	**-0.60'**	**+1.39***	**-1.05***	-0.12
5	**0.78**	**-0.13'**	-0.17	-0.18	**-0.95'**	**+1.89'**	**-1.91'**	+2.36
6	**0.74**	-0.05	+0.30	-0.36	-0.91	**+3.04'**	-1.29	+3.36
7	**0.68**	**-0.08***	**+0.30***	-0.08	+0.34	+0.57	+0.78	+1.01
8	**0.56**	-0.04	+0.10	**-0.78^**	-0.56'	+0.50	+0.28	**+7.63^**
9	**0.70**	-0.02	+0.09	-0.29	**-0.77'**	**+2.52^**	+0.22	+2.78

Multiple linear regression model results for July 2-m temperatures (K) over land within 250 km of Arctic Ocean coastline by sector. **Bold** values are significant at $p < 0.05$. The symbols ', *, and ^ indicate a partial coefficient of determination over 5, 10, and 20%, respectively. Variables include cloud fraction (%), sea level pressure (hPa), 10 m x wind (m/s), 10 m y wind (m/s), and 10 m wind speed (m/s). Snow cover is measured as July percentage in Sectors 1 and 4 and as annual retreat week in all others. Reanalysis data from MERRA.

This may be in part because snow cover usually retreats below 60% in late May or early June and covers on average less than 10% of the land area in July in all but Sector 3 (Taymyr Peninsula; the farthest north). Sea ice concentration, meanwhile, stays above 60% until late June and above 20% until late July or August in all but Sector 1 (Barents Sea; the farthest

south). Accordingly, the strongest relationship with AFZ strength is observed in May and June (see below) for snow cover and in July for sea ice. The difference holds whether using the monthly cover/concentration or the seasonal timing of retreat. This suggests that the AFZ system has a short memory; variations in influencing factors in May and June are important to AFZ strength in May and June, but they are relatively unimportant to AFZ strength in July. Another sign of short memory is that for all sectors, July sea ice concentration is a better predictor of ocean 2-m temperatures than the annual sea ice retreat day.

Turning to surface winds, for most sectors, larger coefficients indicate that, not surprisingly, offshore wind anomalies lead to larger increases in land 2-m temperatures than ocean 2-m temperatures. However, across-shore wind velocity is not a significant factor for land 2-m temperatures in Chukotka (Sector 7) or Alaska (Sector 8).

Complicating the picture further, significant negative relationships exist between land 2-m temperatures and both the local along-shore wind velocity and wind speed. This suggests a role for large scale patterns of atmospheric variability. For instance, the positive mode of the Arctic Oscillation (AO) is associated with a) westerly wind anomalies (positive along-shore anomalies) in nearly all sectors and b) a large swath of negative sea level pressure (SLP) anomalies centered over the Arctic Ocean. Lower 2-m temperatures over land would be a logical consequence, but no significant correlation exists between the AO and 2-m temperatures in any sector. Even measuring SLP more locally yields little evidence of a relationship, as SLP is only significant in Chukotka (Sector 7). Therefore, a sound physical mechanism for the along-shore wind relationship remains elusive.

Cloud fraction is a significant predictor of 2-m temperature for five sectors. Cloud cover may increase during the passage of low pressure systems (SLP and cloud fraction have a negative correlation), but summer Arctic cloud cover is dominated by low-level stratus, whose formation processes are largely independent of synoptic scale dynamics (Klein and Hartmann 1993; Beesley and Moritz 1999). In all sectors, greater cloud cover is associated with lower 2-m temperatures even after controlling for SLP, consistent with the negative cloud radiative forcing in the Arctic during summer (Intrieri et al. 2002).

In conclusion, variation in 2-m temperatures over the ocean for all sectors is most strongly affected by sea ice concentration and the across-shore wind component. Influences over land are more diverse. Clouds have a substantial impact in Sectors 2-5 and are dominant in Sector 7, which is also linked to variation in SLP. Snow retreat timing is the most important factor in Sector 8. Sectors 3-6 and 9 are all strongly dependent on the across-shore wind regime, although 2-m temperatures in Sectors 3-5 are also strongly influenced by wind speed. Along-shore winds have a significant impact on four sectors.

5.4. Models for July AFZ Strength

Whereas the variables for the previous models included only the area on either the land or ocean side of the coastline, the AFZ-var model (**Table 4c**) regresses the July AFZ strength on variables spanning both sides of the coast. Assumedly, any process that makes land 2-m temperatures higher or ocean 2-m temperatures lower should increase AFZ strength and any process that makes land 2-m temperatures lower or ocean 2-m temperatures higher should decrease AFZ strength.

Accordingly, terrestrial snow cover and snow retreat have a negative relationship with AFZ strength and sea ice concentration and sea ice retreat have a positive relationship for all sectors. However, their significance is sector-specific. July snow cover is only significant in Sector 4 (around the Lena River Delta), and snow retreat week in Sectors 2 and 8 (Ob River Estuary and Alaska). Sea ice concentration is only significant in five sectors. Still, sea ice is by far the most important factor in Sectors 7 (Chukotka) and 9 (eastern Beaufort Sea) and is the only significant factor in Sector 1 (Barents Sea).

Table 4c: AFZ-var Models for July

Sector	R^2	Cloud Fraction	SLP	Snow Cover	Sea Ice	X Wind	Y Wind	Wind Speed	Int
1	**0.64**	-0.07’	-0.04	-0.09	**+0.02***	-0.09	+0.30	-0.08	**-0.78***
2	**0.73**	**-0.05’**	-0.04	**-0.23’**	**+0.02***	**-0.29***	+0.14	-0.17	+1.65
3	**0.72**	-0.03	+0.03	-0.07	0.00	**-0.28***	+0.17	**-0.38’**	0.00
4	**0.77**	**-0.05’**	+0.01	**-0.05***	+0.01	-0.18	**+0.61***	**-0.69^**	-1.11
5	**0.76**	-0.03	0.00	-0.06	+0.03	**-0.41***	**+0.89^**	**-0.57***	-1.34
6	**0.56**	-0.02	+0.07	-0.11	**+0.03***	+0.01	**+1.05***	-0.06	-1.34
7	**0.70**	**-0.06***	**+0.19***	-0.12	**+0.04^**	+0.12	+0.15	+0.40	+1.45
8	**0.63**	-0.01	+0.06	**-0.37***	+0.01’	**-0.34***	+0.39	-0.27	**+3.58***
9	**0.66**	-0.02	+0.02	-0.04	**+0.03^**	-0.14	**+0.66’**	+0.13	+0.01

Multiple linear regression model results for July AFZ strength (K/100 km) based on variables within 250 km of Arctic Ocean coastline (both sides) by sector. **Bold** values are significant at $p < 0.05$. The symbols ‘, *, and ^ indicate a partial coefficient of determination over 5, 10, and 20%, respectively. Variables include cloud fraction (%), sea level pressure (hPa), 10 m x wind (m/s), 10 m y wind (m/s), and 10 m wind speed (m/s). Snow cover is measured as July percentage in Sectors 1, 4, and 9 and as annual retreat week in all others. Sea ice is measured as July percentage in Sectors 3 and 7-9 and as annual retreat day in all others. Reanalysis data from MERRA.

Apart from sea ice, the variables affecting AFZ strength are all associated with variation in land 2-m temperatures. When significant, greater cloud fraction, more positive along-shore (westerly) winds, and stronger wind speed, all of which have a cooling effect on land in July, are associated with a weaker AFZ. Similarly, higher SLP, even after controlling for the presence of fewer clouds, is associated with higher 2-m temperatures over land and a stronger AFZ. Perhaps

the most telling example of the primacy of conditions over land is the across-shore wind velocity, which has a positive and significant relationship with AFZ strength in the three Siberian sectors (4-6) and Sector 9 (western Canada). Offshore wind anomalies are associated with higher 2-m temperatures over both land and ocean, but the effect on land temperatures is stronger. The end result is that offshore wind anomalies encourage a stronger summer AFZ despite any increase in ocean 2-m temperatures.

Land 2-m temperatures more strongly control variability in July AFZ strength because they are more readily changed. The standard deviation for the 34-year temperature record is on average 0.67 K greater for land than ocean throughout the AFZ (significant at $p < 0.01$). This difference follows from surface energy balance considerations introduced earlier. If the ocean surface receives more energy, that energy will largely be used to melt more sea ice or heat the large liquid water column and will not substantially affect the atmosphere. However, if the land surface receives more energy, that energy will largely go into the upward sensible heat flux and upward longwave radiation, increasing 2-m temperatures. Land 2-m temperatures change more readily than ocean 2-m temperatures, so they exhibit greater interannual variability. And since they exhibit greater interannual variability, land 2-m temperatures also exhibit greater influence on the interannual variability of AFZ strength.

Nevertheless, the tendency of ocean 2-m temperatures partially offsets the tendency of land 2-m temperatures in affecting summer AFZ strength. Despite having the same number of observations in all models, fewer variables are significant when predicting AFZ strength than when predicting land 2-m temperatures, such as the across-shore wind velocity for Sectors 1-3. The summer AFZ is clearly a complicated system for which the various influencing factors are

interconnected and for which a single factor can have simultaneous and opposite effects. But the variation in land 2-m temperatures is the dominant forcing. This makes the relevance of sea ice notable; it is the only variable that impacts ocean 2-m temperatures without being overshadowed by a simultaneous and opposite impact on land 2-m temperatures.

Table 5a: OceanT-var Models for May

Sector	R^2	Cloud Fraction	SLP	Sea Ice	X Wind	Y Wind	Wind Speed	Intercept
1	**0.75**	+0.02	+0.03	**-0.05^**	**+0.25**	**+0.64***	+0.07	+0.03
2	**0.62**	+0.03'	+0.07	**-0.05***	**+0.50***	**+0.56***	**+0.69***	+0.15
3	**0.51**	+0.01	-0.04	**-0.19^**	-0.51'	+0.16	-0.63'	+0.12
4	**0.52**	-0.03	-0.05	**-0.06^**	-0.12	+0.32	-0.06	**+4.84^**
5	**0.47**	-0.06'	-0.05	-0.27'	-0.37'	+0.63'	-0.34	+0.12
6	**0.53**	**-0.05'**	-0.12	**-0.04***	**-0.56***	+0.54	-0.44	**+3.68***
7	**0.74**	**-0.06'**	-0.11	**-0.16^**	**-0.38'**	+0.01	-0.19	-0.02
8	**0.53**	**-0.09^**	-0.14'	-0.02	-0.38'	**+0.86***	-0.12	0.00
9	**0.73**	**-0.04'**	**-0.19***	**-0.07***	-0.67	**+0.60'**	-0.77	-0.01

Multiple linear regression model results for May 2-m temperatures (K) over ocean within 250 km of Arctic Ocean coastline by sector. **Bold** values are significant at $p < 0.05$. The symbols ', *, and ^ indicate a partial coefficient of determination over 5, 10, and 20%, respectively. Variables include cloud fraction (%), sea level pressure (hPa), 10 m x wind (m/s), 10 m y wind (m/s), and 10 m wind speed (m/s). Sea ice is measured as annual retreat day in Sectors 1 and 2 and as May percentage in all other sectors. Reanalysis data from MERRA.

Table 5b: LandT-var Models for May

Sector	R^2	Cloud Fraction	SLP	Snow Cover	X Wind	Y Wind	Wind Speed	Intercept
1	**0.77**	-0.04	+0.04	**-0.07^**	+0.10	**+1.56***	+0.08	-0.06
2	**0.55**	**+0.04***	**+0.13***	**-0.32***	**+0.31'**	**+0.57***	+0.50'	**+4.14***
3	0.35	+0.02	-0.01	**-0.42***	-0.13	+0.61*	-0.14	**+5.96***
4	0.39	+0.01	-0.03	**-0.48***	-0.54'	+1.00'	-0.38	**+5.69***
5	**0.70**	-0.02	-0.04	**-0.19^**	-0.27	**+2.09***	-0.45	+0.04
6	**0.65**	-0.06	-0.23	**-0.13***	**-1.30***	**+1.54'**	-0.23	-0.09
7	**0.53**	-0.06	-0.01	-0.34'	**-0.93***	**+0.83***	-0.29	+4.00
8	**0.41**	**-0.11***	-0.04	**-0.10***	-0.99*	+1.21'	-0.61	-0.14
9	**0.74**	-0.06	**-0.28'**	**-0.07***	-0.73	**+2.04***	-0.69	-0.15

Multiple linear regression model results for May 2-m temperatures (K) over land within 250 km of Arctic Ocean coastline by sector. **Bold** values are significant at $p < 0.05$. The symbols ', *, and ^ indicate a partial coefficient of determination over 5, 10, and 20%, respectively. Variables include cloud fraction (%), sea level pressure (hPa), 10 m x wind (m/s), 10 m y wind (m/s), and 10 m wind speed (m/s). Snow cover is measured as annual retreat week in Sectors 2-4 and 7 and as May percentage in all others. Reanalysis data from MERRA.

5.5. Seasonal Development and AFZ Regression Models

Although the physical processes do not fundamentally change throughout the development of the summer AFZ, the relative importance of various factors does change. In other words, the sign of coefficients is consistent, but the magnitudes of the coefficients and the partial R^2 values are variable.

Table 5c: AFZ-var Models for May

Sector	R^2	Cloud Fraction	SLP	Snow Cover	Sea Ice	X Wind	Y Wind	Wind Speed	Int
1	**0.74**	-0.01	+0.02	**-1.30^**	0.00	-0.02	**+0.14'**	-0.05	-0.01
2	**0.58**	0.00	-0.01	+0.03	**-0.00***	-0.02	**-0.12^**	-0.05	-0.09
3	0.35	0.00	0.00	**+0.05***	0.00	+0.03	-0.04	0.00	**-0.61***
4	0.38	-0.01	-0.01	-0.03	-0.01'	-0.02	+0.01	-0.07'	+0.37
5	**0.67**	-0.01	0.00	**-2.61***	+0.01'	-0.04	**+0.32^**	-0.01	-1.12'
6	**0.80**	**-0.02**	-0.02	**-3.91^**	0.00	**-0.21'**	**+0.46***	-0.07	+0.10
7	**0.47**	**-0.01***	-0.01	+0.06'	0.00	-0.06'	**+0.12***	**+0.14***	-0.34
8	**0.72**	**-0.04***	-0.04	**-3.03'**	-0.01	**-0.28'**	**+0.55***	+0.04	+0.44
9	**0.85**	-0.01	-0.02	**-2.61^**	0.00	-0.10	**+0.55***	-0.07	-0.04

Multiple linear regression model results for May AFZ strength (K/100 km) based on variables within 250 km of Arctic Ocean coastline (both sides) by sector. **Bold** values are significant at $p < 0.05$. The symbols ', *, and ^ indicate a partial coefficient of determination over 5, 10, and 20%, respectively. Variables include cloud fraction (%), sea level pressure (hPa), 10 m x wind (m/s), 10 m y wind (m/s), and 10 m wind speed (m/s). Snow cover is measured as May percentage in Sectors 1, 5-6, and 9 as annual retreat week in all others. Sea ice is measured as May percentage in Sectors 1, 4, and 9 and as annual retreat day in all others. Reanalysis data from MERRA.

Looking first at the factors affecting 2-m temperatures over ocean (OceanT-var), sea ice and across-shore winds are the most consistently significant factors, but they become more dominant as the summer advances. In May (**Table 5**), sea ice is significant in seven out of nine sectors, but it is significant in all sectors from June (**Table 6**) through August (**Table 7**). Across-shore winds are only significant in May along the Barents and Kara Seas (Sectors 1-2) and the western Chukchi and Beaufort Seas (Sectors 8-9). They are not significant in all sectors until

July. Additionally, even in sectors where significance does not change, the coefficients and partial R^2 values for both variables are higher in July and August than in May and June.

Table 6a: OceanT-var Models for June

Sector	R^2	Cloud Fraction	SLP	Sea Ice	X Wind	Y Wind	Wind Speed	Intercept
1	**0.84**	**-0.09'**	+0.08	**-0.05^**	+0.10	**+0.83^**	+0.33	0.00
2	**0.71**	-0.02	+0.05	**-0.03^**	+0.06	**+0.36'**	+0.08	+0.01
3	**0.52**	-0.02	0.00	**-0.03^**	-0.04	+0.28'	-0.04	+0.02
4	**0.78**	-0.01	+0.06	**-0.06^**	+0.08	**+0.50***	+0.04	+0.08
5	**0.71**	-0.02	+0.01	**-0.09^**	-0.12	+0.30	-0.19	+0.06
6	**0.77**	+0.01	+0.02	**-0.03^**	-0.13	**+0.51***	-0.06	**+2.95^**
7	**0.88**	**-0.03**	**+0.09**	**-0.03^**	-0.01	**+0.63***	+0.10	+0.03
8	**0.69**	**-0.03^**	+0.03	**-0.02***	-0.13	**+0.43'**	-0.23	**+1.43***
9	**0.76**	-0.02	-0.05	**-0.04^**	-0.11	**+0.63'**	-0.17	0.00

Multiple linear regression model results for June 2-m temperatures (K) over ocean within 250 km of Arctic Ocean coastline by sector. **Bold** values are significant at $p < 0.05$. The symbols ', *, and ^ indicate a partial coefficient of determination over 5, 10, and 20%, respectively. Variables include cloud fraction (%), sea level pressure (hPa), 10 m x wind (m/s), 10 m y wind (m/s), and 10 m wind speed (m/s). Sea ice is measured as annual retreat day in sectors 6 and 8 and as June percentage in all other sectors. Reanalysis data from MERRA.

Table 6b: LandT-var Models for June

Sector	R^2	Cloud Fraction	SLP	Snow Cover	X Wind	Y Wind	Wind Speed	Intercept
1	**0.69**	**-0.15^**	+0.16	-0.03'	+0.39	**+1.72^**	+0.38	+0.02
2	**0.73**	-0.05	+0.02	**-0.07^**	-0.34	**+0.80'**	+0.34	-0.14
3	**0.46**	0.00	+0.04	**-0.74^**	-0.01	+0.56	+0.19	**+10.19^**
4	**0.56**	+0.05	+0.09	**-0.07^**	+0.01	**+1.09'**	+0.64	-0.04
5	**0.65**	-0.07	-0.13	-0.03'	-0.29	+1.06	+0.12	-0.02
6	**0.74**	-0.07	-0.12	**-0.40'**	-0.35	**+1.28'**	+0.21	**+4.19'**
7	**0.83**	**-0.13^**	+0.01	**-0.49***	**-0.52**	**+1.45^**	-0.42	**+5.86***
8	**0.69**	**-0.12^**	+0.06	-0.11	-0.69'	**+1.04'**	-0.67	+1.17
9	**0.44**	-0.04	+0.02	-0.22'	+0.41	**+2.10***	+0.77	+2.06'

Multiple linear regression model results for June 2-m temperatures (K) over land within 250 km of Arctic Ocean coastline by sector. **Bold** values are significant at $p < 0.05$. The symbols ', *, and ^ indicate a partial coefficient of determination over 5, 10, and 20%, respectively. Variables include cloud fraction (%), sea level pressure (hPa), 10 m x wind (m/s), 10 m y wind (m/s), and 10 m wind speed (m/s). Snow cover is measured as annual retreat week in Sectors 3 and 6-9 and as June percentage in all others. Reanalysis data from MERRA.

Table 6c: AFZ-var Models for June

Sector	R^2	Cloud Fraction	SLP	Snow Cover	Sea Ice	X Wind	Y Wind	Wind Speed	Int
1	**0.53**	**-0.04***	+0.07’	-0.01	+0.01	+0.01	**+0.44***	+0.22	-0.27
2	**0.80**	-0.02	+0.05	**-0.03^**	-0.01	-0.01	**+0.29’**	+0.12	-0.06
3	**0.54**	-0.02	0.00	**-0.25^**	-0.01	0.00	+0.10	-0.05	**+4.18^**
4	**0.69**	+0.02	+0.08	**-0.02^**	**-0.03’**	+0.06	+0.34	+0.21	+0.02
5	**0.66**	0.00	+0.01	-0.01’	-0.02	**-0.26***	+0.21	+0.10	0.00
6	**0.69**	**-0.05’**	-0.01	**-0.19’**	0.00	**-0.32’**	+0.33	-0.12	**+1.94’**
7	**0.74**	**-0.08^**	+0.04	**-0.21’**	-0.01	-0.17	**+0.52***	-0.17	**+2.49’**
8	**0.72**	**-0.05***	-0.05	-0.07	+0.01	**-0.66***	**+0.68***	**-0.61’**	+0.70
9	**0.56**	-0.02	0.00	-0.01’	**+0.03^**	+0.38	**+0.67***	+0.48	**-2.16^**

Multiple linear regression model results for June AFZ strength (K/100 km) based on variables within 250 km of Arctic Ocean coastline (both sides) by sector. **Bold** values are significant at $p < 0.05$. The symbols ‘, *, and ^ indicate a partial coefficient of determination over 5, 10, and 20%, respectively. Variables include cloud fraction (%), sea level pressure (hPa), 10 m x wind (m/s), 10 m y wind (m/s), and 10 m wind speed (m/s). Snow cover is measured as June percentage in Sectors 1, 2, 4, 5, 9 and as annual retreat week in all others. Sea ice is measured as June percentage in Sectors 2 and 4-8 and as annual retreat day in all others. Reanalysis data from MERRA.

Cloud cover is never a significant factor in Sectors 2-5, and it impacts fewer sectors in each month throughout the development of the AFZ. Cloud cover is not significant in any sector by August. Along-shore winds are only significant in May. The positive coefficients for Sectors 1 and 2 show that the 2-m temperatures over the Barents and Kara Seas are warmer when wind is blowing from the relatively warm North Atlantic instead of the cold Arctic. Sectors 6 and 7 have negative coefficients, which matches the unexplained pattern observed in several sectors for 2-m land temperatures in July.

The models explaining 2-m temperatures over land (LandT-var models) are more complicated than the OceanT-var models in every month. They show a similar trend of across-shore winds becoming more dominant throughout summer AFZ development. However, cloud cover is more important over land than ocean, and unlike over ocean, it is relatively more important over land in July and August than in May and June. Along-shore winds are also more

often significant. And although the sectors for which they are significant vary from May to June to July, Sectors 2, 4, and 9 each has a negative coefficient for the along-shore wind component in both July and August. Wind speed is only significant in July, when the summer AFZ is at its peak strength.

Table 7a: OceanT-var Models for August

Sector	R^2	Cloud Fraction	SLP	Sea Ice	X Wind	Y Wind	Wind Speed	Intercept
1	**0.60**	-0.01	-0.01	**-0.04^**	-0.10	**+0.92^**	-0.07	**+1.39***
2	**0.67**	-0.02	+0.01	**-0.02^**	-0.04	**+0.53^**	+0.13	**+1.74^**
3	**0.82**	+0.02	+0.04	**-0.02'**	-0.07	**+0.65^**	+0.02	+0.03
4	**0.75**	-0.01	-0.01	**-0.07^**	+0.03	**+0.79^**	**-0.40***	-0.10
5	**0.66**	-0.01	-0.02	**-0.04^**	+0.04	**+0.59***	**-0.35'**	-0.11
6	**0.74**	0.03	-0.04	**-0.04^**	-0.09	**+0.86***	-0.02	-0.03
7	**0.81**	-0.02	-0.01	**-0.07^**	-0.14	**+0.65^**	+0.30	+0.05
8	**0.88**	-0.02	0.00	**-0.06^**	-0.09	**+1.06^**	+0.02	+0.06
9	**0.81**	-0.02	-0.09	**-0.10^**	-0.07	**+0.86***	+0.27	+0.06

Multiple linear regression model results for August 2-m temperatures (K) over ocean within 250 km of Arctic Ocean coastline by sector. **Bold** values are significant at $p < 0.05$. The symbols ', *, and ^ indicate a partial coefficient of determination over 5, 10, and 20%, respectively. Variables include cloud fraction (%), sea level pressure (hPa), 10 m x wind (m/s), 10 m y wind (m/s), and 10 m wind speed (m/s). Sea ice is measured as annual retreat day in Sectors 1 and 2 and as August percentage in all other sectors. Reanalysis data from MERRA.

Table 7b: LandT-var Models for August

Sector	R^2	Cloud Fraction	SLP	Snow Cover	X Wind	Y Wind	Wind Speed	Intercept
1	**0.68**	-0.07'	-0.01	+0.09	-0.02	**+2.01^**	+0.31	-0.76
2	**0.81**	**-0.08***	+0.06	-0.13	**-0.38'**	**+1.58^**	+0.46	+1.68
3	**0.73**	-0.04	+0.05	-0.07	-0.17	**+1.71^**	+0.14	-0.01
4	**0.71**	**-0.07'**	+0.10	-0.12	**-0.44'**	**+2.14^**	+0.10	+1.29
5	**0.64**	**-0.14***	+0.03	-0.28	-0.11	**+1.79'**	-0.87	-0.04
6	**0.56**	-0.08	-0.11	-0.14	-0.67	+1.51'	-1.27	+0.02
7	**0.78**	**-0.12***	+0.04	-0.13	-0.58	**+1.35^**	-0.26	+1.58
8	**0.50**	-0.07'	+0.15	-0.40	-0.80	**+1.79^**	-0.85	+3.82
9	**0.69**	+0.01	+0.13	**-0.57***	**-0.69'**	**+2.90^**	+1.08	**+5.15***

Multiple linear regression model results for August 2-m temperatures (K) over land within 250 km of Arctic Ocean coastline by sector. **Bold** values are significant at $p < 0.05$. The symbols ', *, and ^ indicate a partial coefficient of determination over 5, 10, and 20%, respectively. Variables include cloud fraction (%), sea level pressure (hPa), 10 m x wind (m/s), 10 m y wind (m/s), and 10 m wind speed (m/s). Snow cover is measured as August percentage in Sectors 3, 5, and 6 and as annual retreat week in all others. Reanalysis data from MERRA.

Most interesting is the changing importance of snow cover. Snow is especially important in May, but is significant in fewer and fewer sectors as the summer continues. In most years, snow cover has all but disappeared by July, so there is more variability in snow cover in May and June than July and August. (Note that although there is usually no snow in any sector except Sector 3 in August, a month will still have some variability even if one grid cell has snow present in one out of the 30 instances observed.) The disappearance of snow cover in summer makes the snow cover retreat day measurement useful, as the seasonal timing of snow cover retreat may impact summer AFZ strength throughout the summer. But even this measure is only a significant factor for AFZ strength in two sectors in July and one in August, which further emphasizes the short memory of the summer AFZ system.

Table 7c: AFZ-var Models for August

Sector	R^2	Cloud Fraction	SLP	Snow Cover	Sea Ice	X Wind	Y Wind	Wind Speed	Int
1	**0.49**	-0.03’	-0.02	+0.09	+0.12’	+0.02	**+0.45***	+0.19	-0.83
2	**0.80**	**-0.05***	+0.04	-0.18	**+0.06**	**-0.27***	**+0.69^**	+0.20	-0.05
3	**0.64**	-0.03	+0.06’	-0.02	-0.01	-0.05	**+0.60^**	+0.02	-0.02
4	**0.59**	-0.05’	+0.07	-0.13	+0.01	-0.16’	**+0.79^**	+0.13	-0.83
5	**0.63**	**-0.07***	+0.04	-0.11	+0.01	-0.13	+0.38	-0.25	-0.84
6	**0.56**	-0.02	-0.08	+0.14	0.00	**-0.27***	**+0.71***	-0.30	-1.48
7	**0.72**	**-0.05***	+0.03	-0.02	**+0.02***	-0.08	**+0.29***	-0.07	**-1.59***
8	**0.69**	-0.03	+0.05	-0.15	**+0.02***	**-0.40***	**+0.67^**	-0.19	1.35
9	**0.69**	-0.01	+0.02	-0.15	+0.02’	-0.24	**+0.99^**	-0.03	1.36

Multiple linear regression model results for August AFZ strength (K/100 km) based on variables within 250 km of Arctic Ocean coastline (both sides) by sector. **Bold** values are significant at $p < 0.05$. The symbols ‘, *, and ^ indicate a partial coefficient of determination over 5, 10, and 20%, respectively. Variables include cloud fraction (%), sea level pressure (hPa), 10 m x wind (m/s), 10 m y wind (m/s), and 10 m wind speed (m/s). Snow cover is measured as August percentage in Sectors 2-5 and 7 and as annual retreat week in all others. Sea ice is measured as August percentage in Sectors 1-3, 6, 8, and 9 and as annual retreat day in all others. Reanalysis data from MERRA.

Sea ice, on the other hand, lingers at lower concentrations in most sectors long after it retreats below 60% concentration, so it is still significant to 2-m temperatures over ocean in

August. Memory is still short in the system, though. August temperatures are better explained by August concentration than by annual retreat day in Sectors 3 through 9. Only Sectors 1 and 2 are better explained by the retreat day, and they are the only two sectors that usually have 0% sea ice concentration in August.

The shifting importance of factors influencing 2-m temperatures is repeated in the AFZ-var models. The most important factors influencing AFZ strength in May are across-shore winds, snow cover, and cloud cover. As the summer AFZ continues to strengthen, the relative importance of snow cover diminishes. Meanwhile, across-shore winds become even more important. Sea ice variations are relevant in the most sectors in July and are still significant in three sectors in August even after snow cover has become obsolete. Because of its influence on land temperatures, cloud cover is consistently important in at least three sectors during each month, and it is always significant to AFZ strength in Chukotka (Sector 7). Similarly, along-shore winds are always significant in at least two sectors and are always significant in Alaska (Sector 8). SLP and wind speed have limited significance, but both are most relevant in July.

Lastly, a check can be made by looking at the significant variables for Sector 3, which is clearly in a winter mode in May, and Sector 2, which is in the winter mode for slightly more than half of all Mays. As expected, the signs of the significant coefficients are the opposite of sectors in the summer mode. Greater snow cover in May on the Taymyr Peninsula (Sector 3) makes 2-m land temperatures lower than normal and strengthens the winter mode temperature gradients. Meanwhile, winds that are more offshore than normal increase 2-m temperatures over the Ob River Estuary area, which more often than not is weakening winter mode temperature gradients instead of strengthening an incipient summer AFZ. Similarly, later

sea ice retreat usually weakens May temperature gradients slightly in Sector 2 because of its cooling effect on 2-m temperatures over the Kara Sea. The consistency of these results with expectations supports the physical explanations for variation in summer AFZ strength in other months and sectors.

In summary, for all summer months cloud cover and surface wind components are important factors in determining variation in AFZ strength from the long-term average. Snow cover and sea ice are both significant to some sectors in July, but snow cover variations are more important earlier in AFZ development (May and June), while sea ice variations are more important later in AFZ development (July and August). The short-term memory of the AFZ system is evidenced by the insignificance of snow cover variations to August AFZ strength.

5.6. Criticism of the Regression Approach

Using linear regression to address the relative importance of various factors on the monthly strength of the summer AFZ is primarily useful because the results are relatively simple and easily interpreted. Multiple regression also has the benefit of isolating each variable by holding the others constant. For instance, although greater cloud cover is consistently associated with lower 2-m temperatures in several sectors each month, it is also associated with lower sea level pressure. Using regression controls for sea level pressure, and this helps to isolate the impact of cloud cover from a potentially confounding variable. This makes results more robust.

However, the isolation is imperfect because multiple regression cannot assign cause and effect amongst non-independent x variables. It does not know, for instance, that lower pressure

at sea level increases the amount of rising air, which increases upward transport of water vapor, which increases condensation (and thus cloud formation) aloft.

Additionally, whenever multicollinearity exists (whenever an x variable is not really independent, but instead is correlated with the combination of all other x variables), the regression model is uncertain whether some of the explanatory power of a particular x variable should really be attributed to the collection of other x variables. For instance, as shown in **Figure 22** the dominant July wind direction is from the east or northeast in all sectors. Examples of northerly or westerly winds are uncommon and in no sector does any July have a predominantly northwesterly wind direction. The result is that when wind is decomposed into a zonal and meridional component, the more easterly (negative anomaly) zonal winds also typically have stronger (positive anomaly) wind speeds. Stronger wind speeds are also generally observed when wind direction is easterly or northeasterly, not southerly, which exacerbates this tendency. It is difficult to disentangle the perceived impacts of variation in wind speed because those variations are not independent of wind direction.

Multicollinearity is always present, and it always has the result of inflating the standard errors in regression results. The coefficient estimate is not affected, but the size of its error bars increases; the coefficient is less likely to be deemed significant and its partial coefficient of determination (partial R^2) will be smaller. Multicollinearity can be measured using a variance inflation factor (VIF) for each x variable in a model. VIF values for the regression models shown above are usually between 2.0 and 5.0, indicating that multicollinearity is present in at least moderate amounts. In a few cases, the VIF is over 5.0, such as for wind speed in the LandT-var model for Sector 6 in July (Table 4b) . Notice how even though the estimated coefficient for

wind speed in Sector 6 is higher than in Sector 3, the coefficient is significant in Sector 3 and insignificant in Sector 6.

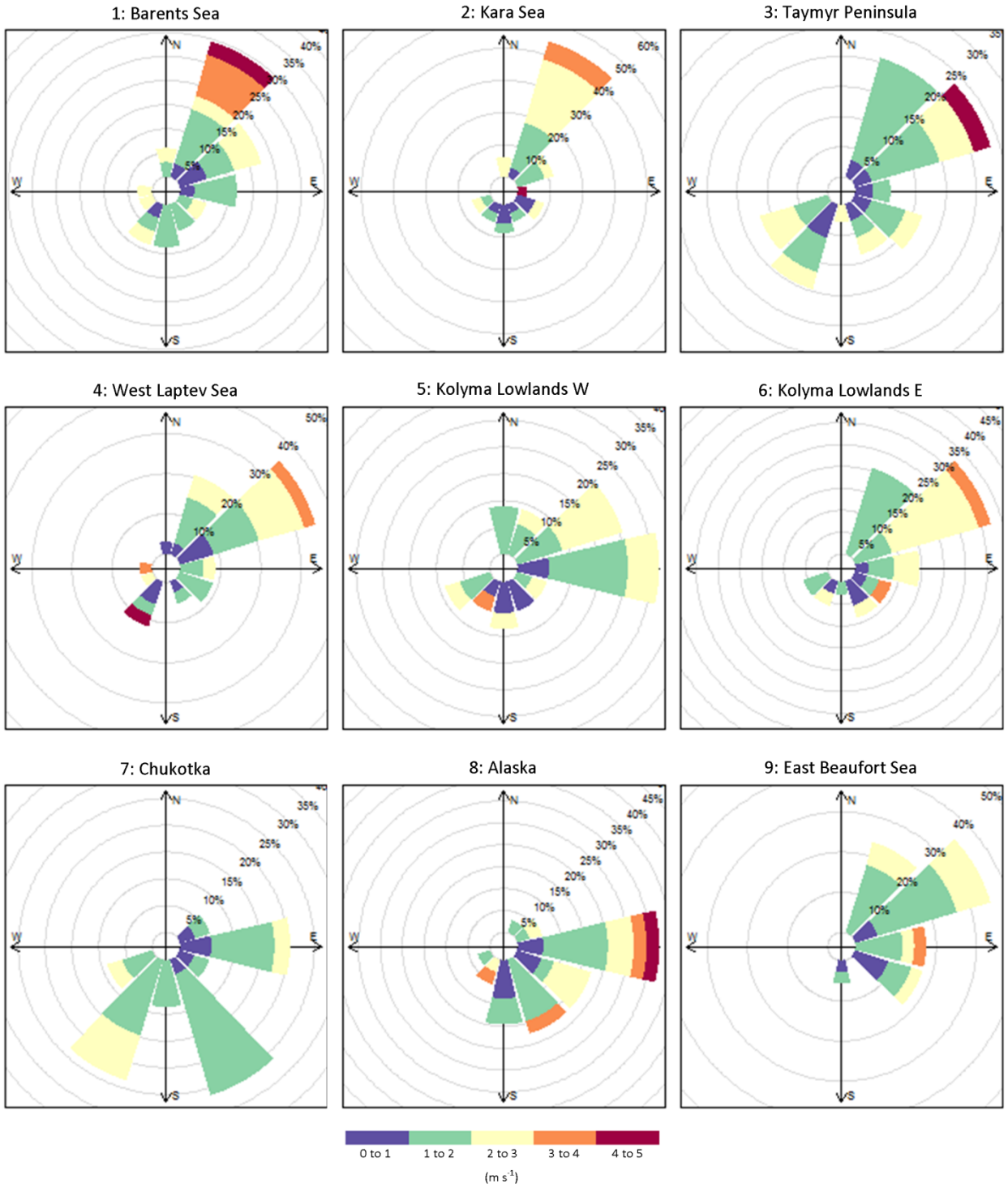

Figure 22: Rose diagrams of monthly July wind direction and speed for 1979-2012 by AFZ Sector. Data from MERRA.

Multicollinearity can be reduced in a regression model by removing problematic variables, but a variable can only be controlled for when present in the model. A more complete data record with more examples of northerly, southerly, and southwesterly winds may provide better results, but a month with predominantly northwesterly winds may never occur. So from a surface wind standpoint, the data record may never contain the gamut of possible of wind directions. For these reasons, linear regression cannot fully disentangle the impacts of all variables affecting the summer AFZ.

In part to address this issue, future research will take an alternative approach to examining the impacts of various surface and atmospheric factors on summer AFZ strength. This approach will include several sensitivity studies using a regional climate model like the Weather Research and Forecasting (WRF) model. Summer AFZ strength could be measured under limiting cases, such as a case where all sea ice is changed to water beginning in the previous September. Sensitivity studies like this will provide a check on the findings in the current study and may further elucidate which factors are most important to summer AFZ development.

Another potential problem can be observed in the intercepts. Although the AFZ-T models showed no substantial model bias in the intercept, some of the other models showed alarmingly high values. In the OceanT-var and LandT-var models in May through July, the intercept was only significant if positive. This indicates that without the intercept, the combination of influencing variables would in general underestimate the 2-m air temperatures and be overly likely to predict a negative anomaly. This sort of model bias may be removed, or at least diminished, with more years of data. Thirty observations are just barely enough to

create a climatology, and models are likely to become more robust with more observations.

Two other likely reasons for the non-zero intercepts are a) that relationships are not linear and b) that important variables have been omitted. Non-linear models were examined, but no alternative model type proved superior in explanatory power to a linear model with consistency when tried for multiple sectors and months.

Therefore, omitted variables may be a more likely cause. **Figure 23** shows one possible omission: the long-term trend of increasing air temperatures related to the increase of greenhouse gas concentration in the atmosphere. This trend would exist with or without change in the influencing variables considered in this study. The 11-year sunspot cycle might also be considered. Such variables were omitted because they operate on a global scale and the focus of this study is on a regional feature. On the other hand, as demonstrated in Sections 5.3 and 5.5, land and ocean 2-m temperatures may exhibit different magnitude responses to the same forcing. Still, only a handful of intercepts indicate the presence of large bias, so the problem may not be widespread enough to merit further complicating the models with variables that operate on different spatial scale and represent decadal or longer temporal variation rather than interannual variation. Instead, the following section considers long-term trends in summer AFZ strength separately.

6. LONG-TERM TRENDS IN AFZ STRENGTH

Increase of near-surface air temperatures during the 1979-2012 period has been well documented in the Arctic (Hansen et al. 2010; IPCC 2013; Cowtan and Way 2014; Simmons and Poli 2014). The linear trend in annual combined land/ocean surface temperature for the Arctic during this period was 0.55 ± 0.15 K per decade (Figure 23). This warming has been linked to changes in other aspects of the Arctic climate system, such as a decline in spring snow cover (Derksen and Brown 2012) and summer sea ice extent (Cavalieri and Parkinson 2012), changes to cyclogenesis and cyclone tracks (McCabe et al. 2001), the frequent development of positive Arctic dipole anomalies (Wang et al. 2009), thawing permafrost (Lawrence et al. 2008), and northward expansion of shrubland and boreal forest into tundra (Tape et al. 2006).

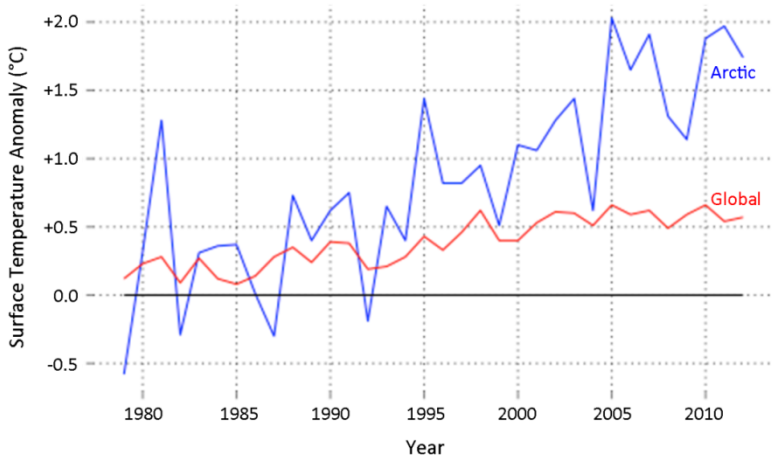

Figure 23: Annual land-ocean surface temperature anomaly from 1951-1980 average.
Arctic domain defined as the area north of 64°N. Data from NASA's GISTEMP.

Some of these changes, such as declining albedo from snow cover and sea ice loss, have acted as positive feedbacks, amplifying recent warming in the Arctic to more than triple the global trend of 0.16 ± 0.03 K per decade (Figure 23; Serreze and Barry 2011). Long-term change

is a prominent feature of the Arctic climate system during the period covered by the reanalysis and satellite data utilized in this study. This section introduces how the AFZ has responded to these long-term regional changes.

6.1. Results from Linear Models of Time Series Data

Table 8 shows the linear per decade change in monthly 2-m meridional temperature gradients for every month and sector during the period 1979-2012. Negative values indicate that gradients are becoming more like the summer AFZ regime, in which 2-m temperatures are warmer over land than over ocean. Positive values indicate that gradients are becoming more like the winter regime, in which 2-m temperatures are cooler over land than over ocean. Therefore, temperature gradients are strengthening when becoming more negative in summer (June through August) or more positive in winter (October through March). Although a crude and simple measure of a time series, the linear trend is easily comparable across all months and sectors. Additionally, no other general model type (power, exponential, logarithmic) explains significantly more of the variation in temperature gradients in more than 10% of cases. For Table 8 and all remaining tables, bold values are significant at the $p < 0.05$ level.

Table 8: Per Decade Change in Monthly 2-m Meridional Temperature Gradient

Sector	Jan	Feb	Mar	Apr	May	Jun	Jul	Aug	Sep	Oct	Nov	Dec
1	**+0.30**	**+0.37**	**+0.23**	+0.06	-0.07	-0.07	0.00	+0.03	-0.01	-0.11	+0.11	+0.17
2	+0.21	+0.16	+0.08	+0.06	**+0.05**	**-0.24**	+0.02	+0.08	-0.05	+0.15	**+0.35**	**+0.23**
3	-0.13	-0.06	-0.04	-0.08	-0.05	**-0.39**	-0.12	-0.04	+0.02	**+0.46**	+0.11	-0.07
4	-0.25	+0.09	+0.04	+0.02	-0.11	**-0.50**	**-0.26**	**-0.31**	**-0.19**	**+0.37**	-0.04	-0.11
5	+0.19	**+0.40**	**+0.20**	**+0.19**	-0.07	**-0.23**	-0.22	**-0.27**	-0.02	**+0.39**	+0.05	+0.16
6	+0.09	**+0.25**	+0.04	+0.11	-0.19	**-0.31**	-0.26	-0.19	-0.01	**+0.57**	+0.03	+0.03
7	+0.05	+0.03	-0.07	-0.02	-0.10	-0.22	+0.19	+0.01	+0.05	**+0.22**	**+0.38**	+0.10
8	+0.12	**-0.40**	+0.01	-0.13	-0.07	-0.11	+0.17	+0.19	+0.10	**+0.57**	**+0.49**	+0.02
9	+0.01	**-0.36**	+0.01	-0.10	-0.16	-0.04	+0.11	+0.10	-0.04	**+0.27**	+0.24	-0.05

Table 9a: Per Decade Change in Monthly 2-m Temperature over Ocean

Sector	Jan	Feb	Mar	Apr	May	Jun	Jul	Aug	Sep	Oct	Nov	Dec
1	+0.11	-0.02	+0.04	**+0.12**	**+0.05**	+0.03	+0.04	+0.02	+0.03	+0.07	+0.05	+0.05
2	**+0.13**	+0.07	**+0.11**	**+0.13**	**+0.07**	**+0.04**	+0.01	+0.01	+0.02	+0.06	+0.09	+0.10
3	**+0.12**	+0.03	**+0.10**	**+0.15**	**+0.11**	**+0.04**	+0.01	+0.03	**+0.07**	**+0.16**	**+0.13**	+0.04
4	+0.08	0.00	**+0.08**	**+0.14**	**+0.10**	**+0.03**	+0.03	0.00	-0.01	**+0.13**	**+0.11**	-0.01
5	+0.05	+0.01	**+0.10**	**+0.15**	**+0.10**	**+0.03**	+0.02	0.00	+0.01	**+0.15**	**+0.12**	+0.02
6	-0.06	-0.07	**+0.12**	**+0.14**	**+0.07**	+0.02	+0.02	+0.03	+0.06	**+0.23**	**+0.11**	+0.04
7	-0.09	-0.07	+0.04	**+0.10**	**+0.06**	**+0.04**	**+0.04**	**+0.06**	**+0.10**	**+0.16**	**+0.15**	+0.03
8	-0.08	-0.01	-0.03	**+0.09**	+0.01	**+0.02**	**+0.05**	**+0.06**	**+0.12**	**+0.23**	**+0.19**	+0.05
9	-0.03	0.00	-0.02	+0.08	+0.04	+0.03	+0.04	+0.03	+0.06	**+0.10**	+0.09	0.00

Table 9b: Per Decade Change in Monthly 2-m Temperature over Land

Sector	Jan	Feb	Mar	Apr	May	Jun	Jul	Aug	Sep	Oct	Nov	Dec
1	+0.07	-0.07	0.00	**+0.10**	+0.06	+0.05	+0.04	+0.02	+0.03	+0.08	+0.03	+0.01
2	+0.09	+0.03	+0.11	**+0.13**	**+0.07**	**+0.10**	0.00	0.00	+0.03	+0.04	+0.02	+0.03
3	**+0.13**	+0.03	**+0.10**	**+0.17**	**+0.12**	**+0.10**	+0.02	+0.03	+0.06	+0.08	+0.10	+0.04
4	**+0.12**	-0.02	+0.07	**+0.14**	**+0.12**	**+0.11**	**+0.06**	+0.05	+0.03	+0.04	+0.08	-0.01
5	+0.02	-0.09	+0.05	**+0.09**	**+0.10**	**+0.07**	+0.07	+0.05	+0.01	**+0.07**	**+0.11**	-0.03
6	-0.06	-0.12	**+0.11**	**+0.11**	**+0.10**	**+0.07**	+0.07	+0.05	+0.04	**+0.10**	**+0.12**	+0.04
7	-0.10	-0.09	+0.06	**+0.11**	**+0.07**	**+0.07**	+0.02	+0.05	**+0.09**	**+0.14**	+0.10	+0.02
8	-0.09	+0.08	-0.05	**+0.11**	+0.03	**+0.04**	+0.02	+0.04	**+0.10**	**+0.13**	+0.08	+0.05
9	-0.03	+0.08	-0.03	**+0.10**	+0.06	+0.03	+0.02	0.00	+0.06	+0.07	+0.06	+0.02

Table 9c: Per Decade Change in Monthly 2-m Temperature over Ocean Minus the Per Decade Change in Monthly 2-m Temperature over Land

Sector	Jan	Feb	Mar	Apr	May	Jun	Jul	Aug	Sep	Oct	Nov	Dec
1	+0.04	**+0.06**	+0.04	+0.01	-0.02	-0.02	0.00	0.00	0.00	-0.01	+0.03	+0.04
2	+0.04	+0.04	0.00	+0.01	0.00	**-0.05**	+0.01	+0.02	-0.01	+0.02	**+0.07**	**+0.07**
3	-0.01	0.00	-0.01	-0.02	-0.01	**-0.06**	-0.02	0.00	+0.01	**+0.09**	+0.03	0.00
4	-0.04	+0.02	+0.01	0.00	-0.02	**-0.08**	-0.03	**-0.05**	-0.03	**+0.09**	+0.03	0.00
5	+0.03	**+0.10**	**+0.05**	**+0.06**	0.00	-0.04	**-0.05**	**-0.05**	0.00	**+0.09**	+0.01	**+0.05**
6	0.00	**+0.05**	+0.01	+0.03	-0.02	**-0.05**	**-0.05**	-0.02	+0.02	**+0.13**	0.00	0.00
7	0.00	+0.02	-0.02	-0.01	-0.01	-0.03	+0.02	+0.01	+0.01	+0.02	**+0.05**	+0.02
8	+0.01	**-0.09**	+0.02	-0.03	-0.02	-0.02	+0.03	+0.03	+0.02	**+0.10**	**+0.11**	0.00
9	0.00	**-0.08**	+0.01	-0.02	-0.02	0.00	+0.02	+0.02	0.00	+0.03	+0.03	-0.02

Each sector has experienced significant change in at least two months during the year, and temperature gradients in every month have changed significantly for at least one sector,

but only June and October show consistent and significant changes throughout most sectors. In October, Sectors 3-9 are all increasing in strength; the winter mode is being enhanced. In June, Sectors 2-6 are all increasing in strength as well, but the summer mode is being enhanced. Sectors 4 and 5 are the only two experiencing a change in strength in multiple summer months. The only two instances of a long-term weakening trend are in Sectors 8 and 9 for February. The spatial and seasonal heterogeneity observed in Table 8 merits closer inspection of the two temperature components of the gradient, as well as the factors that influence AFZ variability.

The per decade change in 2-m surface temperatures overlying ocean and land surfaces within 250 km of the coastline are shown in **Table 9a** and **Table 9b**, respectively. **Table 9c** shows the difference between them. Although cooling might be occurring along the coast in winter months for a few sectors, the predominant pattern is one of warming. Furthermore, all significant trends are positive, regardless of sector, month, or surface type. Significant trends in summer show 2-m temperatures over land warming more rapidly than 2-m temperatures over ocean. In winter, the differences are reversed except in Sectors 8 and 9 for February.

Only two influencing factors show more than one or two significant values for linear trends: sea ice concentration (**Table 10**) and snow cover extent (**Table 11**). Consistent with past observations, sea ice is declining for all spring, summer, and fall months when the trend is significant. Concentration is only increasing in some sectors during February and March, around the annual maximum for sea ice extent. From December through April snow covers the entire land surface of each sector at the spatial resolution observed, so there is no change. Snow cover is declining in summer, but it shows some increases in North America in autumn. Finally, **Table 12** shows the per decade trends in sea ice and snow cover retreat days and the difference

between them. Not surprisingly, the days of retreat below 60% concentration were occurring over two weeks later each year at the beginning of the period than at the end in sectors 1-3, 7, and 9. The only sectors for which there is a significant trend in retreat day difference show that the sea ice retreat day is changing more rapidly than the snow cover retreat day.

Table 10: Per Decade Change in Monthly Snow Cover Extent

Sector	Jan	Feb	Mar	Apr	May	Jun	Jul	Aug	Sep	Oct	Nov	Dec
1	--	--	--	--	-0.34	-0.43	**-0.14**	--	--	+0.30	-0.01	--
2	--	--	--	--	--	**-1.01**	**-0.79**	-0.10	+0.06	+0.29	+0.01	--
3	--	--	--	--	--	**-0.47**	**-0.99**	+0.02	+0.06	-0.05	--	--
4	--	--	--	--	-0.03	**-0.88**	**-0.49**	-0.03	+0.13	+0.25	--	--
5	--	--	--	--	-0.20	-0.54	**-0.29**	-0.03	+0.36	+0.20	--	--
6	--	--	--	--	**-0.43**	**-1.21**	**-0.30**	-0.01	-0.20	-0.08	+0.01	--
7	--	--	--	--	-0.01	**-1.37**	**-0.46**	-0.09	-0.56	**-0.35**	-0.01	--
8	--	--	--	--	-0.09	**-0.75**	**-0.26**	-0.20	-0.57	+0.32	**+0.04**	--
9	--	--	--	--	**-0.67**	**-0.77**	-0.07	**-0.16**	-0.34	**+0.84**	+0.12	--

Table 11: Per Decade Change in Monthly Sea Ice Concentration

Sector	Jan	Feb	Mar	Apr	May	Jun	Jul	Aug	Sep	Oct	Nov	Dec
1	**-0.95**	**-0.57**	**-0.43**	**-0.84**	**-0.93**	**-0.77**	**-0.39**	**-0.07**	**-0.03**	**-0.12**	**-0.49**	**-0.78**
2	**-0.21**	**-0.20**	**-0.11**	**-0.25**	**-0.52**	**-1.17**	**-1.10**	**-0.16**	**-0.06**	**-0.71**	**-0.96**	**-0.61**
3	-0.02	+0.01	+0.02	**-0.11**	**-0.28**	**-0.55**	**-0.92**	**-1.19**	**-1.20**	**-1.55**	**-0.32**	-0.06
4	+0.02	**+0.07**	+0.02	-0.07	**-0.30**	**-0.59**	**-0.94**	**-0.33**	-0.15	**-1.14**	**-0.11**	+0.01
5	+0.02	+0.02	+0.02	--	-0.06	-0.07	**-0.76**	**-0.56**	-0.35	**-1.14**	**-0.13**	-0.01
6	+0.06	**+0.05**	--	--	-0.03	-0.13	**-0.69**	**-1.03**	**-1.08**	**-1.84**	**-0.18**	+0.01
7	+0.04	+0.08	+0.04	+0.02	**-0.24**	**-0.83**	**-0.83**	**-0.54**	**-0.69**	**-1.21**	**-0.99**	**-0.35**
8	+0.06	**+0.11**	**+0.11**	+0.01	-0.13	**-0.64**	**-1.17**	**-1.00**	**-0.96**	**-1.76**	**-0.73**	-0.10
9	+0.05	**+0.11**	**+0.11**	-0.02	-0.30	**-0.82**	-0.58	-0.24	**-0.45**	**-0.97**	**-0.41**	-0.03

6.2. Discussion of Linear Trends

Since both land and ocean 2-m temperatures warmed substantially from 1979 to 2012, the difference between warming over land and warming over ocean is most helpful to understanding the changes to coastal temperature gradients. Although warming occurred in nearly all sectors in May, when the summer AFZ is just beginning to develop, the warming was fairly even over land and ocean. The only sector to experience significant change was Sector 2,

which shifted closer to a winter mode. However, these winter gradients were still essentially neutral (see Figure 11 for the complete distribution).

Table 12: Per Decade Change in Snow and Sea Ice Retreat Days

Sector	Sea Ice Retreat Day	Snow Cover Retreat Day	Retreat Day Difference
1	**-10.68**	-1.78	**-8.90**
2	**-8.64**	**-5.00**	-3.63
3	**-8.27**	**-4.06**	-4.21
4	**-5.92**	-2.07	**-3.85**
5	-0.30	-1.97	+1.66
6	-5.08	**-5.47**	+0.39
7	**-8.82**	**-4.30**	**-4.51**
8	**-9.09**	-1.65	**-7.44**
9	-3.85	**-4.35**	+0.50

Per decade change in the timing of retreat below 60% for snow cover and sea ice concentration within 250 km of the coastline. Positive retreat day difference means that snow cover retreat precedes sea ice retreat.

The greatest changes to the summer AFZ were in June, which saw the monthly meridional temperature gradient strengthen in five out of nine sectors. This occurred because warming over land outpaced warming over ocean. In July and August, ocean warming and land warming were roughly equal in most sectors, so the summer AFZ has experienced little significant change. Sector 4 (Lena River Delta) has strengthened in July, and both Sectors 4 and 5 (Laptev Sea) have strengthened in August. Sector 4 has also experienced enhancement of the summer mode in September, but this change is minor since it would take over two hundred years at this pace for September strength in Sector 4 to match the current July strength.

One more notable feature of the strengthening in June and relative stability of the AFZ in July is that June is becoming more like July. AFZ strength in June surpassed AFZ strength in

July for 18% of cases for the period 1979-1995 and 28% of cases for the period 1996-2012. In other words, the period of peak AFZ strength may be expanding or shifting to earlier in the season. Observations at a finer time scale (weekly or daily) would better address this possibility.

While land 2-m temperatures have warmed faster than ocean 2-m temperatures in summer, the opposite has occurred in winter. The most extreme differences are in October, which has seen the greatest enhancement of the AFZ's winter mode. With September either not changing or becoming more like the summer mode (in Sector 4), this means the transition from summer to winter regimes has become faster and more extreme.

The exceptional changes that occurred in June and October are likely linked to declines in snow cover and sea ice concentration, respectively. June is the month with the most extreme declines in snow cover for every sector except Sector 3. Since June has the most variability in snow cover, the positive feedbacks associated with snow cover loss likely contributed to the exceptional warming over land and strengthening of the June AFZ.

Sea ice, meanwhile, has experienced significant declines in at least seven sectors for all months June through November. But unlike land, which responds to a changing energy balance quickly, the ocean has more thermal inertia and responds slowly. The ocean also stores excess energy until autumn and winter, when the ocean switches of being colder than the overlying atmosphere to being warmer than the overlying atmosphere. Looking at the energy balance terms from Figures 12-15, autumn is when the signs of net radiation (black line) and sensible heat flux (gold line) terms are reversed.

These results are consistent with the seasonal amplifications of Arctic warming reviewed by Serreze and Barry (2011). The snow cover feedback provides an immediate amplification of

Arctic atmospheric warming in late spring over land, while the sea ice feedback provides a delayed amplification of Arctic atmospheric warming that is strongest in autumn and winter. Therefore, snow cover decline has dominated the trend in temperature gradient strength in spring, amplifying warming over land and strengthening the summer AFZ regime, while sea ice decline has dominated the trend in temperature gradient strength in autumn, amplifying warming over ocean and strengthening the winter regime.

The last question to consider with these time series is to project into the future. How is the summer AFZ likely to respond if warming continues? This question was addressed in part by Liess et al. (2011), but they focused their study on the impacts of northward advancement of the boreal forest. By replacing all shrubland with boreal forest in their model, they meant to simulate a change that will take 100-500 years. Although they did observe some increase in monthly temperature gradient strength, the largest observed changes were around 0.15 to 0.20 K/100 km. This maximum observed change, expected to occur over centuries, is less than the per decade changes observed in summer months for many sectors from 1979 to 2012. In other words, observed changes today are an order of magnitude faster than those proposed to accompany a northward advance of the boreal forest. Therefore, the advancement of the boreal forest described by Liess et al. (2011) likely is and will continue to be only a minor agent of change for the summer AFZ.

Rather than changes to vegetation, the state of the summer AFZ over the next century will more likely be determined by changes in snow cover and sea ice concentration. The decline of snow cover in spring will encourage more rapid warming of land 2-m temperatures relative to ocean 2-m temperatures, so the development of the AFZ may occur earlier, increasing June

and possibly even May AFZ strength. Because of the delayed response of the atmosphere to the sea ice feedback, the impact of sea ice decline may not be as acute, but the models in Section 5 show that ocean temperatures are still influenced by sea ice concentration and sea ice retreat. Therefore, AFZ strength may experience weakening from sea ice decline, especially in July and August. Additionally, Table 12 shows that for several sectors, sea ice retreat day is changing more quickly than snow cover retreat day, which may accentuate changes related to sea ice decline in the near future.

7. CONCLUSIONS

The Arctic Ocean coastline from the Kola Peninsula to the Canadian Arctic Archipelago represents a unique boundary that is broad in extent (over 7,000 km long) and broadly zonal in orientation. Differential heating across this boundary produces strong temperature gradients each summer that extend through a considerable depth of the troposphere and help produce a jet-like feature aloft.

The data presented here show consistent depictions of the summer AFZ by three atmospheric reanalyses: CFSR, ERA-Interim, and MERRA, although higher spatial resolution reanalysis data depicts a stronger summer AFZ with more spatial and temporal variance. In all cases, the summer AFZ is located along the coastline, distinctly north of the boreal forest-tundra ecotone.

The summer AFZ is not a homogeneous unit, but is stronger in Siberia and western North America and weaker in Chukotka and along the Barents and Kara Seas. Interannual variations in AFZ strength also occur in a spatially heterogeneous manner, and based on this variability, the summer AFZ can be divided into nine distinct sectors.

Development of the summer AFZ begins when melting snow reveals the underlying land surface. Substantially greater longwave and sensible heat fluxes to the lower atmosphere occur from this exposed land surface than from the ocean/sea ice surface. The resulting temperature differences across the coastline are particularly strong wherever sea ice concentration declines more slowly than snow cover. This development begins in May for most sectors, continues through June, and peaks in July before switching back to a winter mode during September.

Although the summer AFZ develops over the course of several months, year-to-year variation in its monthly strength is most strongly dependent on atmospheric and surface conditions within that month, not on seasonal processes. In general, less snow cover, less cloud cover and more southerly (offshore) winds lead to higher 2-m temperatures over land and a stronger summer AFZ. Lower sea ice concentration, on the other hand, leads to an increase in 2-m temperatures over the ocean and weakens the summer AFZ. The relative importance of these factors varies greatly by sector, and sea level pressure, zonal winds, and wind speed also seem important in some cases. It is nevertheless clear that the strength of the summer AFZ is mostly determined by processes over land, with the exception of sea ice concentration, which impacts ocean 2-m temperatures. The relative importance of these factors also varies by month. In May and June, snow cover is particularly important, while sea ice is more important in July and August. The impact of across-shore winds also strengthens later in the season.

Recent warming in the Arctic has impacted near-surface air temperatures over both land and ocean, so little change has been observed in the peak strength of the summer AFZ. However, the AFZ has become stronger in June in Siberia, the Taymyr Peninsula, and around the Ob River Estuary (Sectors 2-6). This is likely related to seasonal amplification of warming over land by snow cover loss. The amplification of warming due to sea ice loss is primarily felt in autumn and winter and so has not impacted the summer AFZ as strongly.

Future work will examine the development of the summer AFZ at daily and weekly timescales to refine our understanding of how it develops. For instance, the role of advection may prove more important to the exact location of maximum temperature gradient strength on a day-to-day basis. Sensitivity studies using the WRF model will test the conclusions draw from

the linear regression models employed here. Future changes to the summer AFZ will be further explored using the Coupled Model Intercomparison Project Phase 5 (CMIP5) archive of climate models. Lastly, the relevance of the summer AFZ to the broader Arctic climate system will be assessed by exploring the impacts of its interannual variability on cyclone development and Arctic precipitation.

BIBLIOGRAPHY

Bader, J., M. D. S. Mesquita, K. I. Hodges, N. Keenlyside, S. Østerhus, and M. Miles, 2011: A review on Northern Hemisphere sea-ice, storminess and the North Atlantic Oscillation: Observations and projected changes. *Atmospheric Research*, **101**, 809–834, doi:10.1016/j.atmosres.2011.04.007.

Barry, R. G., 1967: Seasonal location of the Arctic front over North America. *Geographical Bulletin*, **9**, 79–95.

Beesley, J. A., and R. E. Moritz, 1999: Toward an Explanation of the Annual Cycle of Cloudiness over the Arctic Ocean. *Journal of Climate*, **12**, 395–415.

Beringer, J., N. J. Tapper, I. Mchugh, F. S. Chapin, A. H. Lynch, M. C. Serreze, and A. G. Slater, 2001: Impact of Arctic treeline on synoptic climate. *Geophysical Research Letters*, **28**, 4247–4250.

Brodzik, M., and R. Armstrong, 2013: Northern Hemisphere EASE-Grid 2.0 Weekly Snow Cover and Sea Ice Extent.

Bryson, R. A., 1966: Air masses, streamlines, and the boreal forest. *Geographical Bulletin*, **8**, 228–269.

Bunkers, M. J., J. R. Miller Jr., and A. T. DeGaetano, 1996: Definition of climate regions in the Northern Plains using an objective cluster modification technique. *Journal of Climate*, **9**, 130–146, doi:10.1175/1520-0442(1996)009<0130:DOCRIT>2.0.CO;2.

Cavalieri, D. J., and C. L. Parkinson, 2012: Arctic sea ice variability and trends, 1979–2010. *Cryosphere*.

Cavalieri, D. J., and Coauthors, 1992: *NASA Sea Ice Validation Program for the DMSP SSM/I: Final Report*. National Aeronautics and Space Administration, Washington, D. C, 126 pp. http://ntrs.nasa.gov/archive/nasa/casi.ntrs.nasa.gov/19920015007.pdf.

Cavalieri, D. J., C. L. Parkinson, P. Gloersen, and H. Zwally, 1996: Sea Ice concentrations from Nimbus-7 SMMR and DMSP SSM/I-SSMIS Passive Microwave Data.

Cowtan, K., and R. G. Way, 2014: Coverage bias in the HadCRUT4 temperature series and its impact on recent temperature trends (in press). *Quarterly Journal of the Royal Meteorological Society*.

Dee, D. P., S. M. Uppala, and A. J. Simmons, 2011: The ERA-Interim reanalysis: Configuration and performance of the data assimilation system. *Quarterly Journal of the Royal Meteorological Society*, **137**, 553–597.

Derksen, C., and R. Brown, 2012: Spring snow cover extent reductions in the 2008-2012 period

exceeding climate model projections. *Geophysical Research Letters*, **39**, L19504, doi:10.1029/2012GL053387.

Dzerdzeevskii, B. L., 1945: Tsirkuliatsionnye skhemy v troposfere Tsentral' noi Arktiki. *Izdatel'stvo Akademii Nauk*, 28.

Gong, X., and M. B. Richman, 1995: On the application of cluster analysis to growing season precipitation data in North America east of the Rockies. *Journal of Climate*, **8**, 897–931, doi:10.1175/1520-0442(1995)008<0897:OTAOCA>2.0.CO;2.

Hansen, J., R. Ruedy, M. Sato, and K. Lo, 2010: Global Surface Temperature Change. *Reviews of Geophysics*, **48**, RG4004, doi:10.1029/2010RG000345.

Hare, F. K., 1968: The Arctic. *Quarterly Journal of the Royal Meteorological Society*, **94**, 439–459.

Hare, F. K., and J. C. Ritchie, 1972: Boreal Bioclimates. *Geographical Review*, **62**, 333–365.

Hewson, T. D., 1998: Objective fronts. *Meteorological Applications*, **5**, 37–65, doi:10.1017/S1350482798000553.

Intrieri, J. M., C. W. Fairall, M. D. Shupe, P. O. G. Persson, E. L. Andreas, P. S. Guest, and R. E. Moritz, 2002: An annual cycle of Arctic surface cloud forcing at SHEBA. *Journal of Geophysical Research*, **107**, 8039, doi:10.1029/2000JC000439.

IPCC, 2013: *Climate Change 2013: The Physical Science Basis*. T.F. Stocker et al., Eds. Cambridge University Press, Cambridge, UK, 33 pp.

Jakobson, E., T. Vihma, T. Palo, L. Jakobson, H. Keernik, and J. Jaagus, 2012: Validation of atmospheric reanalyses over the central Arctic Ocean. *Geophysical Research Letters*, **39**, L10802, doi:10.1029/2012GL051591.

Jakobsson, M., and Coauthors, 2012: The international bathymetric chart of the Arctic Ocean (IBCAO) version 3.0. *Geophysical Research Letters*, **39**, L12609, doi:10.1029/2012GL052219.

Kalkstein, L. S., G. Tan, and J. A. Skindlov, 1987: An evaluation of three clustering procedures for use in synoptic climatological classification. *J. Climate Appl. Meteor*, **26**, 717–730, doi:10.1175/1520-0450(1987)026<0717:AEOTCP>2.0.CO;2.

Key, J. R., 2002: *The Cloud and Surface Parameter Retrieval (CASPR) System for Polar AVHRR*. 4 ed. Cooperative Institue for Meteorlogical Satellite Studies, Univeristy of Wisconsin - Madison, 69 pp. http://stratus.ssec.wisc.edu/caspr/userman.pdf.

Key, J. R., X. Wang, J. C. Stoeve, and C. Fowler, 2001: Estimating the cloudy-sky albedo of sea ice and snow from space. *Journal of Geophysical Research*, **106**, 12489, doi:10.1029/2001JD900069.

Klein, S. A., and D. L. Hartmann, 1993: The seasonal cycle of low stratiform clouds. *Journal of Climate*, **6**, 1587–1606, doi:10.1175/1520-0442(1993)006<1587:TSCOLS>2.0.CO;2.

Krebs, J. S., and R. G. Barry, 1970: The arctic front and the tundra-taiga boundary in Eurasia. *Geographical Review*, **60**, 548–554.

Kurashima, A., 1968: Studies of the winter and summer monsoons in east Asia based on dynamic concept. *Geophysical Magazine*, **34**, 145–235.

Ladd, M. J., and K. Gajewski, 2010: The North American summer Arctic front during 1948–2007. *International Journal of Climatology*, **30**, 874–883, doi:10.1002/joc.1940.

Lawrence, D. M., A. G. Slater, R. A. Tomas, M. M. Holland, and C. Deser, 2008: Accelerated Arctic land warming and permafrost degradation during rapid sea ice loss. *Geophysical Research Letters*, **35**, L11506, doi:10.1029/2008GL033985.

Liess, S., P. K. Snyder, and K. J. Harding, 2011: The effects of boreal forest expansion on the summer Arctic frontal zone. *Climate Dynamics*, **38**, 1805–1827, doi:10.1007/s00382-011-1064-7.

Lüpkes, C., T. Vihma, E. Jakobson, G. König-Langlo, and A. Tetzlaff, 2010: Meteorological observations from ship cruises during summer to the central Arctic: A comparison with reanalysis data. *Geophysical Research Letters*, **37**, L09810, doi:10.1029/2010GL042724.

Lynch, A. H., A. G. Slater, and M. C. Serreze, 2001: The Alaskan Arctic frontal zone: Forcing by orography, coastal contrast, and the boreal forest. *Journal of Climate*, **14**, 4351–4362.

McCabe, G. J., M. P. Clark, and M. C. Serreze, 2001: Trends in Northern Hemisphere Surface Cyclone Frequency and Intensity. *Journal of Climate*, **14**, 2763–2768, doi:10.1175/1520-0442(2001)014<2763:TINHSC>2.0.CO;2.

Overland, J. E., and M. Wang, 2010: Large-scale atmospheric circulation changes are associated with the recent loss of Arctic sea ice. *Tellus A*, **62A**, 1–9.

Pielke, R. A., and P. L. Vidale, 1995: The boreal forest and the polar front. *Journal of Geophysical Research*, **100**, 25755, doi:10.1029/95JD02418.

Reed, R. J., and B. A. Kunkel, 1960: The Arctic circulation in summer. *Journal of Meteorology*, **17**, 489–506.

Rienecker, M. M., and Coauthors, 2011: MERRA: NASA's Modern-Era Retrospective Analysis for Research and Applications. *Journal of Climate*, **24**, 3624–3648, doi:10.1175/JCLI-D-11-00015.1.

Robinson, D., 2013: *Climate Algorithm Theoretical Basis Document (C-ATBD) Northern Hemisphere Snow Cover Extent*. 3rd ed. NOAA, 29 pp.

Rouse, W. R., 1991: Impacts of Hudson Bay on the Terrestrial Climate of the Hudson Bay Lowlands. *Arctic and Alpine Research*, **23**, 24–30.

Saha, S., and Coauthors, 2010: The NCEP Climate Forecast System Reanalysis. *Bulletin of the American Meteorological Society*, **91**, 1015–1057, doi:10.1175/2010BAMS3001.2.

Scott, P. A., 1992: Annual development of climatic summer in northern North America: Accurate prediction of summer heat availability. *Climate Research*, **2**, 1–9.

Serreze, M. C., A. H. Lynch, and M. P. Clark, 2001: The Arctic frontal zone as seen in the NCEP-NCAR reanalysis. *Journal of Climate*, **14**, 1550–1567.

Serreze, M. C., and A. P. Barrett, 2008: The summer cyclone maximum over the Central Arctic Ocean. *Journal of Climate*, **21**, 1048–1065, doi:10.1175/2007JCLI1810.1.

Serreze, M. C., and R. G. Barry, 2011: Processes and impacts of Arctic amplification: A research synthesis. *Global and Planetary Change*, **77**, 85–96, doi:10.1016/j.gloplacha.2011.03.004.

Shahgedanova, M., T. P. Burt, and T. D. Davies, 1998: Synoptic Climatology of Air Pollution in Moscow. *Theoretical and Applied Climatology*, **61**, 85–102, doi:10.1007/s007040050054.

Shapiro, M. A., T. Hampel, and A. J. Krueger, 1987: The Arctic tropopause fold. *Monthly Weather Review*, **115**, 444–454.

Simmonds, I., and I. Rudeva, 2012: The great Arctic cyclone of August 2012. *Geophysical Research Letters*, **39**, L23709, doi:10.1029/2012GL054259.

Simmonds, I., and K. Keay, 2009: Extraordinary September Arctic sea ice reductions and their relationships with storm behavior over 1979–2008. *Geophysical Research Letters*, **36**, L19715, doi:10.1029/2009GL039810.

Simmons, A. J., and P. Poli, 2014: Arctic warming in ERA-Interim and other analyses (in press). *Quarterly Journal of the Royal Meteorological Society*, doi:10.1002/qj.2422.

Strahler, A., D. Muchoney, J. Borak, M. Friedl, S. Gopal, E. Lambin, and A. Moody, 1999: *MODIS Land Cover Product*. 5 ed. Boston, 66 pp.

Stroeve, J. C., J. A. Maslanik, M. C. Serreze, I. Rigor, W. Meier, and C. Fowler, 2011: Sea ice response to an extreme negative phase of the Arctic Oscillation during winter 2009/2010. *Geophysical Research Letters*, **38**, L02502, doi:10.1029/2010GL045662.

Tape, K., M. Sturm, and C. Racine, 2006: The evidence for shrub expansion in Northern Alaska and the Pan-Arctic. *Global Change Biology*, **12**, 686–702, doi:10.1111/j.1365-2486.2006.01128.x.

Tsukernik, M., D. N. Kindig, and M. C. Serreze, 2007: Characteristics of winter cyclone activity in

the northern North Atlantic: Insights from observations and regional modeling. *Journal of Geophysical Research*, **112**, D03101, doi:10.1029/2006JD007184.

Unal, Y., T. Kindap, and M. Karaca, 2003: Redefining the climate zones of Turkey using cluster analysis. *International Journal of Climatology*, **23**, 1045–1055, doi:10.1002/joc.910.

Wang, J., J. Zhang, E. Watanabe, M. Ikeda, K. Mizobata, J. E. Walsh, X. Bai, and B. Wu, 2009: Is the Dipole Anomaly a major driver to record lows in Arctic summer sea ice extent? *Geophysical Research Letters*, **36**, L05706, doi:10.1029/2008GL036706.

Willis, R. A., and G. K. Grice, 1977: The wintertime Arctic front and its effect on Fairbanks, Alaska. *Monthly Weather Review*, **105**, 78–85.

Wu, B., J. Wang, and J. E. Walsh, 2006: Dipole Anomaly in the winter Arctic atmosphere and its association with sea ice motion. *Journal of Climate*, **19**, 210–225, doi:10.1175/JCLI3619.1.

Zhang, J., R. Lindsay, A. Schweiger, and M. Steele, 2013: The impact of an intense summer cyclone on 2012 Arctic sea ice retreat. *Geophysical Research Letters*, **40**, 1–7, doi:10.1002/grl.50190.